

# **SAND REPORT**

SAND2001-3188

Unlimited Release

Printed October 2001

## **Development of the Capabilities to Analyze the Vulnerability of Bulk Power Systems**

Authors: David G. Robinson, Satish J. Ranade, Salvador B. Rodriguez,  
Rudolph G. Jungst, Angel Urbina, Thomas L. Paez  
Editor: David M. Kunsman

Prepared by  
Sandia National Laboratories  
Albuquerque, New Mexico 87185 and Livermore, California 94550

Sandia is a multiprogram laboratory operated by Sandia Corporation,  
a Lockheed Martin Company, for the United States Department of  
Energy under Contract DE-AC04-94AL85000.

Approved for public release; further dissemination unlimited.



Issued by Sandia National Laboratories, operated for the United States Department of Energy by Sandia Corporation.

**NOTICE:** This report was prepared as an account of work sponsored by an agency of the United States Government. Neither the United States Government, nor any agency thereof, nor any of their employees, nor any of their contractors, subcontractors, or their employees, make any warranty, express or implied, or assume any legal liability or responsibility for the accuracy, completeness, or usefulness of any information, apparatus, product, or process disclosed, or represent that its use would not infringe privately owned rights. Reference herein to any specific commercial product, process, or service by trade name, trademark, manufacturer, or otherwise, does not necessarily constitute or imply its endorsement, recommendation, or favoring by the United States Government, any agency thereof, or any of their contractors or subcontractors. The views and opinions expressed herein do not necessarily state or reflect those of the United States Government, any agency thereof, or any of their contractors.

Printed in the United States of America. This report has been reproduced directly from the best available copy.

Available to DOE and DOE contractors from  
U.S. Department of Energy  
Office of Scientific and Technical Information  
P.O. Box 62  
Oak Ridge, TN 37831

Telephone: (865)576-8401  
Facsimile: (865)576-5728  
E-Mail: [reports@adonis.osti.gov](mailto:reports@adonis.osti.gov)  
Online ordering: <http://www.doe.gov/bridge>

Available to the public from  
U.S. Department of Commerce  
National Technical Information Service  
5285 Port Royal Rd  
Springfield, VA 22161

Telephone: (800)553-6847  
Facsimile: (703)605-6900  
E-Mail: [orders@ntis.fedworld.gov](mailto:orders@ntis.fedworld.gov)  
Online order: <http://www.ntis.gov/ordering.htm>



SAND2001-3188  
Unlimited Release  
Printed October 2001

## **Development of the Capabilities to Analyze the Vulnerability of Bulk Power Systems**

Editor:

David M. Kunsman, Risk & Reliability Analysis Department  
Sandia National Laboratories  
P. O. Box 5800  
Albuquerque, NM 87185-0748

Authors:

David G. Robinson, Risk & Reliability Analysis Department  
Sandia National Laboratories  
P. O. Box 5800  
Albuquerque, NM 87185-0748

Salvador B. Rodriguez, Modeling and Analysis  
Sandia National Laboratories  
P. O. Box 5800  
Albuquerque, NM 87185-0739

Rudolph G. Jungst, Lithium Battery Research & Development  
Sandia National Laboratories  
P. O. Box 5800  
Albuquerque, NM 87185-0613

Angel Urbina and Thomas L. Paez, Validation & Uncertainty Quantification  
Sandia National Laboratories  
P. O. Box 5800  
Albuquerque, NM 87185-0557

Satish J. Ranade  
New Mexico State University  
Klipsch School of Engineering and Computer Engineering  
Las Cruces, New Mexico, 88003

## **Abstract**

The electrical grids of North America are an extremely large and complex set of interconnected networks vital to the economic lifeblood and safety of more than 380 million people. These networks are dynamic and constantly changing systems whose operation is vulnerable to significant disruptions due to evolving energy policies as well as from natural and man-made sources. The President's Commission on Critical Infrastructure Protection has identified electric power as a critical infrastructure sector. The 1996 blackouts of the western power system demonstrated the weaknesses of the current power grid reliability analysis tools and highlighted the need for improved techniques to deal with the uncertainties associated with the operation of a bulk power network. An alternative approach involves probabilistic load-flow characterization and is closely related to the analysis methods being developed as part of the nuclear weapon system stockpile surveillance program. Integration of the new probabilistic load-flow analysis techniques and sensitivity analysis methods will provide the tools necessary to statistically characterize the load shedding at each major bus in a very large bulk power system. By probabilistically characterizing the amount of load shed at each network node and then relating this measure to the sensitivity of the grid to failure of this node, the reliability of the grid can be understood more thoroughly. The major objective of this effort was the integration of traditional load-flow analysis packages, advanced optimization methods, and state-of-the-art uncertainty analysis techniques. In parallel with this effort, we addressed issues associated with short-term energy storage devices (e.g., batteries) that might impact the overall reliability of the bulk power system. It was anticipated that a significant impediment to integrating these various tools and techniques was the size of bulk power systems that could be analyzed with this complex suite of tools. Therefore, a secondary objective was the implementation of all software analysis tools on the massively parallel computer systems at Sandia National Laboratories. These risk-based analytical tools can be used for short-term (daily) vulnerability assessment and long-term (yearly) planning for improved network security.

## **Acknowledgment**

The authors sincerely thank Pat Oliver of Tech Reps for her time-challenged editing and integration. Prior to her efforts, this report existed as a collection of numerous memos, letters, and letter reports, and presentations of an ongoing, multiyear effort. Her skills brought together the information presented here into the draft of a coherent whole.

This page intentionally left blank.

# Contents

<b><u>1. INTRODUCTION</u></b> .....	<b>10</b>
<b><u>2. BACKGROUND</u></b> .....	<b>12</b>
<b><u>2.1 THE ELECTRIC POWER SYSTEM IN TRANSITION</u></b> .....	<b>12</b>
<b><u>2.2 TECHNICAL BACKGROUND</u></b> .....	<b>12</b>
<b><u>3. OBJECTIVES</u></b> .....	<b>15</b>
<b><u>3.1 GENERAL OBJECTIVES</u></b> .....	<b>15</b>
<b><u>3.2 SPECIFIC OBJECTIVES</u></b> .....	<b>16</b>
<b><u>4. RESULTS</u></b> .....	<b>19</b>
<b><u>4.1 FIRST YEAR—TRADITIONAL POWER SYSTEM RELIABILITY MODELING</u></b> .....	<b>19</b>
<b><u>4.1.1 Background</u></b> .....	<b>19</b>
<b><u>4.1.1.1 Grid Reliability</u></b> .....	<b>19</b>
<b><u>4.1.1.2 Power-flow Model</u></b> .....	<b>20</b>
<b><u>4.1.2 Accomplishments</u></b> .....	<b>23</b>
<b><u>4.1.2.1 Power Flow Modeling</u></b> .....	<b>23</b>
<b><u>4.1.2.2 Battery Study</u></b> .....	<b>23</b>
<b><u>4.2 SECOND YEAR—OPTIMIZATION AND UNCERTAINTY</u></b> .....	<b>24</b>
<b><u>4.2.1 Background</u></b> .....	<b>24</b>
<b><u>4.2.2 Optimization Module</u></b> .....	<b>25</b>
<b><u>4.2.2.1 SGOPT Software</u></b> .....	<b>25</b>
<b><u>4.2.2.2 Models Using Optimization Software</u></b> .....	<b>26</b>
<b><u>4.2.3 Power-flow Software</u></b> .....	<b>26</b>
<b><u>4.2.4 Uncertainty Module</u></b> .....	<b>29</b>
<b><u>4.2.4.1 CRAX/Cassandra Software Elements</u></b> .....	<b>30</b>
<b><u>4.2.4.2 Cassandra Capabilities</u></b> .....	<b>33</b>
<b><u>4.2.5 Battery Study</u></b> .....	<b>33</b>
<b><u>4.2.6 Accomplishments</u></b> .....	<b>34</b>
<b><u>4.2.6.1 Power Flow Modeling</u></b> .....	<b>34</b>
<b><u>4.2.6.2 Battery Study</u></b> .....	<b>35</b>
<b><u>4.3 THIRD YEAR—MASSIVELY PARALLEL IMPLEMENTATION</u></b> .....	<b>35</b>
<b><u>4.3.1 Background</u></b> .....	<b>36</b>
<b><u>4.3.1.1 Application of the High-performance Computing Initiative</u></b> .....	<b>36</b>
<b><u>4.3.1.2 Sandia National Laboratories' Teraflops Computers</u></b> .....	<b>36</b>
<b><u>4.3.2 Work Performed</u></b> .....	<b>38</b>
<b><u>4.3.2.1 Efforts in the Power Flow Modeling</u></b> .....	<b>38</b>
<b><u>4.3.2.2 Efforts in Battery Storage Modeling</u></b> .....	<b>39</b>
<b><u>4.3.3 Accomplishments</u></b> .....	<b>40</b>
<b><u>5. PROGRAM RESULTS</u></b> .....	<b>41</b>
<b><u>5.1 ACCOMPLISHMENTS</u></b> .....	<b>41</b>
<b><u>5.2 RECOMMENDATIONS</u></b> .....	<b>42</b>
<b><u>6. REFERENCES</u></b> .....	<b>44</b>

## Figures

<a href="#">Figure 4-1 General Uncertainty Module Information Flow</a> .....	30
<a href="#">Figure 4-2 Relationships among CRAX, Cassandra, SGOPT and the Analytical Engine and Physical Models</a> .....	32
<a href="#">Figure 4-3 Effect of Parallel Processing on Computational Speed</a> .....	37
<a href="#">Figure 4-4 Cplant Node Distribution</a> .....	38

# Nomenclature

SNL	Sandia National Laboratories
NMSU	New Mexico State University
IEEE	Institute of Electrical and Electronics Engineers
RTS	Reliability Test System
SCADA	Supervisory Control and Data Acquisition
DAKOTA	<b>Design Analysis Kit for OpTimizAtion</b>
LDRD	Laboratory Directed Research and Development
T&D	transmission and distribution
ISO	Independent System Operator
LOLP	Loss of Load Probability
ESP	Enhanced Surveillance Project
FMEA	Failure Modes and Effects Analysis
WSCC	Western Systems Coordinating Council (Electric Power Grid in Western U.S.)
AC	alternating current
DC	direct current
ERCOT	Electric Reliability Council of Texas
COTS	commercial off-the-shelf
CRAX	<b>Cassandra Exoskeleton</b>
GUI	graphics user interface
Tk	Tool Kit
Tcl	Tool Command Language
CDF	Common Data Form
LHS	Latin Hypercube Sampling
IP	Internet Protocol
MIMD	multiple instruction multiple data
T O/S	Teraflops Operating System
MPI	Message Passing Interface
CORBA	Common Object Request Broker Architecture
EIS	electrochemical impedance spectroscopy

# 1. Introduction

The electrical power transmission grids of North America are an extremely large and complex set of interconnected networks vital to the economic lifeblood and safety of over 380 million people. These networks are dynamic and constantly changing systems whose operation is vulnerable to significant disruptions due to evolving energy policies as well as from natural and man-made sources. The President's Commission on Critical Infrastructure Protection has identified electric power as a critical infrastructure sector, of which these networks are essential components. Furthermore, electric power utilities have been transitioning from a regulated, rate-based, mode of operation in which utilities provide service to areas and customers on an exclusive franchise basis to a mode of competitive energy markets. As this has occurred--as the industry deregulates and competition is introduced--the operation, control, maintenance and expansion of electric power systems have become fragmented, and this trend continues. In the past, regulated electric utilities have had responsibility to insure the reliability of their systems as well as to coordinate efforts to insure system wide reliability. As planning and operating decisions become more and more subject to market forces, it is less clear what processes will ensure reliability under power industry deregulation.

One could thus argue that it was inevitable that the transition to competitive energy markets would impact electric service reliability, and negative impacts were quite evident in California during the winter of 2000-2001. Therefore, there is a need for models and methods to assess the likely reliability impacts of utility deregulation, and to provide guidance to energy providers, regulatory agencies and other government agencies, and the public during this process. Furthermore, these models can be used to ascertain mitigation strategies, such as new transmission capabilities or distributed energy resources, for any reliability deficiencies identified. In addition, there exists an increasing problem of potential physical and cyber sabotage to key power grid elements. There is already a complex interaction between infrastructure elements (communications, power, transportation, etc.) and under restructuring these interactions will increase in scope to a national level. Existing reliability assessment models are based on examining contingencies, one at a time, from the bottom up of the grid system, and are not capable of accurately reflecting and assessing critical reliability issues affecting the transmission grid system in the new market environment. It is one thing to do contingency analyses for a limited monopoly grid and another for a regional, if not national, system. Thus, improved and more comprehensive models are needed. The work described herein, funded internally at Sandia National Laboratories (SNL) as a project of laboratory-directed research and development (LDRD), addressed this need.

An alternative to the existing contingency approaches to reliability analysis involves probabilistic load-flow characterization, which is closely related to the analysis method being developed as a part of the nuclear weapon system stockpile program. Integration of the new probabilistic load-flow analysis technique and sensitivity analysis methods will provide the tools necessary to statistically characterize the load flow. In addition, reliability of bulk power grids can be increased by the judicious incorporation of distributed energy resources. As part of this effort, one such potential resource, rechargeable batteries, has been investigated in this study. Further,

SNL's massively parallel computer systems provide a platform of sufficient speed to integrate the required tools and techniques for large bulk power systems.

This report describes the ongoing effort to develop, improve, and implement probabilistic load-flow characterization of large bulk power systems, for both linear and non-linear applications. The main report is more of a summary of the work with the details provided in the appendices. Also, although this report is self-contained, it really should be considered to be more an initial report, or a first volume, than a final report in that the work, described herein, continues, and additional reports discussing both broader and deeper aspects of the ongoing effort will be forthcoming. The recommendations made in this study for improvements and additions to the models were accepted, and the work to develop and incorporate those improvements and additions has started.

## **2. Background**

### **2.1 The Electric Power System in Transition**

Electric power utility business is in transition. It is changing from a regulated, rate-based mode of operation in which utilities provide service to areas and customers on an exclusive franchise basis to a mode of competitive energy markets. It is inevitable that the transition to competitive energy markets will impact electric service reliability. Therefore, there is a need for models and methods to assess the likely reliability impacts of utility deregulation and to provide guidance to energy providers, regulatory and other government agencies, and the public. Existing reliability assessment models are not capable of accurately reflecting and assessing all of the reliability issues arising from deregulation, and so improved and more comprehensive models are needed.

There are many recent examples of the evolving reliability problems of the North American grid. The 1996 blackouts of the western power system demonstrated the weaknesses of the current power grid reliability analysis tools and highlighted the need for improved techniques to deal with the uncertainties associated with the operation of a bulk power network [1]. A series of isolated failures caused significant disruptions throughout the western states on July 2, 1996. The ensuing investigation revealed several unusual operating conditions in addition to a fault on a 345-kV transmission line. For example, high-power transfers between the Pacific Northwest and California, Idaho, and Utah and the loss of another high-voltage line due to a bad protective device contributed to the loss of power to approximately two million customers in 14 states, Canada, and Mexico. The disruption lasted less than 35 seconds but caused power outages lasting up to seven hours. A similar incident occurred on August 10, 1996, when all major transmission lines between Oregon and California failed. Outages in 10 western states affected 5.6 million customers for up to six hours. Vulnerability of the electrical power network infrastructure to deliberate sabotage is also of concern. Based on these and other recent problems, it is now recognized that there is a national need for a comprehensive, integrated capability that can help respond to these and other stresses. Models and modeling techniques that were adequate for the service-area grid of the regulated utilities cannot accurately address all the issues arising from the new grid operation.

### **2.2 Technical Background**

The reliability of bulk power systems is composed of two fundamental elements: adequacy and security. Adequacy relates to the existence of sufficient facilities within the system to satisfy the consumer load demand. These include the facilities necessary to generate sufficient energy and transmission facilities to transport energy to the consumer load. Adequacy is associated with static system conditions and does not include disturbances that might result from such events as transmission line loss. Security is the ability of the system to respond to disturbances arising within the system and is associated with loss of major generation and transmission facilities, e.g., loss of major portions of the grid in the West resulted primarily from system instabilities. While adequacy has always been an issue during planning, in the future, security will become a major

planning issue as deregulation and the potential for sabotage (cyber or physical) becomes reality. Presently, no method exists to probabilistically evaluate security (only adequacy is statistically characterized). A fundamental reason for this deficiency is that network structures such as the grid can be characteristically noncoherent, i.e., element failure can increase the reliability or the introduction of a redundant element can decrease the system reliability. Current reliability methods require the system to be logically coherent. For example, to assess the impact of a loss of transmission line segment requires that a simulated loss be introduced followed by a redistribution of the available power through the remaining system elements. It is possible that the new system, with the redistributed power flow, will be more stable than the original system. This counterintuitive notion has been shown to be a common effect in, for example, transportation, communications, and water distribution systems (all of the major dynamic elements in the national infrastructure). The concept is often referred to as Braess Paradox after Dietrich Braess, who has shown that the addition of more connections in systems (he specifically analyzed transportation) will not necessarily improve the performance of the system because optimizing individual portions of an overall system (e.g., individual utilities in the overall national grid) does not usually result in an optimized overall system. Furthermore, adding capacity to a portion of the system can degrade the performance of the overall system. The paradox is somewhat akin to the economics insight of the fallacy of the commons, wherein common ownership of a resource results in overuse and thence exploitation as every “owner” extracts an amount which is good for him and not what is best for everyone. (For an explanation of the paradox, see D. Braess, *Nonlinear Approximation Theory*, Amsterdam: Springer-Verlag, 1986.) The paradox does not mean that the reliability of infrastructure systems cannot be analyzed; rather it means that such analyses must be done with great care and that they should be comprehensive (if the problem examined is too narrow, the negative effects might not be evident). Therefore, for the purposes of this research, the result of the paradox is that each possible combination of failure modes must be examined for the effect on the system. The effect cannot be inferred because of the potential non-linearity of adding or subtracting connections. The system must be exercised to determine the extent and severity of the failure combination.

One aspect of the grid that significantly lessens the likelihood of a noncoherent system structure and thereby enhances system security (i.e., the ability of the system to respond to perturbations) is the local availability of excess power. This excess margin might take the form of small localized generation facilities or even power storage facilities, and is often referred to as distributed generation. For example, Pacific Gas and Electric found that transportable battery systems would be economically competitive for deferring substation upgrades for a year in areas experiencing rapid load growth. Energy storage systems improve the benefits available from renewable generators by making the energy dispatchable. System security benefits from storage are currently being realized by the Puerto Rico Electric Power Authority, which is using a 20-MW battery facility to provide a “spinning reserve” capability that stabilizes the frequency on their island system in the event of an outage on a large turbine generator. Southern California Edison studied the possibility of using their Chino battery system to stabilize transmission lines and concluded that it would be possible to do so. Small island utilities such as Metlakatla Power and Light have replaced diesel generators with battery storage systems to manage load spikes on their systems. The analyses of the economic and technical benefits of such systems are generally performed by extremely crude methods and are recognized widely by industry and regulatory

organizations as needing substantial improvement [2]. In addition to the unique difficulties with modeling the traditional generation and transmission network, this ability to characterize the impact of distributed power will be a key element in continuing research at SNL. However, evaluation of system reliability comes at great computational expense—certainly beyond that available to the majority of research institutions in the U.S.

## 3. Objectives

The long-term goals of our effort in the area of the security of the bulk power grid involve fundamental advancements in concepts and computational techniques as applied to uncertainty analysis of the grid. This report summarizes our accomplishments during a three year LDRD project that created an alternative approach to assessing the reliability of the bulk electric power system, an approach which we believe takes us a long way toward that fundamental advancement.

### 3.1 General Objectives

Over the course of three years, our intermediate findings could and did change our additional efforts so that our specific objectives responded to the work as it progressed. Nevertheless, these objectives can be concisely stated as

Year 1—link linear (direct current, DC) power flow models to the uncertainty tools

- initiate development of battery storage models

Year 2—expand the power flow tools to address non-linear (alternating current, AC) power

- incorporate new methods into the uncertainty models

- re-link the updated power flow and uncertainty models

- complete the development of the battery storage models

Year 3—port the developed tools to the massively parallel processors

- demonstrate the operability of the tools on these computers

- link the power flow and uncertainty models with the developed battery storage models

As additional features were added to the models, they were exercised and the results were compared to an IEEE standard grid reliability test problem.

Our alternative approach involved probabilistic load-flow characterization and was closely related to the analysis methods being developed as part of the nuclear weapon system stockpile surveillance program. By probabilistically characterizing the amount of load shed at each network node and then relating this characterization to the sensitivity of the grid to failure of this node, the reliability of the grid can be more thoroughly understood.

From the beginning of the work, our major objectives were the integration of traditional load-flow analysis packages, advanced optimization methods, and state-of-the-art uncertainty analysis techniques. In accomplishing this, we also addressed issues associated with short-term energy storage devices (e.g., batteries) that could enhance the overall reliability of the bulk power

system. Also, at the beginning of the work, we anticipated that a significant impediment to integrating these various tools and techniques would be the size of bulk power systems that could be analyzed with this complex suite of tools. Therefore, a secondary objective for our effort was advanced and realized: the implementation of all software analysis tools on the massively parallel computer systems at SNL. These risk-based analytical tools can be used for short-term (daily) vulnerability assessment and long-term (yearly) planning for improved network security.

## 3.2 Specific Objectives

Specific research objectives for this effort are presented below. As will be seen in the remaining sections of this report, all these objectives were addressed to at least a limited degree. In some instances, however, we discovered that the effort involved much more work than we anticipated, and we continue more detailed work on them via additional LDRD funding. In particular, the stability analysis effort and subsequent application and implementation are more complex than originally thought, and much more effort continues in this area. In addition, alternative distributed energy resource solutions continue to be explored in addition to the batteries examined herein.

Stability analysis of large (national scale) bulk power grids requires the development of a new hierarchical load-flow analysis technique that combines DC and AC approaches for performing deterministic load-flow analyses. Mathematical development of the initial hierarchical model was been completed and ported to the DEC 8400 computer network at SNL, and implemented on the 28-node computer network at New Mexico State University (NMSU). This effort required

- Extending the AC power-flow model to include explicitly the ability to use DC and AC load-flow algorithms simultaneously in a single network analysis.
- Completing initial switching and storage computer modules, and including these in the power-flow model. Specific tasks for this effort include
  - Completing Algorithms and Initial models.
  - Coding to C/C++.
- More thoroughly integrating the uncertainty analysis into the power-flow analysis. This effort also included
  - Developing contingency-based analysis capability.
  - Testing the Cassandra uncertainty library interface.
  - Adding additional, more efficient uncertainty methods.
  - Identifying metrics to characterize the voltage collapse of a large network.

- Applying the results to a small local network involving a nuclear power plant. This effort included
  - Defining grid topology for a small test network.
  - Analyzing switching and storage components as elements in the Institute of Electrical and Electronics Engineers (IEEE) Reliability Test System (RTS).
- Applying the probabilistic power-flow analysis to a large bulk power system using a preliminary hierarchical network-modeling tool. This effort included defining the grid topology for a regional bulk power system.
- Investigating alternative hardware solutions, in particular renewable energy components that might aid in improving power grid reliability. Specifically, this effort modeled the effect that rechargeable batteries could have on the reliability of a power grid.
  - Constructing, for the first time by anyone, anywhere, a model of a renewable generator that is compatible with a power flow model for grid reliability calculations
  - Incorporating in this model a representation of an energy storage device
  - Including all components in the model
  - Representing the operation of the system as realistic as possible, e.g., allowing for operational degradation
- Identifying and testing metrics for statistical characterization of stability. This effort included
  - Identifying possible metrics to statistically describe the sensitivity of network stability to disturbances.
  - Developing capability to output these metrics for selected nodes/buses on the network.
  - Performing two significant literature reviews: probabilistic characterization of power flow in a bulk power system, and combination of dynamic bifurcation and probability theory to characterize voltage instability.
  - Acquiring a thorough understanding of the bifurcations of the nonlinear dynamic (i.e., chaos) process associated with power-flow equations. Identifying and testing metrics for statistical characterization of stability is the most challenging area of research in the project because of the need to acquire this understanding.
  - Investigating possible probability-based stability metrics indicates that an optimal power-flow capability will be necessary.
  - Incorporating a library from the Design Analysis Kit for OpTimizAtion (DAKOTA) into the power-flow analysis.

- Tying to a cooperative research venture between SNL Group 9200, Case Western University, NMSU and SNL Group 6400 to investigate this research topic under a separate optimization project through SNL's Laboratory Directed Research and Development (LDRD) Program.

As noted above, all of these objectives were addressed to at least some degree. The following sections describe the work performed during the course of this LDRD, present the results obtained, and conclude with recommendations for additional work.

## 4. Results

Presented in this chapter are the results of the three year long investigation. As such, the results are described chronologically when appropriate with Section 4.1 being devoted to the first year and 4.2 to the second. In Section 4.3 we present the overall results of the work. We also provide some background information in each section so that the work described therein can be better understood. The details of the discussions, however, are given in Appendices A-D.

### 4.1 First Year—Traditional Power System Reliability Modeling

The primary objective for the first year of the study was to link linear (DC) power flow model to uncertainty tools developed in other programs at SNL.

#### 4.1.1 Background

So that the reader can have some understanding of nature of the work discussed, we present some background information on grid reliability and power flow models.

##### 4.1.1.1 Grid Reliability

Typically, reliability is modeled in a probabilistic manner and is measured by indices such as probability of failure, frequency and duration, etc. In general, reliability analysis of a bulk power system is very similar to a classical reliability analysis of any complex system and involves the following steps:

1. *Define system state.* The steady-state conditions of a power system can be characterized by the status of components (lines, generators, transformers, etc.), and load and generation patterns. The state changes continually because of random outages of equipment and variation in load and generation. If dynamics and stability are to be considered, then the notion of state must be supplemented with that of exogenous disturbances.
2. *Define a probability model for system state.* Equipment is usually characterized by discrete failure models, and load and generation by a continuous distribution.
3. *Define acceptable operation and measures of acceptable operation.* Acceptable operation means that load can be supplied at proper voltage and without overloading components. Unacceptable operation means some portion of the load must be disconnected. This can occur due to insufficient capacity to maintain power balance or due to unstable dynamics.

4. *Define the structure function or test function that maps the system states into acceptable/unacceptable regions.* Typically the structure function decomposes the state space into sets of acceptable ( $\phi(x) > \text{load}$ ) and unacceptable ( $\phi(x) < \text{load}$ ) states, where  $\phi(x)$  = maximum amount of load that can be served in state  $x$  to satisfy constraints.

Once  $\phi(x)$  is known, an appropriate reliability measure can be defined. For example, for a given load level  $L$ , the Loss of Load Probability (LOLP) is defined as  $\text{LOLP} = \text{Prob}(\phi(x) < L)$ .

An analytical description of  $\phi(x)$  greatly helps in this computation. Alternatively, one can enumerate  $\phi(x)$  for desired values of  $x$ , or attempt to approximate  $\phi(x)$  over a desired region, or attempt to develop estimates of indices from estimated properties of  $\phi(x)$ .

5. *In enumeration-based methods, decompose the set of system states based on acceptability.* Due to the much larger state space and complexity of comprehensive models, approximations are made; typically, only steady-state or “adequacy” models are used. Nonetheless, the decomposition of system states into acceptable and unacceptable remains a computationally intensive problem.
6. *Compute indices based upon above decomposition.* Typical reliability indices include loss of load probability, frequency and duration of loss of load, expected unserved energy, etc. These indices are computed on a system basis or for a single load point.

#### **4.1.1.2 Power-flow Model**

Electric power systems are intended to supply customer load with voltages within a specific range, and without overloading components such as transmission lines. A power system fails (commonly referred to as a “blackout” or a “brownout”) when, in response to disturbances such as transmission line outages, a transition cannot be made from one acceptable steady state to another.

Appendix A provides a brief review of the models that describe electric power systems, and Appendix B presents the detailed report on “Power System Reliability Analysis” done for this work by New Mexico State University. In a normal or acceptable state, power balance is guaranteed at all points in the system. Power is generated primarily by rotating machines and is consumed to a large extent by rotating loads. Power balance implies that these machines operate at essentially constant speed as evidenced by an essentially constant frequency while maintaining the stepped energy potentials (voltages) throughout the system. Similarly, loads that regulate their energy consumption (e.g., thermostatic loads) achieve a steady pattern of operation. Any departure from power or energy balance initiates a dynamic response from the generators, loads, and other regulated equipment in an effort to establish a new steady state. A new steady state may be established with power balanced but with unacceptable conditions. On the other hand, the dynamics of the system may be such that the system cannot transition to a new steady state even if one exists. This is referred to as instability.

A failure sequence may take several forms, including the following:

- A disturbance drives the system into a state wherein a steady-state power balance exists, but voltages or loadings are out of limits. Further, the condition cannot be corrected due to time constraints or lack of resources. In this instance, typically, some of the load is disconnected. This is often called “loss of load.”
- A disturbance creates a condition in which changes in power or voltage are so severe that protective apparatus initiates the dropping of load and perhaps separation of the system into islands.
- A disturbance creates a condition in which a steady-state power balance cannot be achieved at all.
- A disturbance creates a condition in which system dynamics/control is unstable. For analytical purposes, such instability is classified as follows:
  - *Transient or angle stability*: the electromechanical dynamics are such that the generators cannot be returned to a common operating speed. The time range of this phenomenon is 1 to 3 seconds.
  - *Long-term stability*: the control systems are underdamped or undamped, resulting in oscillatory behavior over a long period of time (minutes) and actuation of protective systems.
  - *Voltage stability*: involves system response in terms of regulating system voltage and is a function of the ability of the generators to maintain voltage (provide reactive power), the response of loads such as motors to low voltage conditions, and the response of thermostatic load, which may attempt to continue to draw the required energy by cycling more frequently, for example. The result may be a very rapid uncontrolled decline in voltage (voltage collapse) or a very slow decay (period of hours).

In the event of a failure, the above phenomena may occur simultaneously, but depending on the system state, one form may be dominant.

*The general definition of acceptability is that disturbances do not result in loss of load.* Indeed, reliability councils have adopted a deterministic concept of operational reliability as one in which anticipated disturbances do not cause an “uncontrolled loss of load.” The terms “adequacy” and “security” have been standardized in literature to describe power system reliability.

- *Adequacy* refers to the ability of a system to supply load in the steady state. Dynamics of transition are ignored.
- *Security* refers to the ability to return to a steady state, i.e., the stability of state transitions is presumed.

(The consensus on these definitions is less than complete. We have paraphrased based on what appears in the literature. A more common use of the term “security” is in an operational context with reference to a specific state.)

The reason for this distinction is that the study of system dynamics is extremely computationally intensive. Further, the random events that initiate a change of state involve fundamental phenomena, such as lightning-induced short circuits, which are not easily modeled. Adequacy analysis, on the other hand, involves more manageable models. A bulk power system is typically modeled by static, nonlinear models, while random events are more macroscopic, such as the outage of a transmission line. Adequacy analysis provides an upper bound on reliability measures.

Given the computational burden of reliability analysis, approximate models are often used even for adequacy analysis. In terms of the conceptual models given in Appendix A, the following approximations are often used:

- Generation adequacy studies, which ignore the transmission system.
- Transportation-model-based bulk-system studies, which ignore Ohm’s law and merely look at power transfer along capacitated arcs (transmission lines).
- DC load-flow studies, which are a linear approximations to circuit equations and model the nature of real power (watts) flow through the network.
- Static power-flow studies, or AC power-flow studies, which calculate the *operating voltages*, *line power flow*, etc., for a given condition and determine whether these quantities are acceptable.
- Extended static power-flow studies, which include sensitivity analysis, optimization, and operating margin studies.
- Short-term dynamics studies such as transient stability studies, which determine if a proposed disturbance leads to instability. Both time-domain simulations and direct methods are used.
- Long-term dynamic studies such as mid- and long-term stability and voltage collapse.

Most reliability studies are focused on generation systems and bulk system adequacy studies using DC or AC power-flow models. As such, they are not used to direct system planning but as checks on candidate plans. Alternatively, power system expansion planning involves exhaustive studies of a limited number of scenarios with detailed dynamic analyses.

## **4.1.2 Accomplishments**

As noted above, the major accomplishment of the first year was the linking of a linear power flow models to the uncertainty tools. In addition, preliminary work was done in examining potential distributed energy resources that could locally mitigate power grid unreliability.

### **4.1.2.1 Power Flow Modeling**

The first effort was the development of a new approach to the analysis of power flows. Dealing with such analyses at a national level required the development of a new approach to network modeling. The commercially available transmission and DC load flow models can be used to characterize large areas but lack the accuracy to address voltage stability issues. At the same time, however, the necessary AC flow models in general use are too computationally cumbersome for even moderate size power grids. Our preliminary research in this area developed a hierarchical modeling scheme with model fidelity increasing as the network sensitivity increased.

A second area of study needed in order to link power flow and uncertainty models involved the probabilistic characterization of network stability. To address stability issues, a probabilistic load flow methodology was developed. It is supported by the reliability analysis software tools (Cassandra [7]) that had been developed in support of the nuclear weapon stockpile Enhanced Surveillance Program. A prefatory integration of the Cassandra software and the load flow model was then applied to the Modified IEEE Reliability Test System and the results were encouraging. This is discussed at some length in Appendix B.

### **4.1.2.2 Battery Study**

In addition to addressing the adequacy and stability issues associated with power grid reliability, preliminary investigations were undertaken to characterize and model advanced energy generation technologies to determine their suitability for potentially mitigating network reliability problems. Renewable generation, storage, and high speed power electronics and switches were (and are) candidates for solving many of the problems identified above. In this context, we decided to explore, in more detail, rechargeable batteries as they act as the energy storage medium in a photovoltaic system. During this time frame, the groundwork was set to develop software that would analyze the behavior of the batteries. The major areas that were investigated were the solar resource component and the rechargeable battery component. Literature reviews were conducted in order to identify the type of solar data that was readily available and the best way of representing all of that data for this work.

Furthermore, we began the characterization of the probabilistic behavior of rechargeable batteries, specifically such batteries that are recharged from a renewable source that provides power in random increments. We narrowed our focus by concentrating on the damage that can accumulate in rechargeable lead-acid batteries when they are subjected to deep discharge use cycles that last for significant periods of time. In particular it is known that when rechargeable lead-acid batteries remain at a low state of charge, the maximum potential capacity can be

diminished. The maximum potential capacity is defined as the maximum amount of energy that a battery can store at a particular time. This value will not always be equal to the initial capacity of the battery since damage introduced by long duration discharges will tend to degrade the maximum potential capacity of the battery. The degradation will eventually lead to battery failure. Hence, we developed a framework to model battery state of charge and maximum potential battery capacity as functions of time. We introduced the damage effect that occurs during discharge via a non-positive function of duration of discharge and depth of discharge. Because the form of this function is unknown, we modeled it with an artificial neural network whose parameters are trained with experimental data.

These efforts resulted in a comprehensive stochastic-based model for the analysis of a renewable power supply/energy storage/load system. For a more detailed discussion of this work, see Appendix C.

## **4.2 Second Year—Optimization and Uncertainty**

The primary objectives for the second year of the study were to expand the power flow tools to address non-linear (AC) power; to incorporate new methods into the uncertainty models; and to then re-link the updated power flow and uncertainty models.

### **4.2.1 Background**

Research has shown that current commercial codes are excellent for analyzing the adequacy of moderate size networks. Under restructuring, however, it is likely that network stability will become a more critical issue due to lower reserve margins, fewer generators on hot reserve, smaller maintenance crews, etc. For example, unless the costs of having adequate reserves are somehow incorporated into the market pricing schemes, having ready reserves will be a cost to that particular supplier, a cost not borne by other suppliers, and without an immediate benefit to that supplier, thus making his power more expensive and therefore less competitive. Hence, providing for network stability is not in the market interest of an individual supplier by himself. We believe the future computational environment then is one in which stability issues will become more important. In addition, under restructuring, we have been witnessing consolidation of suppliers, similar to what happened in the deregulated airline industry. As suppliers have generators over a wider geographic area and as grid operators cooperate more, the size of the problem needing to be analyzed will grow substantially. So not only will stability become more of an issue but the magnitude of the grid needing a stability analysis will also be larger.

And for the grid analysis industry as it now exists, this is bad news. Computationally intensive AC flow models are required to characterize stability completely, and only small networks can be analyzed using these models. Stability analysis is not an integral part of bulk power reliability analyses, and it is deterministic and distinct from adequacy analysis. What is generally done in industry today will not be able to answer the questions posed by the evolving grid.

The reason then that we expanded our work to examine probabilistically non-linear problems was to be able to address stability issues. We developed a new hierarchical scheme for network analysis. To better integrate stability analysis into traditional network reliability analysis, we utilized the Cassandra uncertainty analysis software to probabilistically characterize network power flow.

(In the third year of the work, we addressed the issue of problem size when we ported the problem over to the massively parallel processes, see below.)

When voltage collapse occurs, more complex stability problems often ensue; voltage collapse can be a precursor to worse problems. The collapse can be modeled based on simple transportation flow models over large areas interfaced with DC flow models over moderate areas, with increasing detail using AC flow models in those areas where the network is sensitive to voltage collapse. Additional detail (AC flow model) can also be used in those areas where specific information is of interest—perhaps to characterize the likelihood of loss of off-site power at nuclear power plants.

## **4.2.2 Optimization Module**

### **4.2.2.1 SGOPT Software**

Including stability analysis in our power flow models required access to optimization algorithms.

An examination of alternatives for optimization algorithms resulted in the selection of the SGOPT libraries from DAKOTA, and the SNL optimization package. SGOPT was selected over NMSU algorithms that would be faster and easier to implement; unfortunately, they were limited in application. SGOPT also can perform optimization in the presence of uncertainty. While the SGOPT libraries require no additional cost and leverage existing and future optimization efforts, their use required extra effort in coordinating research efforts.

The physical model consists of a power-flow code that models the power system, combined with the SGOPT optimizer. The optimizer essentially models operating policy while the power-flow program models the physical system. The optimizer uses the power-flow engine to determine how the system should be controlled and how load would be shed to minimize costs or minimize load shedding. If there is no load shedding then the proposed state can supply load successfully. Otherwise, it is a failed state.

SGOPT generates minimizing directions by iterating over control variable values. In cases where the given load level cannot be supplied in a given system state, SGOPT drives the objective to a minimum (i.e., feasible with respect to violations) by shedding load. Note that in instances where the power flow diverges, cost is set to a very high number.

The power-flow program supplies the following information to SGOPT:

- Number of control variables.
- Control variable maximums.
- Control variable minimums.
- Initial values.
- Gradient of cost with respect to control variables.
- Initial cost.

#### **4.2.2.2 Models Using Optimization Software**

Models for the renewable energy elements in the power grid have been developed. Specifically, a framework for the probabilistic analysis of a photovoltaic power supply/storage/load system has been developed and a reliability analysis performed based on the maximum potential capacity of the batteries (see Appendix C for the final report for this project). Artificial neural networks, both deterministic and stochastic, were used to simulate the various components. This framework can be used to optimize the operational parameters, increase the reliability, or minimize the cost of the system. Consideration for these types of elements has been addressed during the development of the power-flow models. The models have been developed and tested as Matlab models, and they were translated into C/C++ routines. They were then incorporated into the power-flow model at the same time as the optimization library.

#### **4.2.3 Power-flow Software**

Initially, in this work, an existing power-flow analysis program was extended to provide a Failure Modes and Effects Analysis (FMEA) capability (see Appendix B). The program implements the FMEA methodology as summarized below.

- The program can model steady state power-flow conditions in large systems with the AC, DC, or mixed power-flow approaches.
- The program currently analyzes single contingencies (outage of one element), double contingencies, and user-specified higher-order contingencies.
- For a specified system load level, the program first solves the “base-case” power-flow state, i.e., the case with all components intact. Contractual sales between areas and generator limits are modeled. Given this solution, the program evaluates the steady state response to each contingency. If a contingency results in a violation of voltage requirements or loading capability of one or more elements, the program determines the amount of load to be shed at each node. Otherwise, the contingency state is considered as being acceptable.

- Once states are classified, the program can be used to calculate standard probabilistic indices such as Loss of Load Probability, Expected Demand Not Served, and the Distribution of Load Shed. These indices can be calculated at the system or node level.

The most difficult aspect of bulk power system reliability analysis is the evaluation of the structure function  $\phi(x)$  [4]. The state  $x$  is defined in terms of discrete variables (component status) as well as continuous variables (load). Thus, it is difficult to describe  $\phi(x)$  by analytical models or approximations. In most cases, one must calculate  $\phi(x)$  for a given value for  $x$ . Suppose again that

$$\phi(x) = \text{Maximum load that can be supplied in state } x \text{ in the steady state}$$

In this adequacy evaluation, the system is described by the power-flow equations (Appendix A)

$$F(V, C, N, D) = 0$$

The state  $x$  corresponds to the vector of component statuses in  $N$  and the load  $D$ . The nonlinear power-flow equation above must be solved to determine  $\phi(x)$ , the amount of load that can be supplied while meeting constraints.

Approximations are often used for computational simplicity. As outlined in Appendix A, transportation models and DCDC load-flow models are linear approximations to the power-flow equations. The transportation model is a severe approximation but provides two major advantages. First, the model is coherent in the reliability sense. The addition of components cannot make the system fail. Second, the maximum flow theorem directly yields minimal representation for the structure function. The DCDC load-flow models are more realistic. Since the model is linear, extremely efficient analytical methods can be developed. With the complete AC power-flow model above, iterative techniques are required within each evaluation. Some of the approaches are outlined below.

### *Approach 1*

1. First solve the power-flow equations

$$F(V, C+C_0, N, D) = 0,$$

$C_0$  represents the initial control settings and  $C$  represents changes to control settings required by the transition to state  $x$ . From the power-flow solution, determine if voltage limits or line ratings are violated.

2. Determine a combination of control setting and load shedding that will remove constraint violations. This can be done by solving an optimization problem, e.g.,

$$\text{Min } z_1(D_s) + z_2(V, C)$$

$$F(V, C+C_0, N, D-D_s) = 0 \quad C \in C^*, V \in V, D_s \in S$$

where  $D_s$  represents the vector of load shed at a bus.

The optimization problem is usually formulated as a linear problem. The objective function  $z_1$  attempts to model load shedding policies while  $z_2$  models violations and control cost.

This approach is relatively easy to program. However, a major limitation is that it does not model pre-contingency operating strategies adequately. In general, power system operators utilize analysis software and select operating points such that a single contingency will not cause failure. On the other hand, when multiple contingencies occur, a portion of load may be shed so that additional contingencies will not cause uncontrolled loss of load.

### *Approach 2*

The security constrained optimal power flow is a general model designed for use in real-time operation. The optimization-based model solves for control settings that minimize cost, while ensuring relevant contingencies do not cause failure.

The conceptual form is given below.

$$\text{Min } z_1(c) + z_2(v)$$

$$F(V_i, C_i, N_i, D) = 0 \quad C_i \in C^*, V_i \in V, \quad i = 0, 1, 2, \dots, n$$

Where  $N_0$  represents the normal state with intact components, and  $N_1, N_2, \dots$  are contingency states for a given load  $D$ . The function  $z_1()$  models operating cost, while  $z_2()$  models constraints. This type of formulation can be adapted for contingency and structure function evaluation.

### *Approach 3*

The essentially “brute-force” approaches described above are computationally intensive. The computational burden becomes overwhelming when these techniques must be applied to each possible state. Thus, it is important to consider whether techniques can be developed to approximate  $\phi(x)$  in some other way.

Admittedly, the development of the approximation still requires computations of the type described in approach 1 or 2. (In principle, a Monte Carlo simulation falls into this category in that the goal is to estimate parameters of a probability distribution of  $\phi(x)$ ). Several ideas that appear in the literature are listed below:

#### 1. Feasible spaces

In the conceptual formulation, we defined the state  $x$  to be composed of the component status  $N$  and load  $D$ . For a given  $N$ , one can define the subset  $D_f$  of feasible load  $D$  as follows:

$$D_f = \{ D : F(V, C, N, D) = 0, V \in V \}$$

Thus, for a given network configuration  $D_f$  represent loadings that do not cause voltage or loading violations. Reference [5] reviews several techniques, including a pattern recognition based approach, to approximating  $D_f$ . The use of such approximations can help reduce the computational burden.

## 2. Neural network based approximations

Neural networks can approximate any continuous function to some desired accuracy. Additionally, they have the ability to generalize from exemplars. Thus one could treat both  $N$  and  $D$  as continuous variables and build approximations to  $\varphi(x)$ . The obvious disadvantage of neural networks in relationship to the power system reliability problem is again the high dimensionality of the state space. As indicated earlier, no matter which approximation approach one chooses, the approach to developing the approximation will not be purely analytical. Assume then that the approximation will be developed by some sort of state sampling followed by a solution to the power-flow equations.

Perhaps the most important benefit of approximating techniques lies in the fact that it should not be necessary to model detailed operating policy (as in Approaches 1 or 2). For example, suppose a neural approximation is used to model load shedding at a node for different available generation capacities at several other nodes. Given (or, perhaps, assuming) that the neural network does develop an ability to generalize, it does not need to be trained with generation patterns corresponding to actual economic dispatch. In other words, it is necessary to solve the power-flow equations only in the training phase. The network should provide a good approximation to load shed when the input pattern corresponds to a practical generation pattern.

### 4.2.4 Uncertainty Module

To incorporate uncertainty into this effort, we did not “re-invent the wheel.” We used already existing uncertainty models, modified to link with the other models developed in this program. This section briefly describes those uncertainty models, beginning with how they arose.

SNL has been moving toward an increased dependence on model- or physics-based analyses as a means to assess the impact of long-term storage of the nuclear weapons stockpile (for example, see the discussion in Reference [6]). These deterministic models have also been used to evaluate replacements for aging systems, often involving commercial off-the-shelf (COTS) components. In addition, the models have been used to assess the performance of replacement components manufactured via unique, small-lot production runs. In any of these situations, the limited amount of available test data dictates that the only logical course of action to characterize the reliability of these components is to consider specifically the uncertainties in material properties, operating environments, etc., within the physics-based (deterministic) model. This not only provides the ability to characterize the expected performance of the component or system statistically, but also provides direction regarding the benefits of additional testing on specific components within the system. Therefore, an effort was initiated to evaluate the capabilities of existing probabilistic methods and, if required, to develop new analysis methods to support the inclusion of uncertainty in the classical design tools used by analysts and design engineers at

SNL. The primary result of this effort is the CRAX (Cassandra Exoskeleton) reliability and uncertainty analysis software. Only a very brief introduction and review of the CRAX/Cassandra uncertainty module will be presented here. For a more thorough discussion, see for example Reference [7].

#### 4.2.4.1 CRAX/Cassandra Software Elements

CRAX has three major elements: (1) the uncertainty analysis engine, i.e., Cassandra; (2) the user interface, also called CRAX; and (3) the physical model. CRAX is the interface to the users. It uses Tool Command Language/Tool Kit (Tcl/tk) scripting language to create windows and buttons the user interacts with to input data and view results. It uses embedded C++ commands to access the C++ code, which the code used to write the analysis methods. Cassandra is the heart of the code containing all the analysis methods (all are written in C++). The g-function is the problem being analyzed. It can be a C++ routine that can be compiled and then linked with the Cassandra code, or a program or group of programs that can be accessed by using a g-function stub written in C++ that makes a system call to execute the g-function program(s) and communicates input and output through file input/output. The g-function stub is linked to the Cassandra code.

The relationship between these three elements is depicted in Figure 4-1.

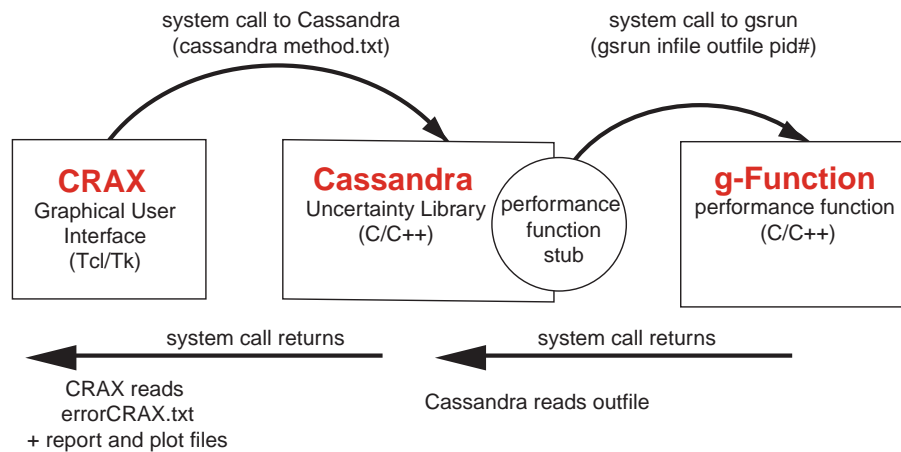


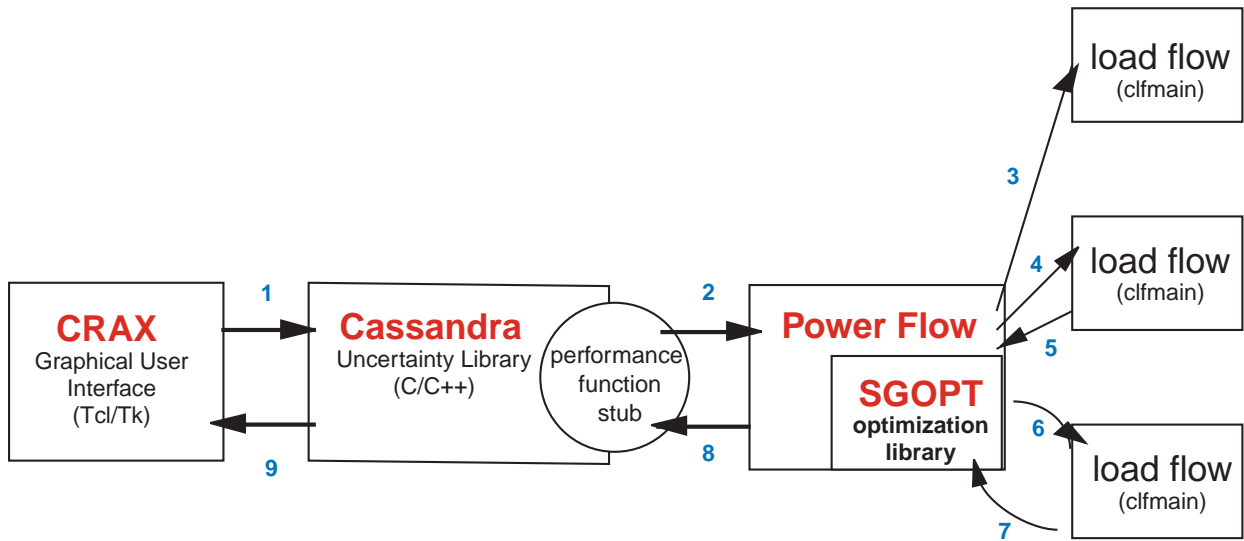
**Figure 4-1 General Uncertainty Module Information Flow**

The heart of the CRAX software is the Cassandra uncertainty analysis engine. This engine consists of a number of software routines that permit the user to select a variety of methods for including uncertainty in their analyses. A number of first- and second-order techniques, maximum likelihood and a variety of other analytical methods are available for application. In addition, the uncertainty analysis engine includes options for using a number of pseudo- and quasi-Monte Carlo methods. Specific methods are constantly being updated and improved, and a recent patent application has been submitted for one of the unique algorithms within the library. Cassandra is written completely in C/C++, making the engine very portable.

CRAX/Cassandra has been used with Win95, WinNT, Power Macintosh, Sun, Silicon Graphics and DEC operating systems. In addition, the software has been ported to one of the large teraflop computers at SNL.

Access to the Cassandra uncertainty analysis engine is gained via the CRAX interface. The CRAX graphical user interface (GUI) is based entirely on the Tcl and associated Tk. The use of Tcl and Tk permits the software to be hosted on any platform and provides a great deal of flexibility in accessing the Cassandra uncertainty engine. Rather than trying to develop a complicated GUI for the user that could handle any situation, the use of Tcl/Tk permits the very quick construction of unique interfaces specific to the problem being analyzed. (A basic/generic interface is available for simple analyses.)

The last element in the CRAX family is the physical model. It was decided early in the development of CRAX to not include any physical modeling tools directly in the software. Rather than develop a modeling tool (e.g., a finite element or thermal analysis package) unique to CRAX, it was decided to let the engineers rely on the existing tools that they were comfortable with and had confidence in. While not the ideal situation in terms of analysis speed, it was felt that for the engineers to become comfortable with incorporating uncertainty into their deterministic models, it was critical to not stretch their belief systems too far. The CRAX GUI effectively “wraps Cassandra around” the existing analysis software, hence the reference to CRAX as an exoskeleton. Figure 4-2 is a block diagram that depicts the relationship among the different model elements of this effort. The load-flow models are the physical models being analyzed, and the power flow model is the analytic engine.



Note: only one load flow program is running at any one time

Figure 4-2 Relationships among CRAX, Cassandra, SGOPT and the Analytical Engine and Physical Models

#### **4.2.4.2 Cassandra Capabilities**

The key to the Cassandra uncertainty library development is the recognition that no single uncertainty analysis method is applicable to every analysis problem. The Cassandra library is a very extensive suite of methods for including uncertainty in complex analysis problems. Analytical techniques include a number of variations of first-order and second-order reliability methods (e.g., Advanced Mean Value). In addition, a wide range of Monte Carlo sampling methods is available for application, e.g., Latin Hypercube Sampling (LHS), Halton (skipped), and Sobol methods. A new method developed at SNL, referred to as the Field Analysis Method, is also available for application.

The data for Cassandra are input via the graphical user interface, CRAX. Existing analyses can be loaded from a text file, and subsequent analyses can be saved as an input file or in a variety of special formats for input to other analysis programs. The plots can be saved as a postscript file for later inclusion in reports. Common Data Form (CDF) files can be saved for later processing in a system-level analysis program. In addition to color-scheme information, the network locations [Internet Protocol (IP) addresses] of the computers performing the uncertainty analysis and the performance analysis can be input interactively and changed “on the fly.”

#### **4.2.5 Battery Study**

The comprehensive stochastic-based model for the analysis of a renewable power supply/energy storage/load system that was developed previously in the work was improved in FY99. Several mathematical techniques, including stochastic, deterministic, and artificial neural network models, were used to develop this simulation capability. These models were combined and solved simultaneously in the Monte Carlo framework to generate realizations of the system behavior.

A kernel density estimation (KDE) approach was incorporated into the solar resource prediction model, and a daily radiation analysis was also implemented for improved efficiency and robustness. This resulted in reduced computational time and increased stability. Groundwork for an improved energy-storage device damage model was laid in several areas. We completed a literature search on applications of electrochemical impedance spectroscopy (EIS) to lead-acid batteries as a diagnostic technique. We also finalized a test plan for the collection of impedance data and cycle testing of GNB 12-5000X photovoltaic reserve batteries in order to gather more experimental battery damage data. Furthermore, we modeled the battery damage surface using the multivariate polynomial spline ANN. This approach provided better accuracy and capability to handle very nonlinear behavior. In addition, we performed a preliminary reliability analysis on the PV/battery system. Finally, we successfully translated the code for the renewable generator model from MATLAB<sup>®</sup> to C<sup>++</sup>. This reduced processing time and enhanced portability of the code for use with other software, and it was a major step as it would allow the integration of our software into the power flow model. These efforts are discussed in more detail in Appendix C.

## 4.2.6 Accomplishments

In the second year, we made great strides in the two areas under investigation: the power flow modeling and the battery study.

### 4.2.6.1 Power Flow Modeling

During the second year, a contingency based reliability analysis capability was developed and preliminary analyses were performed on the IEEE Reliability Test System (RTS) and a model of the Arizona-New Mexico-Texas region within the WSCC (Western Systems Coordinating Council). This program provided the hierarchical capability to model networks involving both AC (accounting for both active and reactive power flow) and DC (an approximation involving only real or active power flow). Two significant literature reviews were also finished. The first emphasized the probabilistic characterization of power flow in a bulk power system, while the second concentrated on recent efforts to combine dynamic bifurcation (a branch of chaos theory) and probability theory to characterize voltage instability. An analysis method that permits the combination of these two techniques has been identified that will permit the static reliability model being developed to be used to statistically characterize dynamic voltage stability.

Developing this contingency based capability required that the model also be able to optimally distribute the available power resources. This analysis capability, planned to be added during the second year of the study, was necessary before static characterization of voltage stability could be fully accomplished. A library from the SNL DAKOTA optimization package was used [3]. An interface was developed between the Cassandra library and a hierarchical power analysis program; however, a great deal of effort was needed to make the analysis tool user-friendly. In addition, the Cassandra software was developed initially to characterize the reliability impact of aging stockpile components, and some minor modifications were required to integrate it fully with the power-flow program.

As to the test problem comparison, the IEEE RTS is a standard test system utilized in reliability studies. The second example used a 400-node model of the Arizona–New Mexico–Texas. These results are also presented in detail in Appendix B.

Two important observations from these comparison studies are:

1. The results from the IEEE RTS were compared with results published by others. Although all results are in the same order of magnitude, they are actually quite different. There are two reasons for the discrepancies. First, implementations differ in terms of how they model operational and load shedding policies. Second, the statistical techniques also differ. *Suffice it to say that a uniform approach to power system reliability analysis does not exist at this time.*

2. The studies showed that uncertainty analysis can identify critical nodes in terms of vulnerability.

#### **4.2.6.2 Battery Study**

In the second year, the behavior of rechargeable batteries was modeled and analyzed using statistical and neural network methods to simulate the behavior of various components of the power system (see Appendix C). Final integration of the model with the new power-flow program would occur in the final year of the program.

The stochastic-based model that was developed in the first year of the study was improved in the second year. Several mathematical techniques, including stochastic, deterministic, and artificial neural network models, were used to develop this simulation capability. These models were combined and solved simultaneously in the Monte Carlo framework to generate realizations of the system behavior.

Specific achievements include

1. Improving the accuracy and computation efficiency of the Markov transition matrices.
2. Enhancing the efficiency and robustness of the solar resource prediction model.
3. Making the theoretical battery damage surface more realistic.
4. Acquiring literature data on lead-acid battery impedance diagnostic and upgrade equipment necessary to perform these measurements on a PV-size battery.
5. Improving the training algorithm and accuracy of the multivariate polynomial spline.
6. Performing initial reliability studies of the rechargeable battery component.
7. Translating the MATLAB<sup>®</sup> analysis code into C<sup>++</sup> language.

### **4.3 Third Year—Massively Parallel Implementation**

The primary objectives for the third year of the study were to port all the developed tools to several different massively parallel processors, demonstrate the operability of all of the tools on these computers, and to then link the power flow and uncertainty models with the developed battery storage models.

### **4.3.1 Background**

This section provides a brief introduction to how the massively parallel computers at SNL were applied to this problem. For a more detailed discussion about massively parallel computation, both its philosophy and approach at SNL, see Appendix D.

#### **4.3.1.1 Application of the High-performance Computing Initiative**

Current bulk power adequacy analysis methods require a compromise between the size of the network to be analyzed and the computational burden of the analysis method. The three approaches used in these analysis methods were linear load flow for a large network, DC load flow for a moderate network, and AC load flow for a small network. In the current climate of utility restructuring, analysis of larger networks is required due to increased area-to-area interactions. As discussed above, the anticipated problems under restructuring will require more detailed flow models. As a minimum, DC has to be added to AC models. One question that needed to be answered was, is there additional benefit in accuracy and in network size to be gained by hosting an existing commercial adequacy analysis software package on a teraflops computer?

The approach to applying high-performance computer initiative capabilities to bulk power systems was to

- Analyze adequacy of a large bulk power network using a PC-based software tool (linear power-flow analysis of WSCC).
- Host the PC-based software tool on a teraflops computer and perform the same analysis (linear power-flow analysis of WSCC).
- Incorporate a more detailed power-flow model into the teraflops-based software and analyze a large network (DC power-flow analysis of WSCC).

#### **4.3.1.2 Sandia National Laboratories' Teraflops Computers**

- Janus

Janus, also known as the Teraflops, is a multiple instruction multiple data (MIMD<sup>1</sup>) massively parallel system that consists of 4663 nodes. Each node consists of two Pentium Pro processors, for a total of 9326 processors. The nodes are used for specific purposes, such as computation, service, I/O, communication, hot standby, and so on. Because Janus is a distributed memory system, every node has its own memory.

Janus uses a minimalized version of a kernel called Cougar that is run on the 4576 compute nodes of the Teraflops, while the Teraflops Operating System (T O/S) operates the service nodes.

---

<sup>1</sup> An MIMD system is capable of both addressing multiple-data streams and executing multiple-instruction streams.

This approach was incorporated in order to minimize the amount of memory required by the operating system. Consequently, executables can run only on the compute nodes, while the service nodes are technically used to compile the code. The key idea is that the compute nodes focus on number crunching, while the rest of the nodes perform all other tasks.

Janus can run interactively or in batch mode.

For a well-tuned parallel system, parallel computing speed, with availability, bandwidth, and other issues aside, is

$$\text{computational speed} \approx n \cdot \log(n)$$

where  $n$  = number of processors.

Figure 4-3 illustrates the speed-up of a 2D PDE solver on four parallel computers.

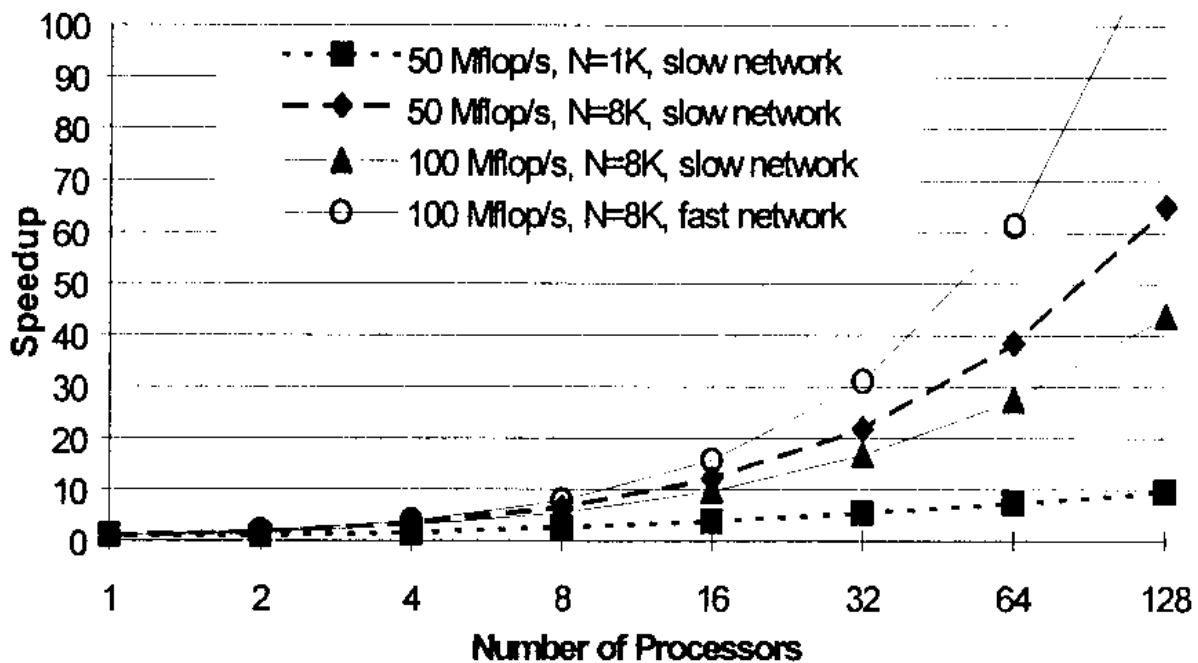


Figure 4-3 Effect of Parallel Processing on Computational Speed

- Cplant

Cplant nodes currently are single processor (433 MHz or 500 MHz) Compaq Alpha machines with about 256 MB of memory. Each has a network connection to a *Myrinet* network, on which application message traffic is carried. The nodes are diskless. All I/O is redirected to one or more I/O servers via message passing or NFS. See Figure 4-4 for Cplant node distribution.

Like Janus, the Cplant consists of server nodes (Juneau) and compute nodes (Alaska). Juneau is used to compile code, and Alaska is used to launch the executables.

Cplant is a MIMD<sup>1</sup> style machine running message-passing applications. An MPI<sup>1</sup> library (MPICH, version 1.2.0) is provided, or applications may use Cplant portals (the software layer below MPI) directly. C, C++, Fortran 77, and Fortran 90 compilers are available. Cplant scripts use native compilers to compile code and link it using special Cplant libraries and portions of the native libraries.

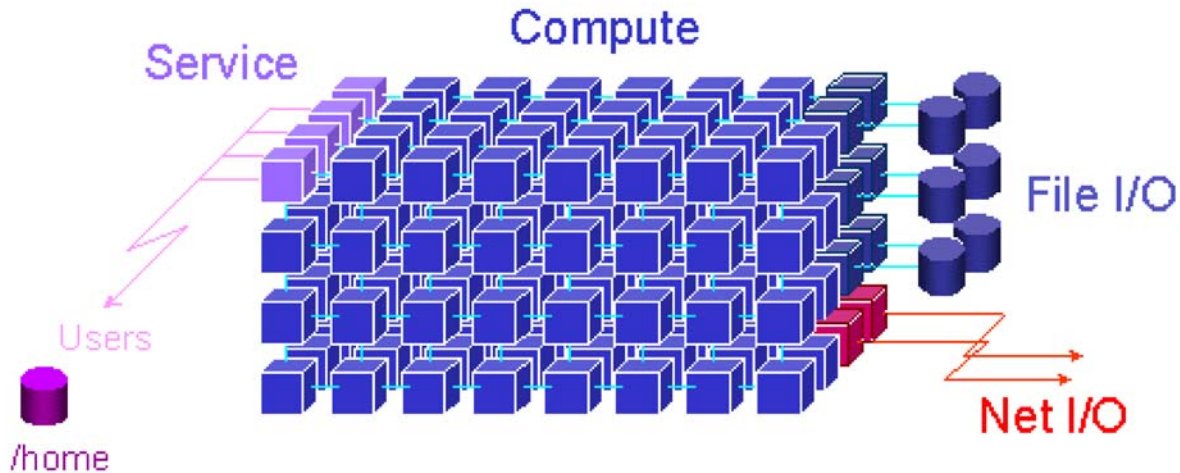


Figure 4-4 Cplant Node Distribution

### 4.3.2 Work Performed

In this section, we present the work that was performed in the areas of power flow and battery storage modeling and the linking of the two.

#### 4.3.2.1 Efforts in the Power Flow Modeling

In the last year of the project, we had three additional goals for the power flow modeling portion of the effort. They were

- to expand the size of the bulk power systems that could be analyzed,

---

<sup>1</sup> MPI (Message Passing Interface). MPI is a popular set of subroutines that transfer data among the parallel processors.

- to build a user interface,
- and to host the software on the massively parallel Teraflops computer at SNL.

Each of these in turn was met.

The size of the networks that could be modeled increased dramatically the last year, and the types of uncertainty analyses were expanded to include new simulation methods being developed at SNL. The software was hosted on a number of massively parallel machines at SNL to explore the unique interface and operational requirements of each platform

Appendix D presents the details concerning the porting of the CRAX/Cassandra software to the DEC 8400 network. (The DEC 8400 network is one of the massively parallel computer processing environments at Sandia.) For incorporating the CRAX/Cassandra software suite, unique modifications were required to allow successful interfacing. Two distinct efforts were involved with getting the CRAX/Cassandra analysis code to execute in a parallel-processing environment:

- Adding MPI coding to the LHS code to cause the *root* CPU to load each other CPU with a different set of input parameters in their own memory space and then to run the *g*-function on every CPU except *root*. *Root* then inquired each other CPU as to the results. *Root* then stores the results in an array and then continues performing all output file generation. (MPI is the communication protocol interface for running on a multiparallel machine, see Appendix D.)
- Changing the communication interface between the three parts of the CRAX/Cassandra analysis code to work in the multiprocessing parallel machine environment.

The DEC 8400 was chosen for the initial implementation primarily due to its accessibility.

#### 4.3.2.2 Efforts in Battery Storage Modeling

Previously in the project, we had used a bivariate Markov process to simulate the direct normal and diffuse horizontal solar radiation data. This technique yields accurate realizations of the random process but it is very CPU intensive. In light of this, we sought out and implemented a faster method that was as accurate as, or more accurate than the original current technique. That new method was canonical variate analysis (CVA) approach to modeling the daily direct normal and diffuse horizontal radiation components. (This is discussed in more detail in Appendix C.)

In addition, we incorporated the PV generator code into the power flow model with the help of a commercially available translator that takes MATLAB<sup>®</sup> code and converts it into C<sup>++</sup> code. As discussed in Appendix C, the converted code was then integrated into the main power flow program and a sample calculation was performed.

Additionally, electrochemical impedance spectroscopy (EIS) measurements were performed on two different lead-acid batteries to evaluate the use of this technique for determining the capacity degradation. The results are documented in detail in Appendix C.

### **4.3.3 Accomplishments**

In the third and final year of the effort, we completed the final development and application of the uncertainty analysis tools to power system applications. This work combined SNL's CRAX/CASSANDRA uncertainty analysis tools, SNL's SGOPT optimization tools, and a power-flow analysis program to create a package for reliability analysis for large power systems. In addition, we successfully linked a battery storage module to this software suite. The complete package, which had been previously tested on a small system, was ported to SNL supercomputers. Databases for standard test systems such as the IEEE RTS and actual systems such as the Arizona-New Mexico system were created for testing.

This work resulted in fundamental advancements in concepts and computational techniques as applied to uncertainty analysis in power systems. We believe that the resulting package is a major contribution towards a capability for conducting uncertainty, reliability and vulnerability studies for large power grids.

See Appendix B for a sample application of the uncertainty analysis package, and Appendix D for a description of the algorithm and process used for analysis.

## 5. Program Results

In this last section, we summarize the accomplishments we achieved during this effort. In addition, during the work, as usually happens when breaking new ground, we discovered additional areas that bear research and development. We shall thus conclude this report with recommendations for that additional work.

### 5.1 Accomplishments

Our accomplishments are many. Before listing them, we recall our original objectives:

Year 1—link linear DC power flow models to the uncertainty tools

initiate development of battery storage models

Year 2—expand the power flow tools to address non-linear AC power

incorporate new methods into the uncertainty models

re-link the updated power flow and uncertainty models

complete the development of the battery storage models

Year 3—port the developed tools to the massively parallel processors

demonstrate the operability of the tools on these computers

link the power flow and uncertainty models with the developed battery storage models

Furthermore, as additional features were added to the models, they were exercised and the results were compared to an IEEE standard grid reliability test problem.

All of these objectives were realized. To achieve them, we

- A contingency-based reliability analysis capability was developed and preliminary analyses have been performed on the IEEE RTS and a 400-node model of the Arizona–New Mexico–Texas region within the WSCC.
- To extend the modeling to address uncertainty and optimization questions, we then combined SNL’s CRAX/CASSANDRA uncertainty analysis tools, SNL’s SGOPT optimization tools, and a power-flow analysis program to create a package for reliability analysis for large power systems.
- This software has been ported to the DEC 8400 computer network at SNL and has been implemented on the 28-node computer network at NMSU. By doing this, we expanded

the size of the bulk power systems that could be analyzed. To do this, we needed to build a user-specific interface.

- Two significant literature reviews were accomplished and are discussed in Appendix B. The first emphasized the probabilistic characterization of power flow in a bulk power system, while the second concentrated on recent efforts to combine dynamic bifurcation (a branch of chaos theory) and probability theory to characterize voltage instability. We identified an analysis method that permits the combination of these two techniques. The method permits the static reliability model we developed to be used to statistically characterize dynamic voltage stability.
- In the last year of the effort, we considered the random failure of various power grid elements and expanded the software to permit the load at each system bus to be randomly variable, possibly as a function of local environmental conditions.
- We modeled the behavior of rechargeable batteries in real-life operational mode so that component degradation due to cycling was explicitly included.
- We analyzed the real-life behavior of the rechargeable battery system using statistical and neural network methods to simulate the behavior of various components of the power system.
- We then linked this model to the power flow package. To our knowledge, having a renewable energy resource model linked with a power flow model is a first by anyone, anywhere.

## **5.2 Recommendations**

As discussed earlier, our long-term goal for this work is to advance fundamentally the approach and computational techniques that are used in analyzing the reliability of the bulk electric power grid. As can be seen from our documenting of the work we have done, we have accomplished much. During this work, we have found, however, that we have not accomplished all. We have identified additional work that needs to be done in order both to make the modeling package as complete as possible for performing uncertainty analyses and to bring the entire package into the marketplace so that it gets wide use and thereby positively affects the operation of the nation's electric power grid. Therefore, we recommend that

- a sensitivity analysis package be added to the linked power flow and uncertainty packages
- SCADA models be developed and then linked to the power flow model
- distributed energy resource models be developed in addition to the battery model developed here

- all of the models be then linked to a commercial power flow model, one that is widely used in the industry
- a marketing capability for the model package be developed.

## 6. References

1. A. Patton, C. Singh, and D. Robinson, *The Impact of Restructuring Policy changes on Power Grid Reliability: Final Report*, SAND98-2178. Sandia National Laboratories, Albuquerque, NM, October 1998.
2. EPRI Report, *Composite-System Reliability Evaluation: Phase 1 – Scoping Study*, EPRI EL-5290. December 1987, p. 3.
3. M. Eldred, *Optimization Strategies for Complex Engineering Applications*, SAND98-0340. Sandia National Laboratories, Albuquerque, NM, February 1998.
4. M. Pereira and N. Balu, "Composite Generation/Transmission Reliability Evaluation," *Proc. IEEE*, Vol. 80, No. 4, April 1992, pp.470-49.
5. F. Wu, Y. Tsai, and Y. Yu, Probabilistic Steady-State and Dynamic Security Assessment in *IEEE Transactions on Power Systems*, Vol. 3, No. 1, pp. 1-9, February 1988.
6. D. Robinson, *Reliability Degradation Due to Stockpile Aging*, SAND99-0975. Sandia National Laboratories, Albuquerque, NM, April 1999.
7. D. Robinson, CRAX/Cassandra Reliability Analysis Software, *AIAA-99-1594, 1999*, [<http://reliability.sandia.gov/crax/SDM99-CRAX.pdf>].
8. R. Allan, R. Billinton, A. Breipohl, and C. Grigg, Bibliography on the Application of Probability Methods in Power System Reliability Evaluation 1967-1991, *IEEE Transactions on Power Systems*, Vol. 9, No. 1, pp. 41-49, February 1994.
9. M. Schilling, A. Leite De Silva, R. Billinton, and M. El-Kady, Bibliography on Power System Probabilistic Analysis (1962-1988) in *IEEE Transactions on Power Systems*, Vol. 5, No. 1, pp. 41-49, February 1990.

This page intentionally left blank.

# Appendix A

## Review of Power System Models

For the purposes of reliability analysis, as discussed in this report, an ac power system can be described by a set of differential-algebraic equations. The differential equations describe slowly varying electromechanical dynamics of turbine generators and their controls, load response, and the response of system control elements. The algebraic part, also called the “power-flow” or “load-flow” equations, describes electric power flow through the network elements. The power system is, of course, subject to faster disturbances such as lightning and switching surges. These, however, affect specific components, and the outage of such components represents the disturbance in the slower dynamic models.

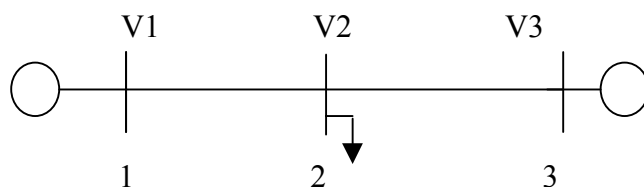


**Figure A-1. Linear Depiction of Power System.**

### A.1 Steady State Model

The powerflow equations can be conceptually written in the form

$$F(V, C, N, D) = 0$$

Where  $V$  = vector of network state variables, e.g., phasor voltages

$C$  = vector of control variables, e.g., generation (MW), generator voltages, transformer taps, etc.

$D$  = vector of demand variables, e.g., load real and reactive power

$N$  = vector of network parameters, e.g., line status, line impedances, etc.

The power flow equations represent real and reactive power balance at each node of the power system. For example, for the system in Figure A-1 the power balance at node  $i$  can be written in the form:

$$Pg_i - Pd_i - \sum_1^N |V_i| |V_j| |Y_{ij}| \cos(\theta_i - \theta_j - \theta_{ij}) = 0$$

$$Qg_i - Qd_i - \sum_1^N |V_i| |V_j| |Y_{ij}| \sin(\theta_i - \theta_j - \theta_{ij}) = 0$$

where:

$P_{g_i}$ ,  $Q_{g_i}$  are the real and reactive power, respectively, supplied by the generator at node  $i$

$P_{d_i}$ ,  $Q_{d_i}$  are the real and reactive power, respectively, demanded by the load at node  $i$

$V_i$ ,  $\theta_i$ , are the magnitude and phase of the ac voltage at node  $i$

$|Y_{ij}|$ ,  $\theta_{ij}$ , represent the  $ij$  term of the network admittance matrix, which is derived from the impedance models of the components.

The summation terms in the above equations measure the power flowing along transmission elements directed away from the node.

In general, only  $2N-1$  equations are independent and it is customary to set the phase angle of a suitable node voltage to zero. Note that a solution may not exist. Such a situation corresponds to load and generation patterns that cause power-flow conditions that exceed the maximum (circuit property based) capability of elements. The condition manifests itself as an unstable dynamic condition, one form of which is voltage stability and voltage collapse.

## A.2 Dynamic Models

The dynamics are described by a set of differential (or mixed differential-difference) equation in the form:

$$\frac{dX}{dt} = G[X(t), U(t), C(t), N(t), D(t), \eta(t)]$$

where:

$X(t)$  = state variable vector that includes control system variables

$U(t)$  = Control variables, e.g., voltage and power commands to a generator

$\eta(t)$  = External disturbance such as a short circuit at a node

For the system in Figure A-1 the simplest model for the dynamics of the generator at node 1 is the “swing” equation

$$H \frac{d\omega}{dt} = (Pm_i - Pg_i)$$
$$\frac{d\theta_i}{dt} = \omega$$

Here  $\omega$  = generator speed

$P_{m_i}$  = Mechanical power input to generator

$P_{g_i}$  = Electrical power output from the generator

Note  $P_{g_i}$  is defined by the power flow equations. Thus the swing equations constitute a nonlinear dynamic system. Conventional power systems are “synchronous;” in the steady state the power flow equations indicate the relative phase angles between nodes, e.g.,  $\theta_i - \theta_j$  must be constant; the swing equations above indicate that all machines must run at a speed corresponding to a common system frequency. If after a disturbance a common frequency is not achieved, generators will continue to accelerate or decelerate and must be disconnected. This situation is called instability (or, more precisely, angle stability).

In general, the dynamic equations include models for the various controllers, and detailed models of generators and loads. Due to model complexity, stability is most commonly studied by simulation. Such simulations are used to determine operating limits on generation so that credible disturbances will not lead to instability. Direct methods for stability analysis, based on energy functions, can also be used.

### A.3 Feasibility

The power flow equations along with the constraints on control variables constitute the so-called “ac power flow model.” A state  $x = (N, D)$  is feasible in the steady-state sense if

$$F(V, C, N, D) = 0, \quad C \in \mathbf{C} \quad V \in \mathbf{V}$$

Here  $\mathbf{C}$  is the set of allowed control variable values and the  $\mathbf{V}$  is the set of allowed state variable values corresponding to voltage and loading limits. For example, the real and reactive power produced by a generator is limited by generator capability, while voltages are usually maintained between 95–105% of nominal values.

A conceptual definition of feasibility with respect to dynamics is: A state  $X(0), N(0), D(0)$  is feasible with respect to disturbances sequences  $\eta(t) \in \boldsymbol{\eta}$  if

$$G(X(t), U(t), C(t), N(t), D, \eta(t)) \xrightarrow{t \rightarrow \infty} 0, \quad \text{for all } \eta(t) \in \boldsymbol{\eta}$$

Note that instability may result from properties of the feedback control systems, or from changes in the network. Also the final and initial states may be different.

## A.4 Simplified Steady-State Models

It is often useful to develop simplified models. These models are outlined below.

### Linearized (Incremental) Models

These are obtained from a Taylor expansion around a steady-state operating point and written as

$$\Delta P = B_v \Delta V$$

$$\Delta Q = B_\theta \Delta \theta$$

Here vectors  $\Delta P$  and  $\Delta Q$  represent changes in real and reactive power injected into nodes and  $\Delta V$ ,  $\Delta \theta$  are corresponding changes in node voltages and phase angles. The matrices  $B_v$  and  $B_\theta$  can be further simplified by assuming nominal voltages to be 1 per unit and angles to be zero. This type of approximation additionally relies on the fact that reactive power primarily affects voltage magnitudes while real power affects phase angles.

### dc Load Flow Model

In many instances one is only interested in real power flow (MW) in the network. Then with nominal voltages assumed to be equal to 1 per unit and angles to be zero the real power flow is described by the linear equation

$$P = B_\theta \theta$$

This is called the dc load flow model.

### Transportation Model

In some instances a transportation model

$$P_i = \sum P_{ij}$$

can be used. Here  $P_{ij}$  represents the power flow on the branch connecting node  $i$  to node  $j$ . In a setting of minimum cost flow in a capacitated network, such a model can be made to mimic actual power flow to an extent.

# **Appendix B**

## **Power System Reliability Analysis**

Draft Final Report

Submitted to

Sandia National Laboratories

By

Satish J. Ranade

The Klipsch School of Electrical and Computer Engineering

New Mexico State University

Las Cruces, NM, 88003



October 2000



## **Abstract**

Sandia National Laboratories (SNL) is involved in a study of electric power system reliability, and more generally uncertainty, analysis within the larger scope of National Infrastructure Surety considerations. The overall objective of the program is to develop tools, techniques, and analyses of the US power system.

This report describes the development and application of uncertainty analysis tools to power system applications. This work combines SNL's CRAX/CASSANDRA uncertainty analysis tools, SNL's SGOPT optimization tools, and a power-flow analysis program to create a package for reliability analysis for large power systems. The package has been developed and tested on a small system and has been ported to SNL supercomputers. Databases for standard test systems such as the IEEE RTS and actual systems such as the Arizona-New Mexico system have been created for testing.

It is believed that the resulting package is a major contribution towards a capability for conducting uncertainty, reliability and vulnerability studies for large power grids.



## Table of Contents

1.	Introduction.....	B-7
1.1	Background.....	B-7
1.2	Uncertainty Analysis in Power Systems.....	B-7
1.3	Motivation.....	B-7
1.4	Objectives.....	B-8
1.5	Summary of Work.....	B-8
1.5.1	Literature Review.....	B-8
1.5.2	A FMEA-Based Toolkit.....	B-10
1.5.3	Uncertainty Analysis Using CRAX.....	B-10
1.6	Conclusions.....	B-11
2.	Power System Reliability Analysis Review.....	B-12
2.1	Preliminaries.....	B-12
2.2	Power System Reliability Terminology-Definition of Acceptable State.....	B-13
2.3	Literature Review.....	B-15
2.3.1	Reliability Analysis Needs/Requirements.....	B-15
2.3.2	Power System Component Models.....	B-16
2.3.3	Power System Models—Evaluating the Structure Function.....	B-17
2.3.4	Reliability Computation.....	B-20
2.3.5	Extension to Security.....	B-20
3.	FMEA Program.....	B-23
3.1	Failure Modes and Effects Analysis.....	B-23
3.2	FMEA Program.....	B-24
3.3	Example 1 --IEEE RTS.....	B-27
3.4	Example 2 -- 400 Node WSCC Submodel.....	B-30
4.	CRAX Uncertainty Analysis.....	B-35
4.1	Overview.....	B-35
4.2	Implementation.....	B-35
4.3	Sample Application.....	B-48
5.	Conclusions.....	B-49
	References.....	B-51

## List of Figures

3.1. FMEA Program.....	B-26
3.2. IEEE Reliability Test System.....	B-28
3.3. Loss of Load Probability by node for the IEEE RTS for a System Load of 2850 MW.....	B-30
3.4. Expected Demand Not Served by Node for the IEEE RTS.....	B-30
3.5. A 400-Bus Submodel from the WSCC System.....	B-32
3.6. LOLP for Some Buses in the 400-Bus System.....	B-34
3.7. Expected Demand Not Served for Some Buses in the 400-Bus System.....	B-34
3.8. The Complementary Distribution of Load Shed at Two Buses in the 400-Bus System.....	B-34
4.1. Power System Uncertainty Analysis using CRAX.....	B-36
4.2. The Test Power System.....	B-37

## List of Tables

2.1 Some Bulk Power System Reliability Analysis Computer Programs.....	B-21
3.1 Contingency List.....	B-29

## **1. Introduction**

### **1.1 Background**

Sandia National Laboratories has initiated a study of electric power system reliability within the larger scope of National Infrastructure Surety considerations. The overall objective of the program is to develop tools, techniques, and analyses of the US power system. The calculation of reliability indices in the traditional sense (e.g., loss of load probability) as well as determining potential scenarios (sequence of events) that lead to failure is of interest. The work reported here is part of SNL's overall program and deals with uncertainty/reliability analysis of power systems.

### **1.2 Uncertainty Analysis in Power Systems**

The purpose of an electric power system is to supply electrical load demanded at an adequate voltage level. The demand and the availability of components are uncertain. Thus, at times demand cannot be supplied without overloading equipment or compromising voltage levels. In such instances load must be disconnected or shed. Load shedding may be localized and controlled or system wide and uncontrolled. The amount of load shed is thus a measure of "failure" of the power system. Probabilistic analysis or Uncertainty analysis in power systems takes many forms, namely:

- **Reliability Analysis:** Reliability analysis involves probabilistic modeling of power system operation in order to calculate the probability of failure; results are expressed in terms of different indices such as loss of load probability, expected demand not served, etc. Reliability analysis generally deals with the entire system and results are used for comparative purposes.
- **Risk Analysis:** Risk analysis is more localized in nature. For example, one might concentrate on a particular load in the system and ask, in a probabilistic sense, what is the risk of not having sufficient power to supply the load. Risk is often measured as a product of event probability and the severity of the effect of the event.
- **Uncertainty Analysis:** This is a more general form of risk analysis. For example, for a specific load in the system we may wish to evaluate the cumulative distribution of supply available to that load.
- **Vulnerability Analysis:** Here the question to be answered is what combination of events is most critical to supplying load? It is desired that the answer take into account the uncertainty in other events.

### **1.3 Motivation**

As industry deregulates and competition is introduced, the operation, control, maintenance and expansion of electric power systems have become fragmented, and this trend continues. In the past, regulated electric utilities have had responsibility to insure the reliability of their systems as well as to coordinate efforts to insure system wide reliability. As planning and operating

decision become more and more subject to market forces, it is less clear what processes will ensure reliability under power industry deregulation. For example:

- Nuclear Power Plants themselves rely on the transmission network for startup and backup power. The separation of generation and transmission ownership might have an adverse effect on the reliability of such supply and therefore the availability of the plant.
- A decrease in maintenance activity could have an adverse impact on the reliability of power delivery, even when adequate capacity exists.
- Loss of a power system control (SCADA) center might significantly reduce reliability for a short period of time.
- Extensive use of renewables and distributed generation can contribute to reliability in some instances and reduce reliability in other instances.

## **1.4 Objectives**

The long-term goals of the work reported here involve fundamental advancements in concepts and computational techniques as applied to uncertainty analysis in power systems. The specific objective is to combine SNL's CRAX/CASSANDRA uncertainty analysis tools, SNL's SGOPT optimization tools, and a power-flow model to create a package for uncertainty analysis for large power systems.

## **1.5 Summary of Work**

### **1.5.1 Literature Review**

An extensive review of literature was conducted as part of this work. Bulk power system reliability analysis has been an active research area for over three decades. Research publications in the area have been periodically listed in bibliographies published in the IEEE Transactions on Power Systems [1,2,3]. Therefore, this report only explicitly lists publications directly relevant to the work described.

A comprehensive computation of probabilistic indices is considered computationally prohibitive. Barriers to such computation include:

- Problem dimensionality: Power Systems are extensively interconnected and may contain 20,000 or more components relevant to system reliability; the state space may not be coherent.
- Discrete nature of failure distributions.
- Successful operation involves both acceptable steady state operation in terms of voltage levels and power-flow conditions, and stability with respect to dynamic conditions. A load-shedding event can occur due to unacceptable voltages or loading in the steady state after an event, the non-existence of steady state equilibria, instability of equilibria or

transitions, and operating policies such as protection schemes. Thus, comprehensive evaluation of even a single state is a difficult problem.

- Complex failure modes of components: Examples are partial failures in generating plant (derated conditions), common-mode failure of system components, etc.
- Temporal dependencies: Parameters such as load, the generation from energy dependent resources, etc., represent stochastic processes.
- Complex operating policies: Power systems are controlled by dispatchers through SCADA. Operator decisions or SCADA failures can compromise a power system.

Some Salient Observations from literature review are given below.

- Typically, reliability studies in published literature address adequacy, i.e., steady-state operation.
- Analytical studies have been limited to generation system adequacy analysis, which is essentially a linear problem. The network is ignored.
- Bulk or composite system reliability analyses utilize the Failure Modes and Effects Analysis (FMEA) method, Monte Carlo simulations, or a combination. The FMEA essentially involves enumeration of selected states followed by an analysis of the steady-state model. Monte Carlo methods involve sampling states from prescribed distributions and analysis based on the steady-state model. Monte Carlo methods can be extended with sequential simulation to model time-evolution of resources such as hydroelectric plant.
- More recent methods have attempted to bridge the gap between enumerative versus analytical approaches by attempting to characterize system operating conditions using neural approximations.
- Typically, reliability studies in published literature address adequacy with system models of about 500 buses. Larger systems have been studied with the DC load flow model. In some instances, deterministic and probabilistic characterizations that include stability considerations have been attempted.
- Commercial and experimental codes exist with a capability to handle large systems. However, it is not clear that existing approaches can be applied directly to solve problems of the magnitude and scope contemplated at SNL.
- A reasonable analysis of the reliability of a specific load point, with some approximations/simplification of network models and models of operating policy, does however seem to be possible with existing techniques implemented on super computers.

### 1.5.2 A FMEA-Based Toolkit

Initially, in this work, an existing power-flow analysis program was extended to provide a FMEA capability. The program implements the FMEA methodology as summarized below.

- The program can model steady state power-flow conditions in large systems with the so-called AC-, DC- or mixed powerflow approaches.
- The program currently analyzes single contingencies (outage of one element), double contingencies and user-specified higher order contingencies.
- For a specified system load level, the program first solves the "base-case" power-flow state, i.e., the case with all components intact. Contractual sales between areas and generator limits are modeled. Given this solution, the program evaluates the steady state response to each contingency. If a contingency results in a violation of voltage requirements or loading capability of one or more elements, the program determines the amount of load to be shed at each node. The contingency state is then classified as failed. Otherwise, the contingency state is considered as being acceptable.
- Once states are classified, the program can be used to calculate standard probabilistic indices such as Loss of Load Probability, Expected Demand Not Served and the distribution of load shed. These indices can be calculated at the system or node level.

The IEEE Reliability Test System is a standard test system utilized in reliability studies. Results for this system are compared with published results. The second example uses a 400-node model of the Arizona-New Mexico-Texas area in the Western US Power System (named the Western Systems Coordinating Council, or WSCC, system). Results are shown for selected nodes in the New Mexico area.

Two important observations from these studies are:

1. The results from the IEEE RTS were compared with results published by others. Although all results are in the same order of magnitude, they are actually quite different. There are two reasons for discrepancies. Implementations differ in terms of how they model operational and load shedding policies. Secondly, the statistical techniques also differ. Suffice it to say that a uniform approach to power system reliability analysis does not exist at this time.
2. The studies showed that uncertainty analysis can identify critical nodes in terms of vulnerability.

### 1.5.3 Uncertainty Analysis Using CRAX

SNL has substantial capabilities in uncertainty analysis. The CRAX package, which includes the CASSANDRA engine, can be combined with physical models to conduct uncertainty analysis. The principal contribution of this work has been the integration of a power system model (power

flow) with CRAX resulting in a sophisticated reliability analysis package. Future research will demonstrate application of this package.

## **1.6 Conclusions**

We believe that, within limitations of model data and modeling assumptions, SNL can conduct credible reliability studies of large-scale power systems. Further development should position SNL as the “provider of choice” for enhancing the surety of energy infrastructures. Necessary enhancements are described in this report.

## 2. Power System Reliability Analysis Review

This task involves a review of literature aimed at establishing the state of the art in power system reliability analysis. The material discussed herein is confined to generally accessible power engineering literature.

### 2.1 Preliminaries

Reliability is the ability of a system to operate as intended over a specific period of time. Reliability is typically modeled in a probabilistic manner and measured by indices such as probability of failure, frequency and duration, etc. In general, reliability analysis involves the following steps:

- Define system state.

The steady state conditions of a power system can be characterized by the status of components (lines, generators, transformers, ...) and load and generation patterns. The state changes continually because of random outages of equipment and variation in load and generation. If dynamics and stability are to be considered, then the notion of state must be supplemented with that of exogenous disturbances.

- Define a probability model for system state.

Equipment is usually characterized by discrete failure models, and load and generation by continuous distributions.

- Define acceptable operation and measures of acceptable operation.

Acceptable operation means that load can be supplied at proper voltage and without overloading components. Unacceptable operation corresponds to a situation when some portion of the load must be disconnected. This can occur due to insufficient capacity to maintain power balance or due to unstable dynamics.

- Define the structure function or test function that maps the system states into acceptable/unacceptable regions.

For example, the structure function given below decomposes the state space into sets of acceptable ( $\varphi(x) > \text{load}$ ) and unacceptable states ( $\varphi(x) < \text{load}$ ).

$\varphi(x)$  = maximum amount of load that can be served in state  $x$  to satisfy constraints

Once  $\varphi(x)$  is known, an appropriate reliability measure can be defined. For example, for a given load level  $L$ , the Loss of Load Probability (LOLP) is

$$\text{LOLP} = \text{Prob}(\varphi(x) < L)$$

An analytical description of  $\phi(x)$  greatly helps in this computation. Alternatively, one can enumerate  $\phi(x)$  for desired values of  $x$ , or attempt to approximate  $\phi(x)$  over a desired region, or attempt to develop estimates of indices from estimated properties of  $\phi(x)$ .

- In enumeration based methods, decompose the set of system states based on acceptability.

Due to the very larger state space and complexity of comprehensive models, approximations are made; typically, only steady-state or “adequacy” models are used. Nonetheless, the decomposition of system states into acceptable and unacceptable remains a computationally intensive problem.

- Compute indices based upon above decomposition.

Typical reliability indices include loss of load probability, frequency and duration of loss of load, expected unserved energy, etc. These indices are computed on a system basis or for a single load point.

## **2.2 Power System Reliability Terminology—Definition of Acceptable State**

Electric power systems are intended to supply customer load with voltages within a specific range, and without overloading components such as transmission lines. A power system fails (commonly referred to as “blackouts” or “brownouts”) when, in response to disturbances such as transmission line outages, a transition cannot be made from one acceptable steady state to another.

Appendix A provides a brief review of the nature models that describe AC power systems. In a normal or acceptable state, power balance is guaranteed at all points in the system. Power is generated primarily by rotating machines and consumed to a large extent by rotating loads. Power balance implies that these machines operate at essentially constant speed as evidence by an essentially constant frequency. Similarly, loads that regulate their energy consumption (e.g., thermostatic loads) achieve a steady pattern of operation. Any departure from power or energy balance initiates a dynamic response from the generators, loads and other regulated equipment, in an effort to establish a new steady state. A new steady state may establish with power balance but unacceptable conditions. On the other hand, the dynamics of the system may be such that the system cannot transition to a new steady state even if one exists. This is referred to as instability.

A failure sequence may take several forms including:

- A disturbance drives the system into a state wherein a steady state power balance exists, but voltages or loadings are out of limit. Further, the condition cannot be corrected due to time constraints or lack of resources. In this instance, typically, some load is disconnected. This is often called “loss of load.”
- A disturbance creates a condition in which changes in power or voltage are so severe that protective apparatus initiates the dropping of load and perhaps separation of the system into islands.

- A disturbance creates a condition where a steady state power balance cannot be achieved at all.
- A disturbance creates a condition in which system dynamics/control is unstable. For analytical purposes such instability is classified as follows:
  - *Transient or “Angle Stability”*: In this case, the electromechanical dynamics are such that the generators cannot be returning to a common operating speed. The time range of this phenomenon is 1-3 seconds.
  - *Long-term stability*: This refers to a situation in which control systems are underdamped or undamped, resulting in oscillatory behavior over a long period of time (minutes) and operation of protective systems.
  - *Voltage stability* involves system response in terms of regulating system voltage and is a function of the ability of the generators to maintain voltage (provide reactive power), the response of loads such as motors to low voltage conditions, and the response of thermostatic load which attempt to continue to draw the required energy by cycling more frequently, for example. The result may be a very rapid uncontrolled decline in voltage (voltage collapse) or a very slow decay (period of hours).

In a failure event, the above phenomena occur simultaneously, of course, but depending on the system one form may be dominant.

*A general definition of acceptability is that disturbances should not result in loss of load. Indeed reliability councils have adopted a deterministic concept of operational reliability as one in which anticipated disturbance do not cause an “uncontrolled loss of load.”*

The terms “Adequacy” and “Security” have been standardized in literature to describe power system reliability.

*Adequacy* refers to the ability of a system to supply load in the steady state. Dynamics of transition are ignored.

*Security*<sup>1</sup> refers to the ability to return to a steady state, i.e., presumes stability of transitions.

The reason for this distinction is that the study of system dynamics is extremely computationally intensive. Further, the random events that initiate a change of state involve fundamental phenomena such as lightning induced short-circuits, which are not easily modeled. Adequacy analysis, on the other hand, involves more manageable models. The power system is modeled by static, nonlinear models, and random events are more macroscopic, such as outage of a transmission line. Adequacy analysis provides an upper bound on reliability measures.

---

<sup>1</sup> The consensus on these definitions is less than complete. We have paraphrased based on what appears in literature. A more common use of the term “security” is in an operational context with reference to a specific state.

Given the computational burden of reliability analysis, approximate models are often used even for adequacy analysis. In terms of the conceptual models given in Appendix A, the following approximations are often used:

- Generation adequacy studies which ignore the transmission system.
- Transportation model based bulk-system studies ignore Ohm's law and merely look at power transfer along capacitated arcs (transmission lines).
- "DC load flow" based studies which are a linear approximations to circuit equations and model the nature of real power (watts) flow through the network.
- Static Power-flow studies, or AC power-flow studies, which calculate the *operating voltages, line power flow, etc.*, for a given condition and determine whether these quantities are acceptable.
- Extended Static Power-flow studies, which include sensitivity analysis, optimization, and operating margin studies.
- Short-term dynamics studies such as transient stability studies, which determine if a proposed disturbance leads to instability. Both time-domain simulations and direct methods are used.
- Long-term dynamic studies such as mid- and long-term stability and voltage collapse.

Most reliability studies are directed at Generation Systems studies, and Bulk system adequacy studies using DC or AC power-flow models. *As such, they are not used to direct system planning but as checks on candidate plans.* Power system expansion planning involves exhaustive studies of a limited number of scenarios with detailed dynamic analyses.

## **2.3 Literature Review**

There exists a vast body of literature in the area of power system reliability. Periodically, working groups in the IEEE, publish extensive bibliographies, e.g., [1,2]. References [3,4] are excellent reviews and also provide extensive references. The references cited in this report were therefore selected so as to cover the full spectrum of research and establish the state of the art. It is convenient to group this literature in terms of SNL program goals and the general reliability analysis approach.

### **2.3.1 Reliability Analysis Needs/Requirements**

References [3,7] summarize current trends in problem definition and solution. Traditionally, reliability analysis has not been used extensively for bulk system planning or operations purposes. This appears to be due to the fundamental limitations of analysis techniques in terms of system size, and the limitations on "observability" of indices (i.e., limitations on measuring results for actual systems). Additionally, at the turn of the eighties in the US, the regulatory and financial climate precluded significant facility construction; as margins eroded, the "weak points"

in systems have perhaps been obvious in a deterministic sense. Reliability analysis appeared unnecessary in identifying these weak points. Reliability analysis larger was used for comparative purposes—to compare alternatives, or to compare reliability of future proposed systems to that of existing systems. The latter is part of reporting requirements. Reference [5], in 1994, identified the following issues:

1. Greater use of cost-based reliability evaluation for system project justification.
2. Introduction of reliability and productivity indices in incentive-based performance evaluation.
3. Continued need for efficient means to include dynamic models into reliability evaluation.
4. Need to correlate major component reliability and safety criteria with system reliability criteria.

Note that the reference appeared immediately prior to FERC open-access order 988.

With deregulation, there is now a growing recognition that traditional deterministic (worst-case) criteria are no longer appropriate particularly in the operations area. Thus, current trends are towards risk analysis, where risk is the product of “probability and consequence.” [7]

Risk analysis can be applied to very specific, localized, situations, such as establishing limits on the power output of a generating plant area, as illustrated in [8]. Closely related issues include probabilistic production costing used in pricing and quantifying economic risk [9], and probabilistic transfer capability assessment which is of interest to transmission providers [10].

The problem of infrastructure surety has only been discussed in rather general terms in power engineering literature. More precisely, general research and methodological developments in large-scale reliability analysis are recommended. These do not focus explicitly on the issues being addressed by SNL. Surety concerns are more in the purview of the National Electric Reliability Council (NERC), local reliability councils, and regulatory and other governmental agencies. Some of this work, and in particular work that relates to national security interests, of course does not appear in open literature.

### 2.3.2 Power System Component Models

Component models used in power system reliability analysis are outlined below.

1. Components such as transmission lines, generators, transformers and other equipment are typically characterized by multi-state Markov models, and associated transition rates. The simplest model is the two-state model with a corresponding mean time to failure (or failure frequency) and mean time to repair. Multistate models are useful in representing events involving derated capacity operation of generating plant, and simultaneous (e.g., common-mode) failures of lines.

2. Power System Loads are modeled by a probability distribution or a Markov model. A critical problem is modeling of loads and their correlation at different nodes in the system.
3. Reference [2] includes a section listing references on Equipment Outage Data. Historical data and methods listed therein provide a source for estimating reliability data for components.
4. The models above are pertinent to the adequacy type reliability evaluation. When security (dynamics) is modeled, then additional events must be considered. One of the most significant disturbances as related to dynamics is the occurrence of a short circuit. This event leads to severe power imbalances, and acceleration and deceleration of machines. It now becomes necessary to develop probabilistic models for short circuits and their duration. The duration is determined by subsequent events such protective system operation/failure and line tripping [11]. Some models based on Discrete Event Systems approaches exist, but the availability of data is quite limited. Further use of a probabilistic model for short circuits comes in conflict with using historical data for, say, line outages which themselves are caused by short circuits to a large extent.

### 2.3.3 Power System Models—Evaluating the Structure Function

The most difficult aspect of bulk power system reliability analysis is the evaluation of the structure function  $\phi(x)$  [3]. The state  $x$  is defined in terms of discrete variables (component status) as well as continuous variables (load). Thus, it is difficult to describe  $\phi(x)$  by analytical models or approximations. In most cases one must calculate  $\phi(x)$  for a given value for  $x$ . Suppose again that

$\phi(x)$  = Maximum load that can be supplied in state  $x$  in the steady state

In this adequacy evaluation, the system is described by the powerflow equations (Appendix A)

$$F(V, C, N, D) = 0$$

The state  $x$  corresponds to the vector of component statuses in  $N$  and the load  $D$ . The non-linear power-flow equation above must be solved to determine  $\phi(x)$ , the amount of load that can be supplied while meeting constraints.

For computational simplicity, approximations are often used. As outlined in Appendix A, transportation models and DC load flow models are linear approximations to the power-flow equations. The transportation model is a severe approximation but provides two major advantages. First, the model is coherent in the reliability sense. The addition of components cannot make the system fail. Second, the maximum flow theorem directly yields minimal representation for the structure function. The DC load flow models are more realistic. Since the model is linear, extremely efficient analytical methods can be developed. With the complete AC power-flow model above iterative techniques are required within each evaluation. Some of the approaches are outlined below.

### *Approach 1*

First, solve the power-flow equations

$$F(V, C+Co, N, D) = 0,$$

$Co$  represents the initial control settings and  $C$  represent changes to control settings required by the transition to state  $x$ . From the power-flow solution determine if voltage limits or line ratings are violated.

Determine a combination of control setting and load shedding that will remove constraint violations. This can be done by solving an optimization problem, e.g.,

$$\text{Min } z1(Ds)+z2(V,C)$$

$$F(V,C+Co,N,D-Ds)=0 \quad C \in C^*, V \in V, Ds \in S$$

where  $Ds$  represent the vector of load shed at a bus. The optimization problem is usually formulated as linear problem. The objective function  $z1(Ds)$  attempts to model load shedding policies while  $z2(V,C)$  models violations and control cost.

This approach is relatively easy to program. However, a major limitation is that it does not model pre-contingency operating strategies adequately. In general, power system operators utilize analysis software and selects operating points such that a single contingency will not cause failure. On the other hand, when multiple contingencies occur, a portion of load may be shed so that additional contingencies will not cause uncontrolled loss of load.

### *Approach 2*

The security constrained optimal power flow is a general model designed for use in real time operation. The optimization-based model solves for control settings that minimize cost, while ensuring relevant contingencies do not cause failure.

The conceptual form is given below.

$$\text{Min } z1(c) + z2(v)$$

$$F(Vi,Ci,Ni,D)=0 \quad Ci \in C^*, Vi \in V, \quad I=0,1,2\dots n$$

where  $No$  represents the normal state with intact components, and  $N1, N2, \dots$  are contingency states for a given load  $D$ . The function  $z1(c)$  models operating cost, while  $z2(v)$  models constraints. This type of formulation can be adapted for contingency and structure function evaluation. To the author's knowledge this has not been done in commercial or experimental programs.

### *Approach 3*

The essentially “brute-force” approaches described above are computationally intensive. The computational burden becomes overwhelming when these techniques must be applied to each possible state. Thus, it is important to consider whether techniques can be developed to approximate  $\phi(x)$  in some other way.

Admittedly, the development of the approximation still requires computations of the type described in approach 1 or 2. (In principle, a Monte Carlo simulation falls in this category in that the goal is to estimate parameters of a probability distribution of  $\phi(x)$ .) Several ideas that appear in literature are listed below.

#### 1. Feasible spaces

In the conceptual formulation, we defined the state  $x$  to be composed of the Component status  $N$  and load  $D$ . For a given  $N$ , one can define the subset  $D_f$  of feasible load  $D$  as follows

$$D_f = \{ D : F(V,C,N,D)=0, V \in \mathbf{V} \}$$

Thus, for a given network configuration  $D_f$  represent loadings that do not cause voltage or loading violations. Reference [15] reviews several techniques, including a pattern recognition based approach, to approximating  $D_f$ . The use of such approximations can help reduce the computational burden.

#### 2. Neural Network Based Approximations

Neural networks can approximate any continuous function to some desired accuracy. Additionally they have the ability to generalize from exemplars. Thus one could treat both  $N$  and  $D$  as continuous variables and build approximations to  $\phi(x)$ . The obvious disadvantage of Neural Networks in relationship to the power system reliability problem is again the high dimensionality of the state space. As indicated earlier, no matter which approximation approach one chooses, the approach to developing the approximation will not be purely analytical. Assume then that the approximation will be developed by some sort of state sampling followed by a solution to the powerflow equations.

Perhaps the most important benefit of approximating techniques lies in the fact that it should not be necessary to model detailed operating policy (as in Approaches 1 or 2). For example, suppose a neural approximation is used to model load shedding at node for different available generation capacities at several other nodes. Given (or, perhaps, assuming) that the neural network does develop an ability to generalize, it does not need to be trained with generation patterns corresponding to actual economic dispatch. In other words, it is necessary to solve the powerflow equations only in the training phase. The network should provide a good approximation to load shed when the input pattern corresponds to a practical generation pattern.

### 2.3.4 Reliability Computation

There are two commonly used approaches to evaluating bulk power system reliability, namely FMEA and Monte Carlo Simulation.

FMEA [4,16,17] is an enumeration method. Essentially, one starts with an intact system and load level and computes a power-flow solution that reasonably models operating policy. Next, a power-flow computation is performed for contingency. A contingency may involve one or more outages. The number of outaged elements is usually called the contingency level. It is common to evaluate all Level 2 contingencies for transmission contingencies and Level 4 or Level 5 for generating unit contingencies (the failure probability of generating units is higher than that of transmission lines). The solution of each contingency can be quite involved since corrective measures and load shedding policy must be modeled. The results of the analysis provide a classification of states according to the desired index or structure function. The process is then repeated for other load levels. Once the decomposition is achieved, steady state indices such as Loss of Load Probability are easily calculated. The calculation of indices such as frequency and duration require construction of a detailed Markov model.

The FMEA method requires a judicious, experience-based, choice of contingencies; even then, the number of simulations required to achieve usable accuracy can be very large.

Monte Carlo simulation [4,17-20] involves sampling from the distribution of system state. A power-flow solution is then computed for the state as in the FMEA method. The contribution to the reliability index is then computed. The number of states that must be sampled depends on the desired accuracy for the index to be computed. With advanced sampling techniques [4] the number of samples required can be substantially less than the number of contingency evaluations in the FMEA method.

The technique can be extended to sequential or chronological Monte Carlo simulation so that the temporal considerations such as generating unit commitment patterns and engage limited or renewable resources such as hydroelectric generation can be modeled.

Table 2.1 provides an overview of typical computer programs described in literature.

### 2.3.5 Extension to Security

As indicated earlier typical reliability studies address the adequacy issue or steady-state considerations. In power system reliability definitions “security” is used to describe reliability models that take into account system failures due to stability problems as well. Examples of conceptual approaches are given in [14] and [21].

The dynamic equations governing the system may be visualized as

$$\frac{dX}{dt} = G(X(t), U(t), C(t), N(t), D(t), \eta(t))$$

Here  $X(t)$ ,  $N(t)$ ,  $D(t)$  represent system state in terms of electrical and mechanical variables, network status and load, respectively.  $U(t)$  and  $C(t)$  represent controls.  $\eta(t)$  represents a disturbance sequence—for example, a short circuit that is subsequently removed by network changes represented by  $N(t)$ .

**Table 2.1 Some Bulk Power System Reliability Analysis Computer Programs**

Code	Adequacy(A) or Security(S)	Powerflow type	Operating/Load Shedding Model	System Size <sup>2</sup>	Approach
COMREL[17]	A	Ac or DC	Linear Sensitivities/LP/Heuristics	600	FMEA
CREAM[3]	A	DC/May support AC	Linear Sensitivities/LP	600	Monte Carlo
TRELLS[[22]	A	Ac	Advanced Approaches	1000(?)	FMEA
(TEXAS A&M)[19]	A	DC	Sensitivities	5000	Monte Carlo with modifications
MEXICO[20]	A	Dc	?	600	Monte Carlo/Chronological
RECS[23]	A	Ac	Optimization	1000	FMEA
This Report	A	Ac	Heuristic	400	FMEA
This Report		Ac	Optimization	Tested on small systems	CRAX/CASSAN DRA

A conceptual definition of feasibility with respect to dynamics is: A state  $X(0)$ ,  $N(0)$ ,  $D(0)$  is feasible with respect to disturbances sequences  $\eta(t) \in \eta$  if

$$G(X(t), U(t), C(t), N(t), D, \eta(t)) \xrightarrow{t \rightarrow \infty} 0, \text{ for all } \eta(t) \in \eta$$

Note that instability may result from properties of the feedback control systems, or from changes in the network. In addition, the final and initial states may be different. References [14] and [21] provide conceptual approaches to studying reliability with such models included. In both cases the steps adopted are:

- Define a set of disturbances  $\eta$
- Separately compute a stability measure for a given initial state or a set of initial states
- Both references use time domain simulation for this computation

Once a description of feasible states is obtained, [14] illustrates how a Markov model can be set up for analytical purposes. The vector differential-equation model is used to estimate a distribution

<sup>2</sup> The system size listed is based on the size of system used by the authors for illustration. The code in itself likely does not limit system size.

of time to failure. In [21], the authors use the description of feasible state in a Monte Carlo simulation to develop security-based reliability indices.

### 3. FMEA Program

#### 3.1 Failure Modes and Effects Analysis

As part of this phase of work, a power system reliability analysis tool has been developed. The tool is based on the conventional Failure Modes and Effects Analysis (FMEA). In this method, credible component failures are defined and system operation evaluated for each case. With knowledge of states that correspond to unacceptable operation, reliability indices can be calculated. Although the FMEA method does not look at all possible states (and one cannot prove completeness using it), it can in many applications provide reasonable results (particularly when comparing different expansion plans or operating strategies) if the probability of a large number of random outages is inherently low. When the probability of a large number of simultaneous events is not small, these can be *a priori* identified and listed in the FMEA.

The simplest FMEA approach consists of the following steps:

##### Type 1 FMEA

1. Prepare a list of states to be evaluated. State variables are usually the status of components such as transmission line, load levels, and generation patterns.
2. Build an intact system or “base-case” model. Solve the power-flow case.
3. Evaluate each state using a power-flow model (or approximation). If there are any violations, classify state as unacceptable.
4. Compute reliability indices.

This FMEA corresponds to conventional system level “Adequacy” analysis with the AC power-flow model. Since unacceptable operation at any point in the system constitutes a system failure, the indices are less sensitive to the specifics of operation and control practices. If operational policies are to be considered additional “base cases” can be developed.

The above FMEA process can be modified to compute reliability indices for each node or bus in the power system as outlined below.

##### Type 2 FMEA

1. Prepare a list of states to be evaluated. State variables are usually the status of components such as transmission line, load levels, and generation pattern.
2. Build an intact system or “base-case” model. Solve the power-flow case.
3. Evaluate each state using the power-flow model.
4. If the state is unacceptable, attempt to remedy the violations by using available controls.

5. If the unacceptable state remains, apply control action to the base case to remedy problems in the outage cases.
6. For the final set of unacceptable cases, shed load based on load-shedding policies until the case is acceptable.
7. Compute reliability indices.

This approach properly models operating policies as well as computes the load that can be supplied at each bus. Steps 4-6 in this approach can usually be implemented in an optimization framework.

### **3.2 FMEA Program**

The FMEA developed here follows the Type 2 FMEA approach, above. An existing power-flow analysis program was modified for this purpose. Specific descriptions of the FMEA steps follow:

1. The program uses an input file wherein the user can list contingency groups known to be significant in terms of impact. Each group defines up to five simultaneous outages.

The program develops contingencies to be studied as combination of

- Single element contingencies for every element with a nonzero forced outage rate.
- Double element contingencies for each pair of elements with a nonzero forced outage rate.
- Each Single element contingency along with each contingency group listed in a user-input file.
- Each Double element contingency for each pair of elements with a nonzero forced outage rate along with each contingency group listed in a user-input file.

Thus, the program models all single and double contingencies and a limited set of higher order contingencies.

2. Build an intact system or “base-case” model. Solve the power-flow case.

The fast decoupled load flow technique is used to solve the power-flow model. As the iterations begin to converge, generator powers and voltages are adjusted to enforce contractual interchange and generator limits. Note that economic or other dispatch policies to set generator output are not modeled at this time. In other words, system operation is not optimized.

3. Evaluate each contingency state using the power-flow model.

For each contingency, the power-flow problem is solved again. Generation adjustments are made based on governor action alone. In this step (as well as in step 2) non-convergence of the power flow is possible. A simple rule is used to detect non-convergence.

Reasons for non-convergence are listed below.

- Isolated system with inadequate generation to support load in an island. The trivial case is an isolated load bus.
- Load in excess of or close to steady state stability (voltage or angle) limit.
- Numerical divergence.

For each contingency, the model checks for voltage levels below 90 % and for emergency rating violations. If either of these exist, then the contingency is considered a failed state from a system perspective.

If needed, load shedding is performed based on the nature of the problem until the problem is resolved. A simple heuristic algorithm is used. Load is shed in 10% steps at buses where the voltage is low or lines are overloaded; if necessary, load shedding is expanded to neighboring buses and thence to the rest of the system. If there is inadequate generation, however, load is shed at all buses by a common percentage. Any bus where load is shed is considered a failed bus.

#### 4. Compute reliability indices.

In the actual implementation, results of the FMEA are stored. Reliability is then calculated by a separate program. The calculations are shown below.

$$BusLOLP = \sum_{Contingencies\ for\ which\ Load\ Shed\ at\ Bus > 0} Contingency\ Probability$$

$$BusEDNS = \sum_{Contingencies\ for\ which\ Load\ Shed\ at\ Bus > 0} Contingency\ Probability * Load\ Shed$$

Because Fortran 90 compilers are available on certain SNL supercomputers, the existing power-flow code was modified to compile under Fortran 90. As described presently the code was also modified so that the power-flow calculation can be spawned on an external computer. Thus, while the conversion to C code continues, the Fortran program can be utilized on a single host machine at SNL, or a combination of a host PC for user interaction and a super computer for engine execution. The program has been separated into two programs as described below.

1. User interface for setting up case.
2. FMEA engine that performs power-flow calculations for the given data.

Figure 3.1 illustrates this setup.

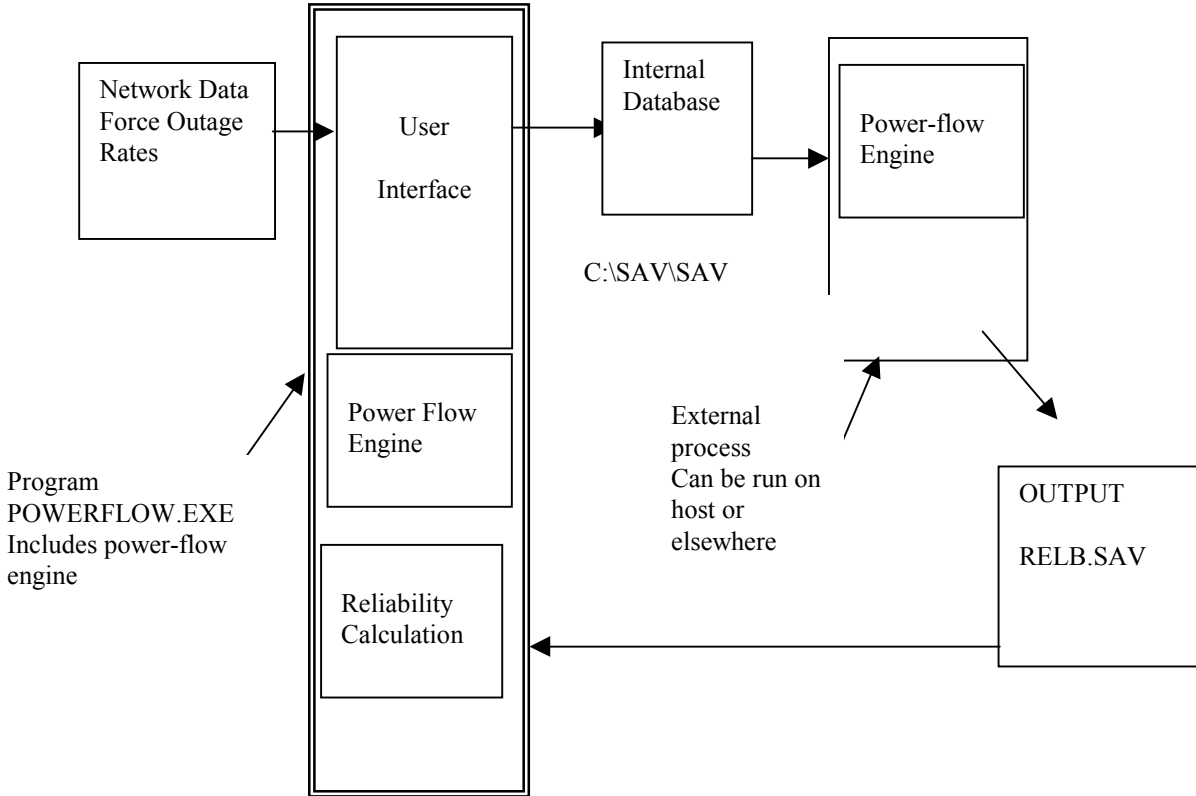


**Figure 3.1. FMEA Program.**

The FMEA program is executed from a menu option in the power-flow program.

1. The power-flow program POWERFLOW.EXE is started and a data case is selected.
2. Next the data case can be modified and checked.
3. The FMEA option is selected. The user is prompted for the starting load level in percent of case load contingency level (1 for single or 2 for single and double).

At this point, a binary data file c:\sav.sav is created. The binary file is created by the power-flow program from the original system data file. Then the FMEA is spawned as an external process.

4. The FMEA reads the input data file (binary file sav.sav) and executes the FMEA process.

The FMEA produces an output file, which is placed in the same directory as the executable LF.EXE. The file BRELB.SAV lists each failure contingency, the type of problem and the load shed at each bus.

5. The program returns to the main user interface and performs the reliability index calculation.

Note: the user can repeat these calculations at will, for example, with a different set of outage rates.

### 3.3 Example 1—IEEE RTS

The FMEA program was used to conduct a study of the IEEE Reliability Test System (RTS)[24-26]. The original RTS [24], which has 20 nodes, is used here. It is shown in Figure 3.4. The following modifications were made:

1. The system was divided into two areas A and B. Area A consist of 230 kV buses while area B consists of all 138 kV buses. The total system load is 2850 MW and the installed generation capacity is 3950 MW.
2. It was assumed that Area A generators supply or “sell” 600 MW to area B.
3. Figure 3.2 shows several generator buses. Each of these “plants” can contain more than one generator. Generating unit transformers were added for each generator, but were assumed to be perfectly reliable.

The FMEA outage list file is shown in Table 3.1. Recall that the program generates its contingency list all combinations of single and double contingencies, along with each contingency listed in the file. As such, all single and double contingencies and a number of triple contingencies are considered. The characteristics of the run are summarized below.

System load MW	2850 MW
Number of contingencies evaluated	32305
Probability corresponding to evaluated contingencies	0.9803
Probability of unevaluated contingencies	0.0197

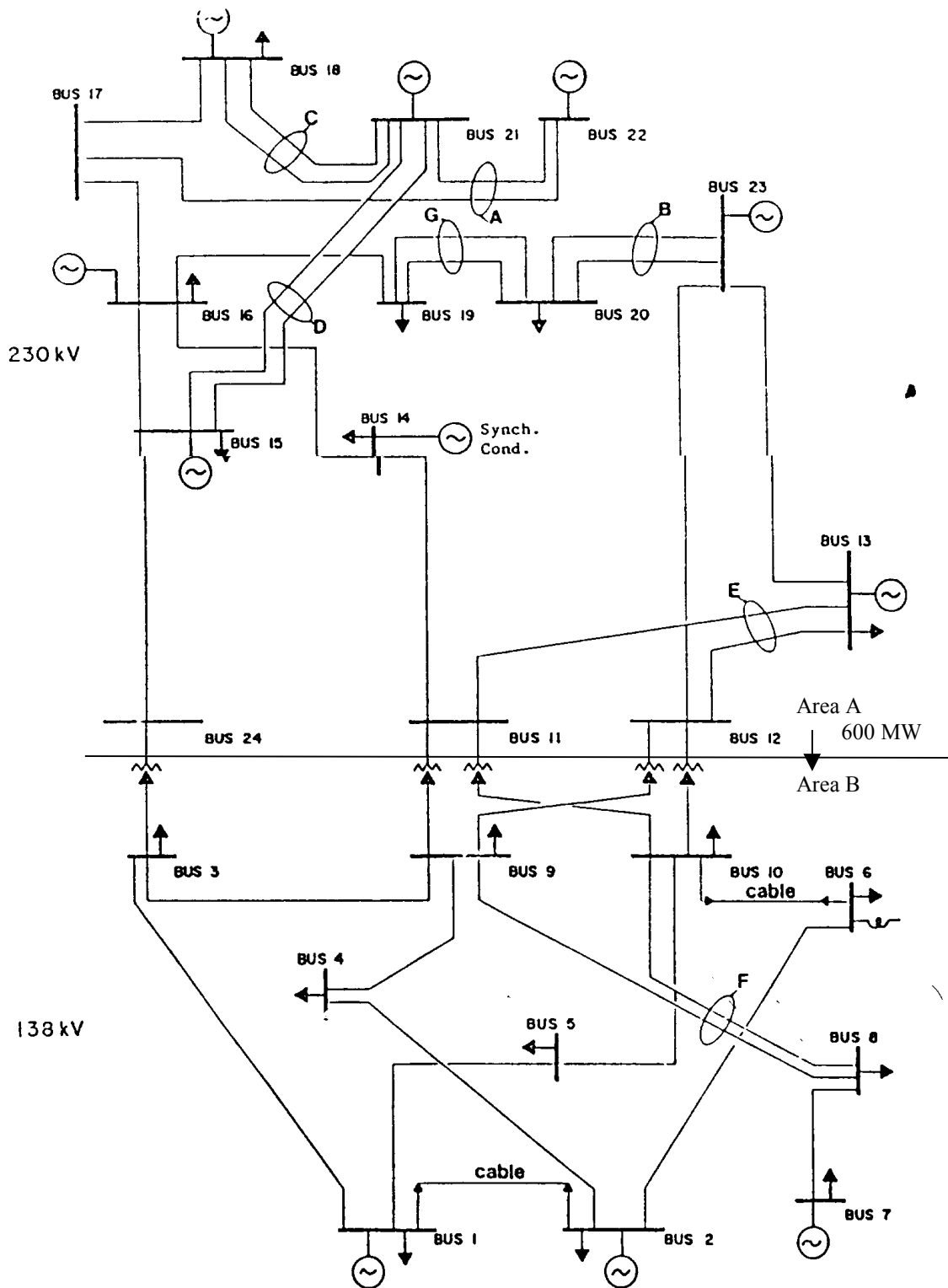


Figure 3.2. IEEE Reliability Test System.

**Table 3.1 Contingency List**

GEN23-3	15		
SIXTEEN	230	GEN23-3	15
EIGHTEEN	230		
TONE	230		
GEN23-1	15		
GEN23-3	15		
ELEVEN	230	FOURTEEN	230
TWELVE	230T	THREE	230
FIFTEEN	230T	FOUR	230
SEVENTEEN	230T	TWO	230
FIFTEEN	230T	ONE	230
NINE	138	ELEVEN	230
TEN	138	TWELVE	230

Recall that the FMEA program solves the AC load flow model for each contingency. During the solution, the constraints on generator reactive power are enforced. If the contingency involves a generator outage power is redistributed to other units. If the solution indicates acceptable voltages (> 90% of nominal) and loading within emergency ratings, the contingency is considered acceptable. If the case is not acceptable load is shed at appropriate nodes until the performance becomes acceptable. Any load shedding at a node is considered a node or load point failure as well as a system failure.

#### System Loss of Load Probability

In this example, the probability of system failure or Loss of Load Probability is evaluated at 0.00459. As discussed previously this number represents a lower bound since events with a combined probability of 0.01970 were not evaluated. If coherency were assumed, the estimate of the Loss of Load Probability is 0.01912. In summary

Loss of Load Probability	0.00459
Loss of Load Probability assuming coherency	0.01912
Upper Bound	0.02371

#### Load Point Loss of Load Probability

Figure 3.3 shows the Loss of Load Probability by node. Only nodes with nonzero connected load are shown. Also shown are the loss-of-load probability results presented by Vidal, et al. [18] and by Salvaderi and Billinton, [17], for a load of 2850 MW. The LOLP estimate in Vidal [18] is based on a Monte Carlo sampling with a DC load flow based model, and is generally higher than results from the FMEA. The results in [17] were obtained from both a FMEA and a Monte Carlo simulation. The FMEA results are based on an AC load flow model and are referenced here. The results are different from both our FMEA and those in [18]. In addition, for example, Bus 1 has a

significantly higher LOLP than Bus 2 in [18], but in the FMEA in this report and in [17], Bus 2 and Bus 1 have a similar probability of failure. It is believed that these differences are a result of the load shedding model used. Vidal, et al. [17] use a linear optimization model; therefore, it is suspected that whenever there are generator outages, load is shed at small number of buses. In the FMEA developed here, a generation shortage at the system level leads to load shedding and such shedding is spread uniformly across the system. This tends to level the LOLP index.

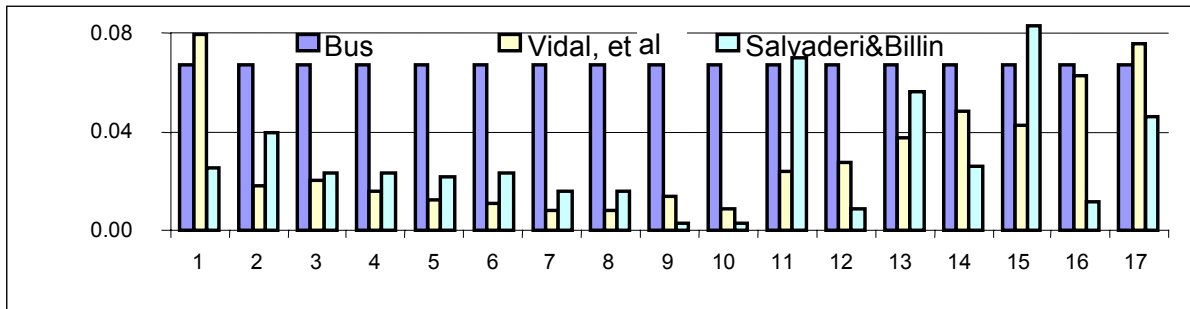


Figure 3.3. Loss of Load Probability by Node for the IEEE RTS for a System Load of 2850 MW.

### Expected Demand Not Served

The Expected Demand Not Served Index is shown in Figure 3.4 and its pattern is very close to that in [18]. Differences are seen at buses with relatively large load; as discussed previously, the linear optimization approach likely sheds load at a few heavily loaded buses closest to the generation outage.

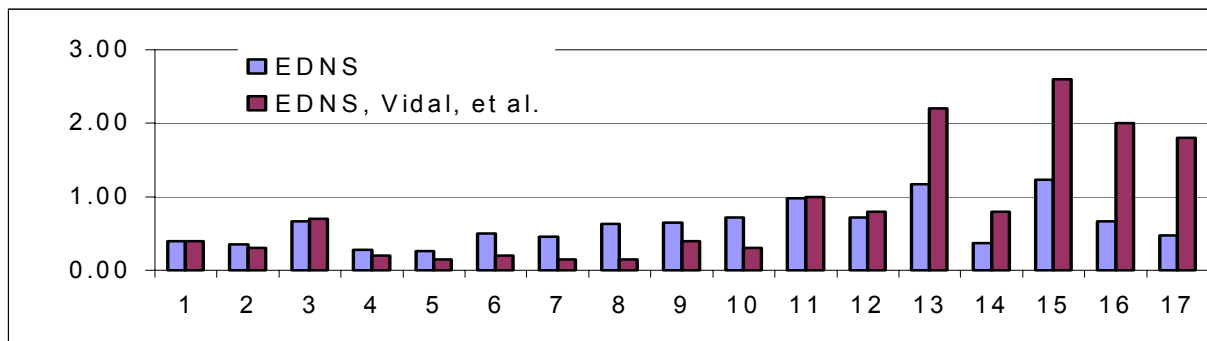


Figure 3.4. Expected Demand Not Served by Node for the IEEE RTS.

### 3.4 Example 2—400 Node WSCC Submodel

In this example, we consider the New Mexico-Far West Texas-Arizona system shown in Figure 3.5. A 400-node model of this system was extracted from a WSCC Summer 1995 case. The nodes connecting Arizona to Nevada and Southern California, and New Mexico to Colorado

were terminated in generator/load buses. A more accurate approach would entail developing an equivalent circuit to model the external systems.

In order to limit computation time to about six hours on a 300-MHZ microcomputer, the FMEA was set up as follows:

1. Single and double contingencies, and triple contingencies based on the contingencies in the FMEA file were considered.
2. In the Arizona area, generating units of capacity less than 100 MW and transmission lines/transformers with voltage lower than 230 kV, were not considered in the single and double contingency list.
3. All elements in the New Mexico and El Paso areas were included in the contingency analysis.
4. The third contingencies specified in the FMEA list included all 500-kV lines, all generating units in excess of 300 MW, and all 345-kV lines terminating in New Mexico/Texas or within New Mexico/Texas
5. Generation unit forced outage rates were assumed to be 0.05; transmission line and transformer forced outage rates were assumed to be 0.001.

The characteristics of the run are summarized below.

System load MW	14367 MW
Number of contingencies evaluated	110160
Probability corresponding to evaluated contingencies	0.35
Probability of unevaluated contingencies	0.65

Note the very high probability of unevaluated contingencies.

The solution for each contingency requires between 7 and 25 load flow iterations. Figure 3.6 shows the Loss of Load Probability for a few of the nodes in the system. Since arbitrary forced outage rates were assumed, and because a small model was used, these results are only indicative. However, the pattern is consistent with known system behavior such as the higher sensitivity of the Northern New Mexico area to outages of the 345 kV transmission (Buses labeled Zia, Taos, for example). Figure 3.7 illustrates the corresponding expected demand not served.

Figure 3.8 shows the complementary distribution of the load shed at two buses. In this instance, the FMEA study was conducted for a fixed load level. It should be noted that the distribution depends on the given level of load, and implicitly then on the operating condition or policy for this load level. In this sense, it is a conditional distribution. To completely characterize the distribution, the FMEA would have to be repeated for different load levels.





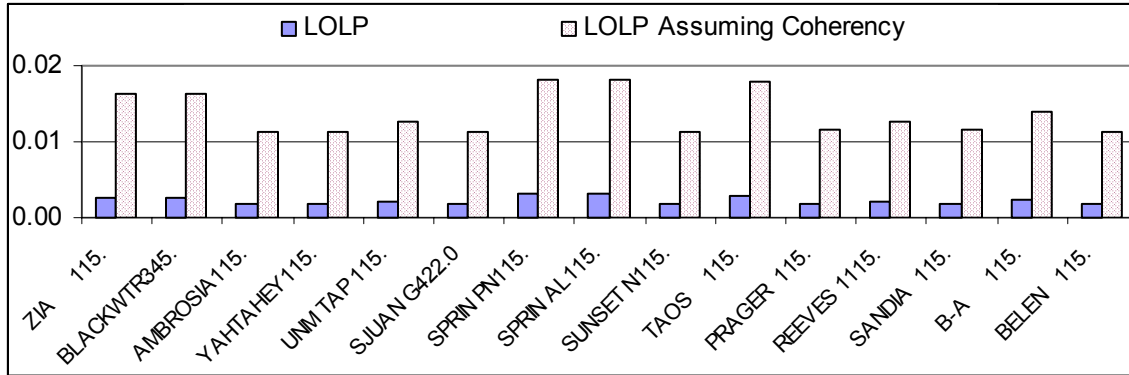


Figure 3.6. LOLP for Some Buses in the 400-Bus System.

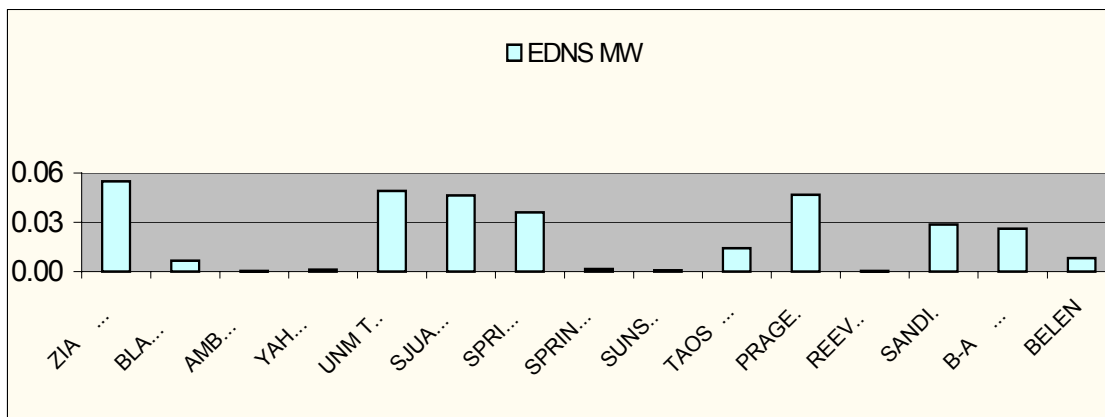


Figure 3.7. Expected Demand Not Served for Some Buses in the 400-Bus System.

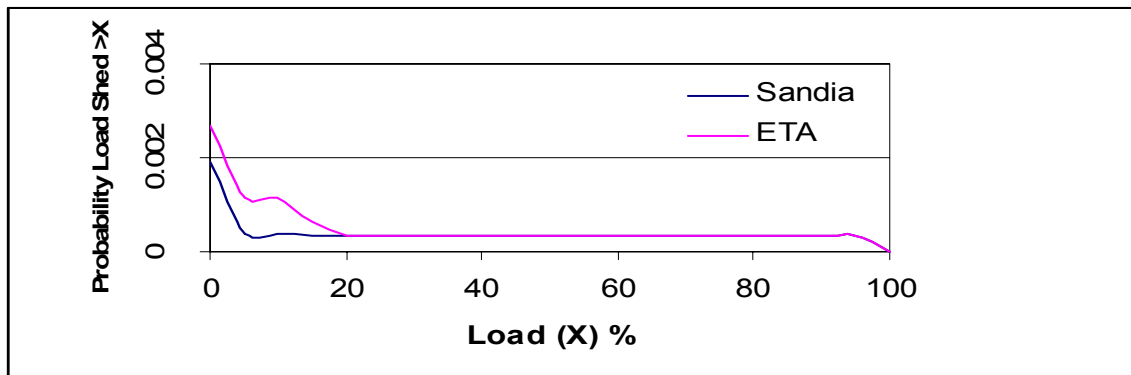


Figure 3.8. The Complementary Distribution of Load Shed at Two Buses in the 400-Bus System.

## 4. CRAX Uncertainty Analysis

### 4.1 Overview

In an effort to include uncertainty analysis in classical design tools, Robinson and others at SNL have developed an uncertainty analysis tool called CRAX [27]. The tool consists of :

- The uncertainty analysis engine CASSANDRA. This is a collection of software routines including pseudo-Monte Carlo and quasi-Monte Carlo techniques
- A graphical interface CRAX
- Physical model(s) of the system under study

The Common Object Request Broker Architecture (CORBA) interface permits a user to combine the three units to form a sophisticated uncertainty analysis package.

In order to apply CRAX to power system reliability analysis, the “Physical Model” of a power system was implemented and integrated (Figure 4.1). Recall that reliability analysis involves the evaluation of power system performance using a model. For a given state of the system, for example, it is first necessary to model the normal operating pattern. Then, if an element were outaged, it is necessary to determine the amount of load that might have to be disconnected or shed, in order to maintain system operation. The physical model consists of a power-flow code which models the power system combined with an optimizer SGOPT (part of SNL’s DAKOTA package). The optimizer essentially models operating policy while the power-flow program models the physical system.

The application of this package to reliability analysis can be illustrated as follows. It is assumed that the pseudo-Monte Carlo approach, specifically Latin Hypercube sampling will be used.

1. CRAX generates a sample which represents the state of the power system.
2. The optimizer uses the power-flow engine to determine how the system should be controlled and how load would be shed to minimize costs or minimize load shedding. If there is no load shedding then the proposed state can successfully supply load. Otherwise it is a failed state.
3. CRAX accumulates statistics by node and repeats steps 1-2 until convergence.

### 4.2 Implementation

#### Interprogram Communication and Control

Communication between the modules is provided by two text files:

1. State.txt

This file contains:

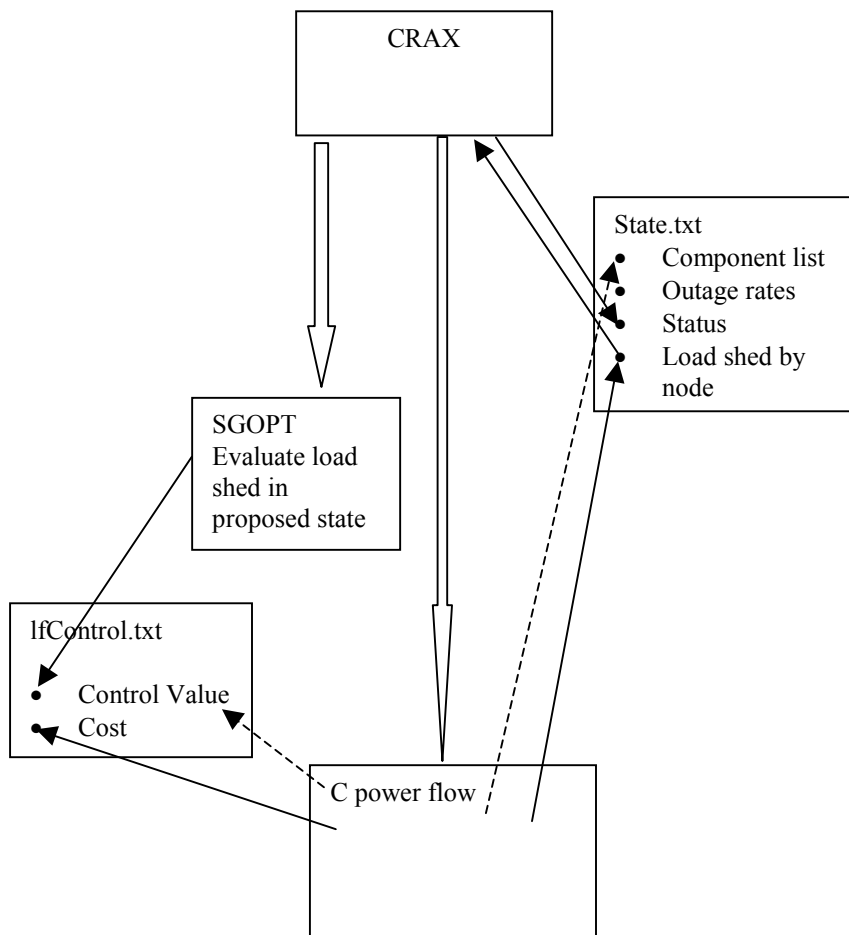


**Figure 4.1. Power System Uncertainty Analysis using CRAX.**

- Number of components--initialized by power flow.
- Component list, type, and statistical data--initialized by power flow.
- Component status-- set by CRAX.
- Load shed by bus--updated by power flow.

## 2. Control.txt

This file contains:

- Number of control variables, maximum, minimum values -- initialized by power flow.
- Control values --initialized by power flow, updated by SGOPT.
- Gradient- initialized and updated by power flow.

- Cost--initialized and updated by power flow.

The specific steps in this process are listed below.

1. Initialization
  - a. CRAX calls power-flow program with PMODE parameter set to 1.
  - b. Power-flow program creates the state.txt file with all components assumed intact.
2. State Evaluation
  - a. CRAX reads state.txt.
  - b. CRAX method selects a state to evaluate and writes state to state.txt.
  - c. CRAX calls SGOPT.
  - d. SGOPT calls power-flow program with PMODE parameter set to 2.
  - e. Power flow reads state.txt, performs power-flow solution, initializes control.txt.
  - f. SGOPT iterates with power flow with PMODE parameter set to 2 until optimal solution is obtained. Power flow updates state.txt with load shed information at each iteration.
  - g. SGOPT returns control to CRAX.

State Evaluation, Problem Variable Description, Interface Structure

The operation of the programs can be illustrated using the test system in Figure 4.2. At each step the program:

1. Samples a system state (CRAX).
2. Evaluates acceptability in terms of load shed(SGOPT/power flow).

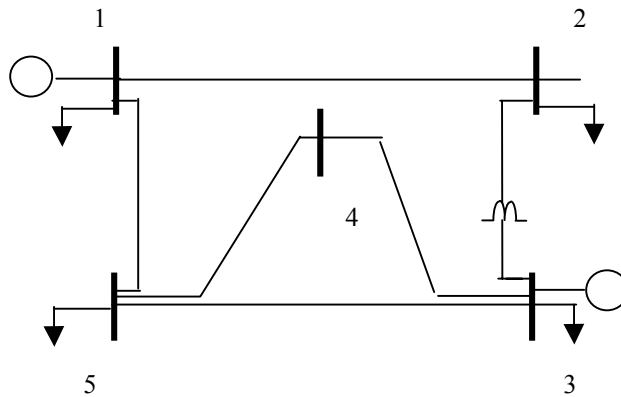


**Figure 4.2. The Test Power System.**

## CRAX State Sampling

CRAX generates samples based upon the statistical failure models of components. With respect to Figure 4.2 components are defined to be the following entities:

Transmission Lines (Type L)  
Transformers (Type T)  
Loads (Type P)  
Generators (Type G)

For the present experiment, Lines, Generators, and Transformers will be modeled as two state components characterized by a Forced Outage rate (FOR), interpreted as the probability of failure. Loads will be modeled as deterministic or by an average and a variance.

Thus, at the start of the calculation CRAX must be provided with the following information from the power-flow database:

Number of components (Integer)  
Initial component status (integer 1=in service 0 = out of service)  
Component type (Not used yet)  
Statistical parameters  
Forced outage rate (Float)  
Load level

For each sample CRAX will need to update the following

Component status  
Capacity scale factor  
Load level

The load level and capacity scale factor are not used at this time but are intended to vary load level and model continuous generator capacity distributions.

The SGOPT/power flow develops an OPF solution and returns to CRAX the following variables

Node number  
Load supplied as fraction of actual

Thus, load supplied of 1 implies no load shed, while 0 implies complete load shedding

These data have been collected in a single file as shown below.

The SGOPT-based OPF seeks a solution of the following problem:

13 ←				# of components	
1	L	1	0.001000	1.000000	5 transmission lines
2	L	1	0.001000	1.000000	
3	L	1	0.001000	1.000000	
4	L	1	0.001000	1.000000	
5	L	1	0.001000	1.000000	
6	T	1	0.000600	1.000000	1 Transformer
7	P	1	0.100000	1.000000	5 Loads
8	P	1	0.100000	1.000000	
9	P	1	0.100000	1.000000	
10	P	1	0.100000	1.000000	
11	P	1	0.100000	1.000000	
12	G	1	0.003000	1.000000	2 generators
13	G	1	0.003000	1.000000	
1			1.000000		Generated by power flow 5 loads Load #, Load supplied(fraction)
2			1.000000		
3			1.000000		
4			1.000000		
5			1.000000		

Min z

C

$$F(C,X)=0$$

where C = control variables

X= Power system variables

F(C,X) =0 represents the power-flow model equations

Control variables C consist of:

Generator MW

Generator voltage

Transformer tap

Transformer phase

Scale factor for load at each node

The scale factor for node at each node is used to model load shedding. A factor of 1 implies all load is intact, while 0 implies all load is shed.

The objective function z has the following components:

Generator fuel cost

Component overload penalty function

Voltage violation penalty function

Load shedding penalty function

SGOPT generates minimizing directions by iterating over control variable values. In cases where the given load level cannot be supplied in a given system state SGOPT will drive the objective to a minimum (i.e., feasible with respect to violations) by shedding load. Note that in instances where the power flow diverges, cost is set to a very high number.

The power-flow program supplies the following information to SGOPT:

- Number of control variables
- Control variable maximums
- Control variable minimums
- Initial values
- Gradient of cost with respect to control variables
- Initial cost

At each SGOPT iteration, SGOPT supplies new values for control variables, and the power-flow program returns the objective function value as described in the interface file below.

#### SGOPT Interface file lfControl.txt

SGOPT interfaces to the power flow through an ASCII data file. The header clfgopt.h describes the interface variables and the function prototypes used to read and write the file. The file lfcontrol.txt shown below provides the interface (note that rows are wrapped around in this display and annotation added).

```
Ten control variables: 1 generation MW, 2 generator voltages, transformer tap, phase, 5 load factors
(Note: If a component associate with a control variable is removed, the control variable is removed
from the control list.)
10

Maximums
300.000000 1.100000 1.100000 1.100000 30.000000 1.000000 1.000000 1.000000 1.000000 1.000000

Minimums
20.000000 0.900000 0.900000 0.900000 -30.000000 0.000000 0.000000 0.000000 0.000000 0.000000

Control status (0 fixed 1 changeable)
1 1 1 1 1 1 1 1 1 1

Initial values
100.000601 1.040000 1.020000 0.971831 20.000000 1.000000 1.000000 1.000000 1.000000 1.000000

Gradient
-25855.1 33650.53 -77762.94 -32483.72 1907.91 4882.97 23000.99 1823 23541.87
COst

8292.493802
```

The file consists of the following records:

1. # of control variables (integer)
2. Maximum values for control variables (float,space(s) separated)
3. Minimum values for control variables (float,space(s) separated)
4. Active flag for controls (integer space(s) separated)
5. Initial values of controls (float,space(s) separated)
6. Gradient values of controls (float,space(s) separated)
7. Cost

The above set is repeated for each SGOPT iteration.

Initially, the lfcontrol.txt is empty. When the power flow is executed with mode parameter PMODE set to 2, it initializes records 1-7. At each iteration from this point on SGOPT writes new control values and the power flow (PMODE=3) returns gradient and cost.

### Illustration

The power-flow program clfmain can be called as an external process with appropriate command line arguments:

Clfmain n

(The declaration of the main is: void main (int argc, char \*argv[ ], char \*envp[ ].)

n is an integer corresponding to argv and is interpreted as follows:

- Clfmain 1 : CRAX command for power flow to initialize state (lfstate.txt)
- Clfmain 2 : SGOPT command for power flow to initialize controls (lfcontrol.txt)
- Clfmain 3 : SGOPT command for power flow to update cost for an updated control (lfcontrol.txt)

The program executable was created with MS c++ as a console application. To run the program in various modes the user opens a DOS window and types one of the above commands.

The Steps described in Section 2 are illustrated below for two example samples generated by CRAX.

### Example 1

#### Step 1:CRAX Initialization

Clfmain 1 initializes the state file lfstate.txt as shown below. Note all components are in service and the load shed records are absent.

File lfstate.txt

```
13
1 L 1 0.001000 1.000000
2 L 1 0.001000 1.000000
3 L 1 0.001000 1.000000
4 L 1 0.001000 1.000000
5 L 1 0.001000 1.000000
6 T 1 0.000600 1.000000
7 P 1 0.100000 1.000000
8 P 1 0.100000 1.000000
9 P 1 0.100000 1.000000
10 P 1 0.100000 1.000000
11 P 1 0.100000 1.000000
12 G 1 0.003000 1.000000
13 G 1 0.003000 1.000000
1 1.000000
2 1.000000
3 1.000000
4 1.000000
5 1.000000
```

Step 2: CRAX state sample

CRAX samples the state and updates the state file as shown below, illustrative of all components in service and loads at nominal values.

```
13
1 L 1 0.001000 1.000000
2 L 1 0.001000 1.000000
3 L 1 0.001000 1.000000
4 L 1 0.001000 1.000000
5 L 1 0.001000 1.000000
6 T 1 0.000600 1.000000
7 P 1 0.100000 1.000000
8 P 1 0.100000 1.000000
9 P 1 0.100000 1.000000
10 P 1 0.100000 1.000000
11 P 1 0.100000 1.000000
12 G 1 0.003000 1.000000
13 G 1 0.003000 1.000000
1 1.000000
2 1.000000
3 1.000000
4 1.000000
5 1.000000
```

Step 3: OPF Initialization

CRAX starts SGOPT for state evaluation. The first step is to initialize the problem by executing CLFmain 2. This results in the control file shown below.

Step 4: OPF Iteration

SGOPT generates a direction and updates the control file as shown below. The SGOPT iteration was simulated manually and the lfcontrol.txt file after several iterations is shown on the next page.

```

10
 300.000000 1.100000 1.100000 1.100000 30.000000 1.000000 1.000000 1.000000
1.000000 1.000000
20.000000 0.900000 0.900000 0.900000 -30.000000 0.000000 0.000000 0.000000
0.000000 0.000000
 1 1 1 1 1 1 1 1 1
100.000601 1.040000 1.020000 0.971831 20.000000 1.000000 1.000000 1.000000
1.000000 1.000000
-25855.103031 33650.531987 -77762.940936 -32483.725652 1907.911978
4882.972831 23000.996773 18238.735786 23541.871462 30555.249624
8292.493802
  ← Note high cost due to generator capacity violations

```

Recall that the control variables are:

- Generation (MW) at node 3
- Voltage at node 3 generator
- Voltage at node 1 generator
- Transformer tap
- Transformer phase
- Load multiplier node 1
- Load multiplier node 2
- Load multiplier node 3
- Load multiplier node 4
- Load multiplier node 5

The lfcontrol.txt file is annotated to show how SGOPT might change control variables towards an optimum.

#### Step 5: Completed State Evaluation

No load is shed and the final lfstate file indicates all loads are at nominal values.

## File lfcontrol.txt for Example 1

```
Initial
300.000000 1.100000 1.100000 1.100000 30.000000 1.000000 1.000000 1.000000 1.000000 1.000000
20.000000 0.900000 0.900000 0.900000 -30.000000 0.000000 0.000000 0.000000 0.000000 0.000000
1 1 1 1 1 1 1 1 1
100.000601 1.040000 1.020000 0.971831 20.000000 1.000000 1.000000 1.000000 1.000000 1.000000
-25855.103031 33650.531987 -77762.940936 -32483.725652 1907.911978 4882.972831 23000.996773
18238.735786 23541.871462 30555.249624
8292.493802
Note high cost do to non optimal generation, reactive overload, and line overload

Iteration 1 Raise Generation(MW) at node 3 to 200 MW(Gradient, -25855 is negative)
200.000601 1.040000 1.020000 0.971831 20.000000 1.000000 1.000000 1.000000 1.000000 1.000000
-34.804376 -725.985901 -1196.868458 -755.090126 12.017794 199.734598 401.870274 220.363184
231.475858 266.262932
1922.132690
A better solution due to reduction of fuel cost and overloads

Iteration 2 Raise node voltages to maximum of 1.05
200.000601 1.050000 1.050000 0.971831 20.000000 1.000000 1.000000 1.000000 1.000000 1.000000
-44.553016 -781.769700 -1288.957794 -827.742613 16.120104 199.684489 415.064850 227.186870
240.957399 274.493906
1921.895001
Further improvement in cost primarily due to reduced power loss. Note voltage gradient remains large
--voltage will generally hit bounds

Iteration 3 Raise tap to 1.05
200.000601 1.050000 1.050000 1.05 20.000000 1.000000 1.000000 1.000000 1.000000 1.000000
-52.615823 -836.412755 -1429.827007 -979.702271 17.622841 199.684352 430.233627 232.829274
245.476753 277.134307
1921.886898

Iteration 4 Change phase to 10
200.000601 1.050000 1.050000 1.05 10.000000 1.000000 1.000000 1.000000 1.000000 1.000000
-49.369648 -891.269811 -1389.232027 -784.008908 10.759028 199.485709 417.410029 230.558050
245.824219 280.734460
1920.953446

Iteration 5 Reduce phase further to 1 degree
200.000601 1.050000 1.050000 1.1 10.000000 1.000000 1.000000 1.000000 1.000000 1.000000
29.639992 557.357902 524.905339 1170.174330 -13.562525 199.526659 234.582224 175.249169
208.282737 250.516237
1962.425432
Cost goes up gradient is negative

Iteration 6
200.000601 1.050000 1.050000 1.05 5.000000 1.000000 1.000000 1.000000 1.000000 1.000000
-48.554370 -916.804322 -1363.442160 -680.824677 8.233683 199.502616 411.221833 229.987681
246.286827 282.677071
1921.034501

Iteration 7
211.000601 1.050000 1.050000 1.05 5.000000 1.000000 1.000000 1.000000 1.000000 1.000000
-28.644974 -939.970743 -1372.671142 -690.042274 7.970480 192.404683 398.806569 222.211018
238.037770 273.517983
1919.395840
Stop
```

Case is close to optimum. No load has been shed.

## File lfstate.txt for Example 1

```
13
1 L 1 0.001000 1.000000
2 L 1 0.001000 1.000000
3 L 1 0.001000 1.000000
4 L 1 0.001000 1.000000
5 L 1 0.001000 1.000000
6 T 1 0.000600 1.000000
7 P 1 0.100000 1.000000
8 P 1 0.100000 1.000000
9 P 1 0.100000 1.000000
10 P 1 0.100000 1.000000
11 P 1 0.100000 1.000000
12 G 1 0.003000 1.000000
13 G 1 0.003000 1.000000
1 1.000000
2 1.000000 All loads at nominal values; no load shed.
3 1.000000
4 1.000000
5 1.000000
```

## Example 2

This example is a continuation of Example 1. After the first state with all components intact has been evaluated, CRAX samples the next state. In this second sample, the line from node 1 to node 5 is out of service.

### Step 2: CRAX State Sample

CRAX samples the state and updates the state file as shown below, illustrative of all components in service and loads at nominal values.

```
13
1 L 1 0.001000 1.000000
2 L 0 0.001000 1.000000
3 L 1 0.001000 1.000000
4 L 1 0.001000 1.000000
5 L 1 0.001000 1.000000
6 T 1 0.000600 1.000000
7 P 1 0.100000 1.000000
8 P 1 0.100000 1.000000
9 P 1 0.100000 1.000000
10 P 1 0.100000 1.000000
11 P 1 0.100000 1.000000
12 G 1 0.003000 1.000000
13 G 1 0.003000 1.000000
1 1.000000
2 1.000000
3 1.000000
4 1.000000
5 1.000000
```

### Step 3: OPF Initialization

CRAX starts SGOPT for state evaluation. The first step is to initialize the problem by executing CLFmain 2. This results in the control file shown below.

```
10
300.000000 1.100000 1.100000 1.100000 30.000000 1.000000 1.000000 1.000000 1.000000 1.000000
20.000000 0.900000 0.900000 0.900000 -30.000000 0.000000 0.000000 0.000000 0.000000 0.000000
1 1 1 1 1 1 1 1 1
100.001640 1.040000 1.020000 0.971831 20.000000 1.000000 1.000000 1.000000 1.000000 1.000000
-60128.471336 375647.764746 119149.535284 123534.125839 -3660.115530 8838.980201 102192.328154
46238.093564 39382.476514 30660.243612
65903.353060 Note high cost due to severe overloads on loss of line
←
```

### Step 4: OPF Iteration

SGOPT generates a direction and updates the control file as shown below. The SGOPT iteration was simulated manually and the lfcontrol.txt file after several iterations is shown on the next page.

### Step 5: Completed State Evaluation

Load is shed and the final lfstate file indicates the amount of load shed.

## File lfcontrol.txt for Example 2

```
Initial
10
300.000000 1.100000 1.100000 1.100000 30.000000 1.000000 1.000000 1.000000 1.000000 1.000000
20.000000 0.900000 0.900000 0.900000 -30.000000 0.000000 0.000000 0.000000 0.000000 0.000000
1 1 1 1 1 1 1 1 1 1
100.001640 1.040000 1.020000 0.971831 20.000000 1.000000 1.000000 1.000000 1.000000 1.000000
-60128.471336 375647.764746 119149.535284 123534.125839 -3660.115530 8838.980201
102192.328154 46238.093564 39382.476514 30660.243612
65903.353060
Cost is high due to overloads on loss of line

Iteration 1 Adjust generation

188.001640 1.040000 1.020000 0.971831 20.000000 1.000000 1.000000 1.000000 1.000000 1.000000
-222.167439 15207.799255 5171.151815 -3724.054671 -324.872919 209.406169 3397.724336
344.779709 1194.758690 2086.765804
2292.736211

Iteration 2 Drop Voltages(Compare example 1 where voltages were raised)

188.001640 1.000000 1.020000 0.971831 20.000000 1.000000 1.000000 1.000000 1.000000 1.000000
1757.503914 4520.244880 10656.076586 -1549.572525 -190.782722 209.517518 -29.259957 -
1040.993625 132.800759 1272.198984
2162.961563

Im[rovement but cost still high due to minor overloads

Iteration 2 Drop Voltages Further

188.001640 1.000000 1.000000 0.971831 20.000000 1.000000 1.000000 1.000000 1.000000 1.000000
-642.454858 4125.290135 -12239.433174 -9438.769126 -251.870842 209.782641 3408.024322
639.021016 2936.049472 2815.688165
2584.745247
oops.

Iteration 2 Drop Voltages(Compare example 1 where voltages were raised)

188.001640 1.000000 1.010000 0.971831 20.000000 1.000000 1.000000 1.000000 1.000000 1.000000
700.524417 4216.254451 496.446283 -5464.236126 -226.263639 209.636818 1572.887701 -
301.089423 1332.889917 1932.266285
2277.138628
Iteration 5 Change tap

188.001640 1.000000 1.010000 0.99 20.000000 1.000000 1.000000 1.000000 1.000000 1.000000
1652.133828 3779.959430 8059.455503 637.233659 -126.230579 209.628677 -517.857362 -
967.228396 825.108692 1543.425998
2202.564354

Iteration 6 Change phase

188.001640 1.000000 1.010000 0.99 25.000000 1.000000 1.000000 1.000000 1.000000 1.000000
1654.370526 3763.359769 8057.651375 640.584504 -125.998855 209.624020 -523.234115 -
968.794068 823.151988 1541.073033
2202.128240
Iteration 7 Shed load

185.001640 1.000000 1.010000 0.99 45.000000 1.000000 1.000000 1.000000 1.000000.96000000
1068.233378 1568.017983 3616.168365 588.502665 -60.046525 209.258532 -416.153344 -560.168986
597.482288 490.297930
2032.261486
Iteration 8

185.001640 1.000000 1.010000 0.99 45.000000 1.000000 1.000000 1.000000 1.000000.93000000
419.041494 723.544984 -84.143182 332.933081 -23.293035 207.474376 19.733503 -105.727793
541.610724 -187.048350
1971.453703
Iteration 9 Shed load

185.001640 1.000000 1.010000 0.99 45.000000 1.000000 1.000000 1.000000.960000.955000000
639.628063 961.511636 1839.435450 370.978685 -35.764499 206.931271 -127.836694 -260.142155
-87.190943 27.995380
1959.872750
Case is close to optimum. Load has been shed.
```

## File Ifstate.txt for Example 2

```
13
1 L 1 0.001000 1.000000
2 L 0 0.001000 1.000000
3 L 1 0.001000 1.000000
4 L 1 0.001000 1.000000
5 L 1 0.001000 1.000000
6 T 1 0.000600 1.000000
7 P 1 0.100000 1.000000
8 P 1 0.100000 1.000000
9 P 1 0.100000 1.000000
10 P 1 0.100000 1.000000
11 P 1 0.100000 1.000000
12 G 1 0.003000 1.000000
13 G 1 0.003000 1.000000
1 1.000000
2 1.000000
3 1.000000
4 0.960000 ← Load at bus 4 is 96% of nominal i.e., 4% has been shed
5 0.955000 ← Load at bus 5 is 95.5% of nominal i.e., 5.5% has been shed
```

### 4.3 Sample Application

This section illustrates the use of the uncertainty analysis package. We consider the system of Figure 4.2. It is assumed that each load in system is described by an independent random variable. The network however is fixed, i.e., line and generator outages are not considered.

The goal of the uncertainty analysis is to determine if these loads can be supplied. If there are combination in which load cannot be supplied then the amount of load shed is to be determined. Finally we wish to describe the probability of being able to supply load at a bus.

When running a Latin Hypercube sample analysis with CRAX/Cassandra, the user must give values for the random variables and the deterministic variables. The random variables are the five requested loads at different points in the network and for this example are all set to have a mean value of 1.0 and a coefficient of variation of .01. The deterministic variables represent the other elements of the power network (i.e., transmission lines, generators, etc.). Each of the 13 deterministic variables has a value of 1 or 0 representing on or off, respectively. For this example all elements are turned on (value 1) except Transmission Line 2, which is turned off (value 0). The user then chooses how many samples are to be generated and used in the analysis. For this example, one analysis is performed with 10 samples and a second analysis is performed using 100 samples. 10 and 100 sample vectors are generated respectively during an analysis. Each vector is made up of the five different loads. During the analysis, Cassandra passes each vector of random loads to the power-flow program which then returns a vector answer representing the percent of each load that is supplied. (1.0 meaning 100%). Cassandra then collects all the responses and presents them to the user as a cumulative distribution function of load shed for each load. These results can then be viewed by the user either in graphical form or as dials overlaid on a schematic of the network.

The results are as follows:

### 10 samples

load 1 no load shedding  
load 2 no load shedding  
load 3 no load shedding  
load 4 20% of samples shed 10% load  
load 5 80% of samples shed 10% load

### 100 samples

load 1 No load shedding  
load 2 No load shedding  
load 3 No load shedding  
load 4 about 22% of samples shed load starting at 5% and increasing to maximum of 10%  
load 5 about 98% of samples shed load starting at 5% and increasing to maximum of 10%

With 10 samples the loss of load probability for Bus 4 is about 20%; Using 100 samples improves the estimate to 22%.

## **5. Conclusions**

The work described here seeks to develop a reliability analysis methodology for large power systems. In the first phase, a literature review was conducted and a computer program developed to study the reliability of a power system using the Failure Modes and Effects Analysis (FMEA) technique. In the second phase, a physical model was formally integrated into the CRAX system to provide a sophisticated capability for reliability analysis.

The complete CRAX-based system has been ported and tested on SNL's DEC8400 parallel machine, which will allow studies of larger systems.

*We believe that, within limitations of model data and modeling assumptions, SNL can conduct credible reliability studies of large-scale power systems. Further development should position SNL as the "provider of choice" for enhancing the surety of energy infrastructures.*

To properly assess energy infrastructure surety, it will be necessary to properly model the key uncertainties in the power system, namely

- Component failures.
- Load and generation patterns in the deregulated market.
- Operating policies.

The current implementation supports the modeling of components failures. However, the comprehensive modeling of load/generation and operating policies should be investigated.

The key issue regarding the load is modeling the inherent uncertainty as well as *load shedding policy*. Market models are necessary to describe generation patterns. Finally operating policies will be dictated by how deregulation unfolds. All three areas are intricately tied into modeling the SCADA-based control systems. The central operator through the SCADA system becomes the clearinghouse for all control actions. Therefore, the principal extension needed is a SCADA model. In the remainder of this section, we speculate on this area.

Power systems are controlled by a central Energy Management Systems (EMS). These systems comprise of three subsystems, namely

- SCADA—Supervisory Control and Data Acquisition Systems which represents the monitoring, communication and control hardware used to open and close breakers, change transformer taps, etc.
- Real-time sequence (sometimes considered a part of SCADA)—this involves real-time control of generation including economic dispatch, state estimation, possibly very slow load shedding.
- Advanced Applications—These include state estimation, power flow, contingency analysis, and possibly unit commitment.

The EMS utilizes redundant computer and communication systems; at the very least a backup SCADA exists and is located at a separate geographical location.

The operator, through the EMS, can supervise and initiate several functions as listed below:

- Real-time control.
- Tactical control in responses to changing requirements or disturbances, e.g., adjusting taps based on voltages that are getting too high or low, rescheduling generators to eliminate overloads, etc. In some instances, the real-time power-flow function is used, but by and large, a set of predetermined rules is provided to the operator.
- Strategic control: The operator, using advanced applications or predetermined procedural rules, can open/close devices, change generation, etc., so credible disturbances will not cause failure.

With this as background, one can speculate on the need for and means to model EMS/SCADA in reliability studies and uncertainty analyses. In conventional system modeling one assumes that, within appropriate time frames, control action can be exercised in response to disturbance, in order to mitigate overloads or poor voltages, or collapse. Thus, if we wish to determine if a certain system state can supply a certain load, then the power-flow model is solved assuming that generation can be rescheduled or taps can be changed. Absent an operator with SCADA capability, this assumption is not valid, and the state may turn out to be a failed state. It certainly appears that EMS/SCADA modeling may be desirable.

## References

1. Schilling, M., Leite De Silva, A., Billinton, R., El-Kady, M., "Bibliography on Power System Probabilistic Analysis (1962-1988)," IEEE Transactions on Power Systems, Vol. 5, No. 1, February 1990, pp. 41–49.
2. Allan, R. Billinton, R., Breipohl, A., Grigg, C., "Bibliography on the Application of Probability Methods in Power System Reliability Evaluation 1967-1991," IEEE Transactions on Power Systems, Vol. 9, No. 1, February 1994, pp. 41–49.
3. Pereira, m., Balu, N., "Composite Generation/Transmission Reliability Evaluation," Proc. IEEE, Vol. 80, No. 4, April 1992, pp. 470–49.
4. "Reliability Assessment of Composite Generation and Transmission Systems," IEEE Tutorial Course 90EH0311-1-PWR, Feb. 1990.
5. APM Bulk Power Indices Task Force, Sub-Task Force on Future Needs, "Bulk Power System Reliability Criteria and Indices Trends and Future Needs," IEEE Transactions on Power Systems, Vol.9, No. 1, February 1994, pp. 181–188.
6. Porretta, B., Neudorf, E. "Conceptual Framework for Evaluation and Interpretation of the Reliability of the Composite Power System," IEEE Transactions on Power Systems, Vol.10, No. 2, May 1995, pp. 1094–1103.
7. Reliability, Risk and Probability Applications Subcommittee, "Reliability Issues in Today's Electric Power Utility Environment," IEEE Transactions on Power Systems, Vol.12, No. 4, November 1998, pp. 1708–1712.
8. McCalley, J., Fouad, A., Agrawal, B., Farmer, R.G., "A Risk-based Security Index for Determining Operating Limits in Stability-Limited Electric Power Systems," IEEE Transactions on Power Systems, Vol.12, No. 3, February 1997, pp. 1210–16.
9. Lee, F., Lin, M., Briehpol, A., "Comparison of Probabilistic Production Costing Simulation Methods," IEEE Transactions on Power Systems, Vol.4, No. 4, November 1989, pp. 258–264.
10. Meliopolous, A., Xia, X, "Method for Probabilistic Simultaneous Transfer Capacity Analysis," IEEE Transactions on Power Systems, Vol.11, No. 3, November 1996, pp. 258–264.
11. Allan, R., "Effects of Protection Systems Operations and Failures in Composite System Reliability Evaluation," Electric Power and Energy References Systems Journal, Vol. 10, No. 3, July 1988, pp. 180–189.

12. "Bulk System Reliability- Predictive Indices," IEEE Task Force on Predictive Indices, IEEE Transactions on Power Systems, Vol. 5, No. 4, October 1990, pp.1204–13.
13. "Bulk System Reliability - Measurement and Indices, A Report by the IEEE Working Group on Measurement and Indices," IEEE Transactions on Power Systems, Vol. 4, No. 3, August 1989, pp. 829–835.
14. Singh, C., "Calculating the Time-specific Frequency of System Failure," IEEE Transactions on Reliability, Vol. R-28, 1979, pp. 20–29.
15. Wu, F., Tsai, Y., Yu, Y. "Probabilistic Steady-State and Dynamic Security Assessment," IEEE Transactions on Power Systems, Vol. 3, No. 1, February 1988, pp. 1–9.
16. Kanetkar, J., Ranade, S. "Compact Representations of Power System Security--A Review," Proc. 24th North American Power Symposium, Reno, NV, October 1992, pp. 310–321.
17. Salvaderi, L., Billinton, R., "A Comparison Between Two Fundamentally Different Approaches to Composite Reliability Evaluation," IEEE Transactions on Power Apparatus and Systems, Vol. PAS-104, No. 12, December 1985, pp. 3486–92.
18. Rios, M., Vidal, V., Kiguel, D., "Bus-Based Reliability Indices and Associated Costs in Electric Power Systems," IEEE Transactions on Power Systems, Vol.13, No. 3, August 1998, pp. 41–46.
19. C. Singh, Kim, Y., "An efficient Technique for Reliability Analysis of Power Systems Including Time Dependent sources," IEEE Transactions on Power Systems, Vol.3, No. 3, August 1988, pp. 1090–96.
20. Dodu, J. Merlin, A., "An Application of Linear Programming to the Planning of Large-Scale Power Systems MEXICO Model," Proc. 5<sup>th</sup>. PSCC, Cambridge, September 1975. Pereira, M, Pinto, L, "A New Computational Model for Composite Reliability Evaluation," IEEE Transactions on Power Systems, Vol.7, No. 1, February 1992, pp. 258–264.
21. Leite da Silva, A., Endrenyi, J., Wang, L., "Integrated Treatment of Adequacy and Security In Bulk Power System Reliability Evaluation," IEEE Transactions on Power Systems, Vol.3, No. 1, March 1993, pp. 275–282.
22. EPRI Report, RP1530-1, July 1982.
23. Meliopoulos, A., Bakirtizis, A., Kovacs, R., Beck, R., "Bulk Power System Reliability Assessment Experience with the RECS Program," IEEE Transactions on Power Systems, Vol.3, No. 1, March 1993, pp. 275–282.

24. Reliability Task Force of the Application of Probability Methods Subcommittee, "IEEE Reliability Test System," IEEE Transactions on Power Apparatus and Systems, Vol. PAS-98, No. 6, Nov./Dec. 1979, pp. 2047–2054.
25. Allan, R., Billinton, R., Abdel-Gawad, N., "The IEEE Reliability Test System-Extensions to and Evaluation of the Generation System," IEEE Transactions on Power Systems, Vol.7, No. 4, November 1986, pp.1–7.
26. IEEE RTS Task Force of the APM Subcommittee "The IEEE Reliability Test System 1996" IEEE PES Winter Meeting Paper 96 WM326-9 PWRS, Baltimore, MD, Jan. 21–25, 1996.
27. Robinson, D. G., "CRAX/CASSANDRA Reliability Analysis Software," AIAA-99-1594.

# **Appendix C**

## **Probabilistic Analysis of Rechargeable Batteries in a Renewable Energy Supply System**

Angel Urbina and Thomas L. Paez  
Information, Computation, and Engineering Sciences Division  
Rudolph G. Jungst  
Weapon Systems Division  
Sandia National Laboratories  
Albuquerque, NM 87185

### **ABSTRACT**

The objective of this project is to develop a working model of a renewable energy generation/rechargeable battery storage system so these components can be included in calculations to estimate the reliability of the United States electricity grid system under different outage scenarios. This modeling capability will allow the reliability benefit of renewable generation to be quantified as well as providing a tool to optimize the design of these systems. Our work has focused on a specific system comprised of a photovoltaic generator and a lead-acid battery. We present in this report the various methods that were investigated for predicting the solar resource, the development of a robust damage model for the lead-acid battery and the translation of the existing MATLAB<sup>®</sup> code to C<sup>++</sup> and its subsequent integration into a power-flow calculation.



## Contents

1.0	Introduction.....	C-5
2.0	Renewable Generation System Characteristics .....	C-5
3.0	Summary of Fiscal Year 1998 Work.....	C-6
3.1	Solar Resource Model Development.....	C-6
3.2	Lead-Acid Rechargeable Battery Modeling.....	C-8
3.3	Sample Calculation.....	C-9
4.0	Summary of Fiscal Year 1999 Work.....	C-12
4.1	The Solar Resource Model.....	C-13
4.2	The Rechargeable Battery Model.....	C-16
4.3	Reliability Analysis.....	C-21
4.4	C <sup>++</sup> Code Translation.....	C-23
5.0	Summary of Work for Fiscal Year 2000.....	C-23
5.1	Canonical Variate Analysis.....	C-23
5.2	Test Case and Results.....	C-25
5.3	Code Integration into Power-Flow Model.....	C-26
5.4	EIS Measurements on Lead-Acid Batteries.....	C-29
6.0	Conclusions.....	C-34
	References.....	C-36
	Appendix C.1: Lead-Acid Battery Diagnostics – Literature Search on Electrochemical Impedance Spectroscopy.....	C-40
	Appendix C.2: GNB Sunlyte™ 12-5000× Battery Test Plan.....	C-47

## Figures

Figure 3.1.	The Initial Battery Damage Model.....	C-9
Figure 3.2.	Charge/Discharge Time History.....	C-10
Figure 3.3.	Maximum Potential Capacity.....	C-10
Figure 3.4.	PDF on M(t) (@ hour 1000).....	C-11
Figure 3.5.	PDF on M(t) (@ hour 6000).....	C-11
Figure 4.1.	Cartesian Space of Direct Normal and Diffuse Horizontal Radiation (day, j).....	C-13
Figure 4.2.	Cartesian Space of Direct Normal and Diffuse Horizontal Radiation (day, j+1).....	C-13
Figure 4.3.	Mean Curve Comparison for August.....	C-16
Figure 4.4.	Mean Curve Comparison for December.....	C-16
Figure 4.5.	The Battery Damage Model.....	C-18
Figure 4.6.	Local Polynomial Models.....	C-20
Figure 4.7.	First Passage Probability of M <sub>c</sub> (t) (tilt angle = 21°).....	C-22
Figure 5.1.	Measured Total Hourly Insolation for January 1978.....	C-26
Figure 5.2.	Simulated Total Hourly Insolation for 31 January Days.....	C-26
Figure 5.3.	PV Generator Interface Diagram.....	C-27

Figure 5.4. Sample Power Grid.....	C-28
Figure 5.5. Impedance of Power Sonic PS-4100 Batteries Fully Charged at 4.3 V.....	C-30
Figure 5.6. Impedance of Power Sonic PS-4100 Batteries at About 50% SOC.....	C-30
Figure 5.7. Impedance of Power Sonic PS-4100 Batteries at About 0% SOC.....	C-31
Figure 5.8. Impedance of Hawker Cyclon Batteries near Full Charge (11.83 V). ....	C-32
Figure 5.9. Impedance of Hawker Cyclon Batteries at About 50% SOC.....	C-32
Figure 5.10. Impedance of Hawker Cyclon Batteries at About 25% SOC.....	C-33
Figure 5.11. Impedance of Hawker Cyclon Batteries at About 0% SOC.....	C-33

## 1.0 Introduction

The goal of this project in the Power Grid Reliability LDRD is the development of a working model for a renewable energy generation and storage system that can then be included as one of the components in a calculation of power flow for a significant portion of the U.S. electricity grid. An overall objective is to be able to use the electricity grid model to estimate the reliability of the grid system under different outage scenarios. Distributed renewable generation and storage has been suggested as a method for improving grid reliability and this modeling capability will allow that benefit to be quantified. The most effective locations on the grid for distributed generation and storage can also be investigated.

Although some commercial software is available to carry out some types of power-flow calculations for portions of the electricity grid, it does not contain a representation for renewable generators. Additionally, it is desirable to include energy storage devices along with the renewable generator since storage allows for dispatchability beyond the periods when the renewable resource (photovoltaics (PV), wind, etc.) is available. Existing software is not capable of modeling the behavior of energy storage over time in a typical renewable energy cycling environment (or in other applications, for that matter). The challenge is then to construct an accurate, flexible renewable generator model that will be computationally efficient enough to be used with the larger power-flow model for grid reliability calculations. Earlier attempts have been made to characterize portions of a renewable system (e.g., the solar resource, flat plate PV collectors), but a complete and efficient generator model has previously not been constructed for high-speed calculations. Some components of the system have not in the past even been modeled in a way that is useful for the purposes of this effort. This is particularly true for the energy storage system, where some performance models existed for batteries, but they did not include the degradation factors that can rapidly accumulate under typical renewable generation profiles.

Meeting these project goals, therefore, required new developments in a number of areas. These included the accurate realizations of the renewable resource in a computationally efficient manner, modeling of the damage to energy storage devices that results from use in a renewable energy operating environment, and integration of several analysis codes. None of these had previously been accomplished. In addition, a new artificial neural network structure developed at Sandia for good robustness and accuracy in nonlinear situations was applied to this type of problem for the first time.

## 2.0 Renewable Generation System Characteristics

Different renewable energy sources (PV, wind, etc.) and energy storage devices (battery, capacitor, flywheel, superconducting magnetic energy) could be envisioned as a combined system. Because they have been more commonly fielded and some efforts have previously been made to describe the output profiles, a PV/battery combination has been chosen for this initial study. However, the general architecture of the model is expected to be compatible with a variety of renewable generation/storage combinations so that it can be easily expanded to include them in the future.

Photovoltaics describes a technology in which radiant energy from the sun is converted to direct current (DC) electricity. This electricity can be used directly, stored in batteries, or fed into an electric utility's grid system. Although the scientific basis of the photovoltaic effect has been known for nearly 150 years, the modern photovoltaic cell was not developed until 1954. Only four years later, the first cells were providing power for U.S. spacecraft. Some of these early systems are still operating in space today and attest to the reliability and durability of the technology. Most solar cells are made of silicon semiconductor material treated with special additives. When the sunlight strikes the cells, a flow of electrons is generated proportional to the intensity of the sunlight and the area of the cell. A solar cell 10 cm. on a side will produce about 3.5 amperes in full sunlight. Each solar cell produces approximately one-half volt. Higher voltages are obtained by connecting the solar cells in series. The typical photovoltaic module used for terrestrial applications contains 36 silicon solar cells, which when connected in series provides enough voltage to charge a 12-volt battery.

Photovoltaic modules produce electricity for a connected load when the sun is shining – some electricity is even produced on cloudy days. However, for many applications electrical energy is needed at night so storage batteries are required. In these cases, the photovoltaic system can be considered an uninterruptible power supply with battery charging provided daily by the photovoltaic modules. Lead-acid batteries are widely used as the storage device mainly due to their relatively low cost, good performance and generally adequate cycle life.

It is important to understand the specific requirements of batteries when designing a PV system. This includes an understanding of the amount of energy that will be produced by the PV array and the amount of energy lost in battery charging. Overestimating these battery charging losses results in a larger PV array than required, whereas underestimating them results in unanticipated loss of load support as well as the possibility of damaging the batteries due to an inability to provide a periodic recharge to a high state-of-charge. The failure modes and the circumstances under which they occur have not been clearly identified. These failures are irreversible in field applications, and when they occur, the battery must be replaced. Since the application in PV systems requires a reliable battery system, it is of critical importance to predict the battery performance and to be able to identify any degradation as it occurs.

### **3.0 Summary of Fiscal Year 1998 Work**

The following sections summarize the work accomplished on the project during FY98. During this time frame, the groundwork was set to develop software that will analyze the behavior of rechargeable batteries as they act as the energy storage medium in a photovoltaic system. The major areas that were investigated during this period were the solar resource component and the rechargeable battery component.

#### **3.1 Solar Resource Model Development**

The first step was to conduct a literature search to identify the type of solar data that was readily available. The database compiled by the National Renewable Energy Laboratories (NREL) based in Golden, Colorado, and entitled National Solar Radiation Database (NSRDB) [1] covering the

period from 1961 through 1990 was used in this study. In this database, there are values of global, direct, and diffuse solar radiation (either measured with a pyranometer or calculated) that were used to develop the solar insolation model described in subsequent sections. The NSRDB was selected because (1) it is easily accessible (the data are available through the Internet) and (2) the database contains hourly records of the main components of the solar resource.

With this available database, it was necessary to reduce the data to accommodate the parameters of various solar collectors. An additional literature search yielded a set of existing mathematical models that served this purpose [2,3,4 and 5]. Using the basic solar measurements, a series of models were used to calculate the solar energy received by a flat plate collector tilted at any angle and located at an arbitrary latitude. Equation 3.1 identifies the fundamental quantities and their relation:

$$E_o = E_{bc} + E_d + E_{gr} \quad (3.1)$$

where  $E_o$  is the total solar energy received by an inclined plane,  $E_{bc}$  is the direct beam contribution,  $E_{gr}$  is the ground reflected energy, and  $E_d$  is the diffuse (or sky) energy. These quantities were calculated using a series of deterministic models, which accounted for the latitude and orientation of the collector.

An objective of this study is to perform a probabilistic analysis in a Monte Carlo framework and solve some preliminary problems in the probabilistic characterization of system behavior. Previous attempts to model the various components of the solar data have been attempted with various degrees of success. Aguiar et al. have used a stochastic technique using Markov chains to generate daily solar radiation data via the simulation of clearness indices [6]. Knight et al., described a similar approach with the incorporation of a first-order autoregressive model [7]. Aguiar et al., described an ARMA (Auto-Regressive Moving Average)-based model to simulate hourly radiation sequences [8]. Finally, Remund et al., described a combination of models including stochastic and deterministic models to simulate hourly short-wave radiation data [9]. In this study, a different approach was chosen to capture the stochastic nature of the solar data. We chose a bivariate, first order Markov chain to simulate two of the main components of the solar radiation: the direct normal radiation and the diffuse horizontal radiation. This approach takes advantage of the measured data without the need to calculate an intermediate parameter, such as the clearness index. The underlying framework for the Markov chain creates bins for the joint values of the diffuse horizontal radiation and the direct normal radiation at each hour and identifies the system state according to the bin occupied by the radiation value at that hour. The probability mass function (PMF) specifying the chance that the system-state occupies a particular bin at a particular hour is known as the state probability. The objective in using the Markov chain is to determine the state probabilities at all times, for all measures of behavior of interest, for the system under consideration. This is accomplished, in the Markov chain framework, by specifying the initial state PMF, estimating (or otherwise deriving) the transition PMF, and using the two to propagate state probabilities through time. Some attractions of the Markov chain framework for analyses are (1) that the state probabilities need not follow a normal law and (2) that the procedure for propagation of the state probabilities is simple, fast, and efficient. This technique was implemented by writing a series of MATLAB<sup>®</sup> [10] functions and the resulting simulations had an acceptable degree of accuracy when compared to the actual data.

### 3.2 Lead-Acid Rechargeable Battery Modeling

One focus of the overall investigation is to characterize the probabilistic behavior of rechargeable batteries that are recharged from a renewable source that provides power in random increments. Further, we narrowed our focus more by concentrating on the damage that can accumulate in rechargeable batteries, specifically lead-acid batteries, when they are subjected to deep discharge use cycles that last for significant periods of time. In particular it is known that when rechargeable lead-acid batteries remain at a low state of charge, the maximum potential capacity can be diminished. The maximum potential capacity is defined as the maximum amount of energy that a battery can store at a particular time. This value will not always be equal to the initial capacity of the battery since damage introduced by long duration discharges will tend to degrade the maximum potential capacity of the battery. This will eventually lead to battery failure. In view of these things, we developed a framework to model battery state of charge and maximum potential battery capacity as functions of time. We introduced the damage effect that occurs during discharge via a non-positive function of duration of discharge and depth of discharge (DOD). Because the form of this function is unknown, we modeled it with an artificial neural network (ANN) whose parameters are trained with experimental data. O’Gorman et al., [11] and Paez and Hunter [12] have successfully modeled battery performance and other complex systems using ANNs, thus providing a motivation to incorporate the ANN methodology into this study. A detailed presentation of the various types of ANNs is given in Freeman et al. [13]. At the initial stage of the study, the ANN model was trained with data we considered plausible since sufficient experimental data did not exist. We introduced notation for the current demanded from the battery,  $I_B(t)$ , and the recharge current available to the battery,  $I_R(t)$ , for use in the development of the system’s governing equations [14]. In terms of these quantities, the state of charge in the rechargeable battery can be expressed as:

$$C(t) = \begin{cases} \int_{t_0}^t \gamma(\tau) [I_R(\tau) - I_B(\tau)] d\tau + C(t_0) & t \geq t_0, C(t) \leq M_C(t) \\ M_C(t) & \text{otherwise} \end{cases} \quad (3.2)$$

The function  $M_C(t)$  is the maximum potential battery capacity at time  $t$ . The function  $\gamma(t)$  is the recharge efficiency that establishes the rate at which recharge can occur. In general, as a lead-acid battery nears its maximum potential capacity,  $\gamma(t)$  approaches zero, and at lower capacity levels  $\gamma(t)$  is near one. Battery testing would be required in the future to establish the specific form and parameters of this function (a plausible form for  $\gamma(t)$  was initially chosen).

Because the function  $M_C(t)$  tracks the maximum potential battery capacity as a function of time and because we take damage to a lead-acid battery caused by discharge as irreversible when used in a photovoltaic application,  $M_C(t)$  must be a monotone non-increasing function. We choose the following as the form for  $M_C(t)$ :

$$M_C(t) = \int_{t_0}^t \delta_M(\tau) d\tau + M_C(t_0) \quad t \geq t_0 \quad (3.3)$$

The function  $\delta_M(t)$  must be non-positive and must indirectly characterize damage to the maximum potential capacity of the rechargeable battery during discharge. For present purposes

we assume that  $\delta_M(t)$  is a function of the time duration of a discharge above a threshold,  $T(t)$ , and the depth of discharge above a threshold,  $D(t)$ . Therefore, we write

$$\delta_M(t) = g_\delta(T, D) \quad (3.4)$$

We specify that  $g_\delta(T, D)$  is zero for  $T(t)$  below its threshold value or  $D(t)$  below its threshold value, but beyond this we do not know the exact form of  $g_\delta(T, D)$ . It is anticipated that an explicit form for  $g_\delta(T, D)$  cannot be easily derived, so we choose to model the function using an ANN. In this phase of the project, we used a particular form of the layered perceptron [13] ANN to model  $g_\delta(T, D)$ . The advantage of using an ANN here is that given sufficient training data, it learns rapidly. Further, ANNs are accurate and efficient. The initial battery damage model used to model  $g_\delta(T, D)$  in this investigation is shown in Figure 3.1. This model will be only applicable to the particular type of battery used in this project.

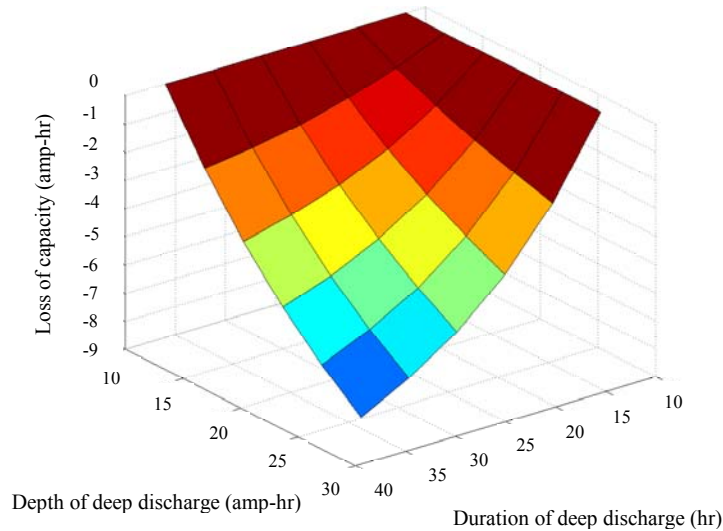


**Figure 3.1. The Initial Battery Damage Model.**

### 3.3 Sample Calculation

The analyses performed were done within the Monte Carlo framework, that is, simulations of the random processes of interest were performed, and realizations were generated and stored (see Figures 3.2 and 3.3). Statistical analyses were then performed on the realizations (Figures 3.4 and 3.5). Here the probability density functions (PDF) at two selected hours are shown.

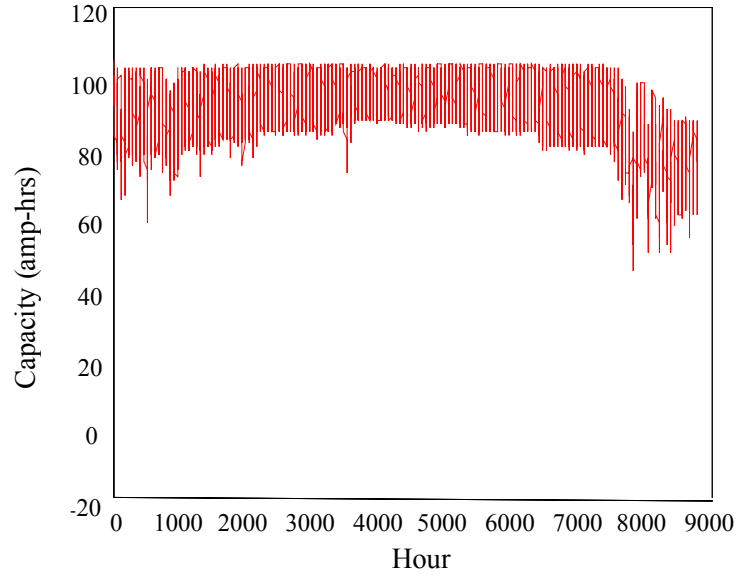


**Figure 3.2. Charge/Discharge Time History.**

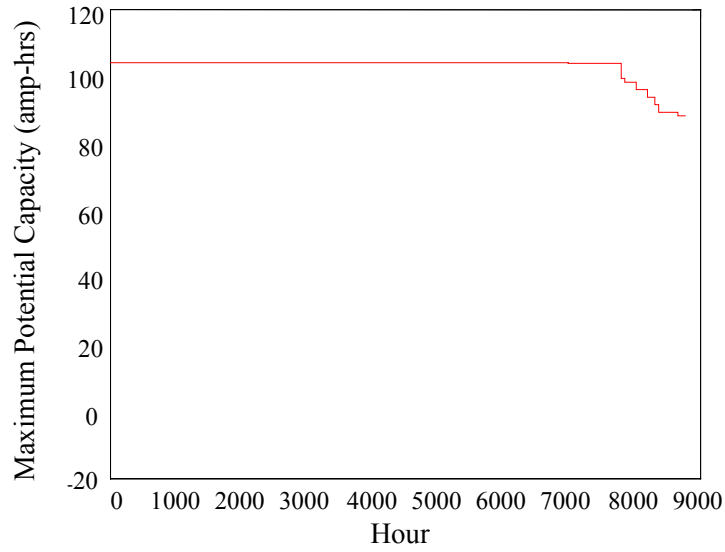


**Figure 3.3. Maximum Potential Capacity.**

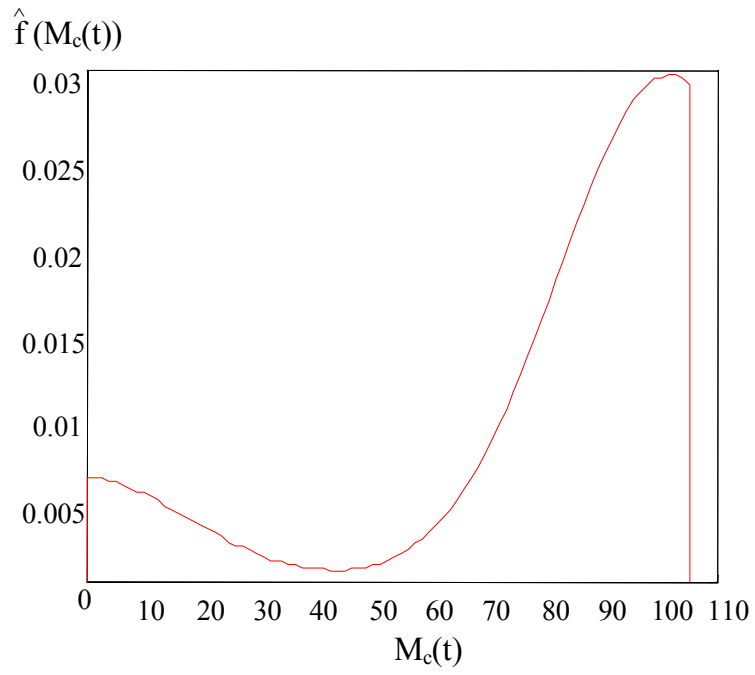


**Figure 3.4. PDF on  $M(t)$  (@ hour 1000).**

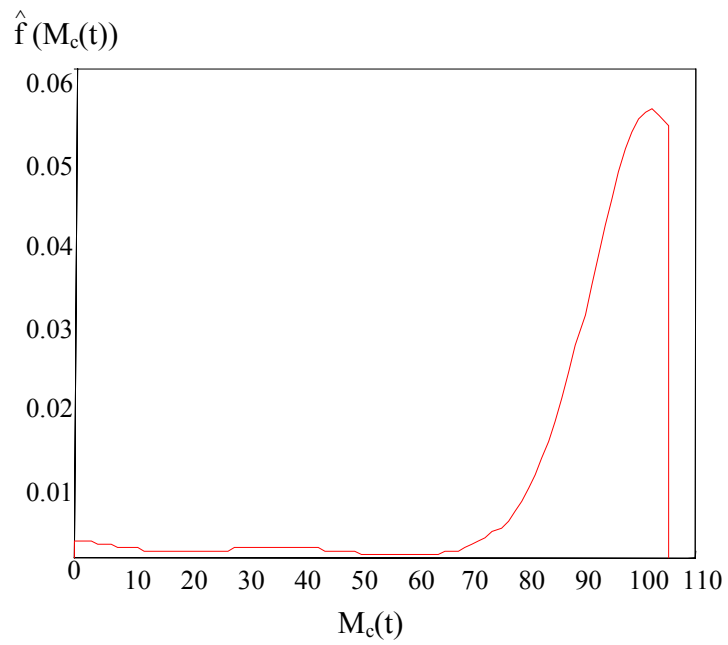


**Figure 3.5. PDF on  $M(t)$  (@ hour 6000).**

The fundamental subprocess modeled as random in this study is the insolation random process. The randomness included in this sub-model causes the simulated quantities of interest in the overall model to also behave randomly; thus, the probabilistic nature of the photovoltaic power supply/energy storage system was established in the initial phase of the project.

#### **4.0 Summary of Fiscal Year 1999 Work**

The comprehensive stochastic-based model for the analysis of a renewable power supply/energy storage/load system that was developed in FY98 was improved in FY99. Several mathematical techniques, including stochastic, deterministic, and artificial neural network models, were used to develop this simulation capability. These models were combined and solved simultaneously in the Monte Carlo framework to generate realizations of the system behavior.

The solar resource prediction model now uses a kernel density estimation (KDE) approach and a daily radiation analysis was implemented for improved efficiency and robustness. Computational time has been reduced and stability increased. Groundwork for an improved energy-storage device damage model has been laid in several areas. A literature search has been completed on applications of electrochemical impedance spectroscopy (EIS) to lead-acid batteries as a diagnostic technique. A test plan has been written for the collection of impedance data and cycle testing of GNB 12-5000X photovoltaic reserve batteries in order to gather more experimental battery damage data. The multivariate polynomial spline ANN is now being used to model the battery damage surface. This provides better accuracy and capability to handle very nonlinear behavior. A preliminary reliability analysis has been performed on the PV/battery system. Finally, the code for the renewable generator model was successfully translated from MATLAB<sup>®</sup> to C<sup>++</sup>. This has reduced processing time and will enhance portability of the code for use with other software. This is a major step for it will allow the integration of our software into the power flow model (see Appendix B). Work activities pursued during FY99 are discussed in the following subsections and are summarized as follows:

1. Improve the accuracy and computation efficiency of the Markov transition matrices.
2. Make the theoretical battery damage surface more realistic.
3. Acquire literature data on lead-acid battery impedance diagnostic and upgrade equipment necessary to perform these measurements on a PV-size battery.
4. Improve the training algorithm and accuracy of the multivariate polynomial spline.
5. Perform initial reliability studies of the rechargeable battery component.
6. Translate MABLAB<sup>®</sup> analysis code into C<sup>++</sup> language.

## 4.1 The Solar Resource Model

The solar resource model was modified to improve its accuracy and efficiency. In the following paragraphs, we describe a different approach in which the Markov transition matrices (MTMS) are created to capture the daily variation in the solar insolation.

In FY99, a new approach based on using the daily solar insolation to calculate the Markov transition matrices was developed and implemented. This technique proved to be computationally more efficient and more accurate than previous techniques. We begin this analysis by considering the total amount of direct normal and diffuse horizontal radiation for each day of a particular month. It is noted that the random variables representing direct normal solar radiation and diffuse horizontal radiation are dependent, and that their joint probability distribution is non-Gaussian. A bivariate Markov chain was again chosen to model the solar radiation phenomenon. A detailed description of a Markov chain can be found in Isaacson et al. [15]. The Cartesian space of daily direct normal solar radiation and diffuse horizontal radiation can be subdivided into a rectangular grid like the one shown in Figure 4.1.

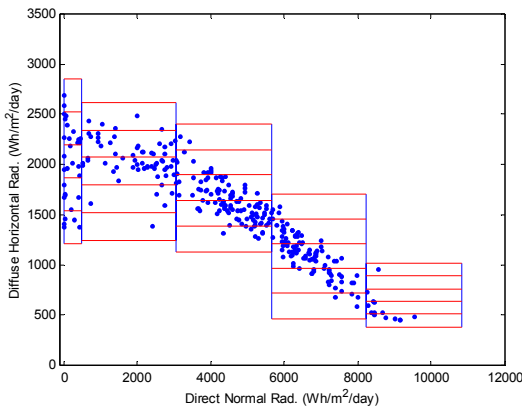


**Figure 4.1. Cartesian Space of Direct Normal and Diffuse Horizontal Radiation (day,  $j$ ).**

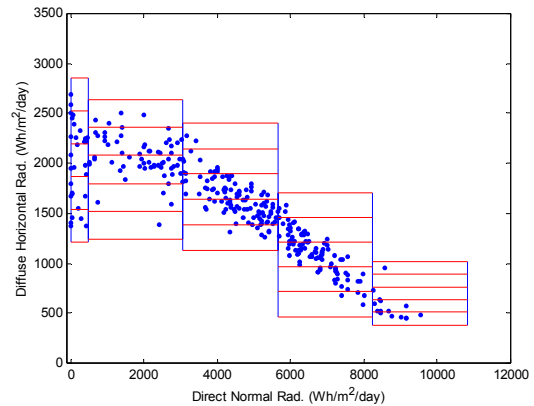


**Figure 4.2. Cartesian Space of Direct Normal and Diffuse Horizontal Radiation (day,  $j+1$ ).**

The data points in Figure 4.1 are 310 realizations of direct solar radiation and diffuse horizontal radiation, and the rectangles group the radiation realizations into states of the Markov chain. Furthermore, Figure 4.1 shows data that spans between January 1 through January 31 for ten years. Figure 4.2 is similar to Figure 4.1 but covers the period between January 2 through February 1 (also for ten years of data).

At any time, the solar radiation stochastic process occupies a state, and there is a probability mass function that describes the chance that each of the states is occupied. This is the state probability mass function, denoted  $p_j$ , and defined as

$$\mathbf{p}_j = \begin{cases} P(\mathbf{X}_j = \mathbf{s}_1) \\ P(\mathbf{X}_j = \mathbf{s}_2) \\ \vdots \\ P(\mathbf{X}_j = \mathbf{s}_N) \end{cases} \quad j = 0, \dots, n-1 \quad (4.1)$$

where  $P(j)$  indicates the probability of the event described in parentheses,  $\mathbf{X}_j$  is a random variable in the random process  $\{\mathbf{X}_j, j = 0, \dots, n-1\}$  that is the bivariate Markov chain, and  $\mathbf{s}_i, i = 1, \dots, N$ , are the system states.

The probability that the solar radiation random process state transitions from  $\mathbf{s}_{i_1}$  at analysis time  $j$ , to  $\mathbf{s}_{i_2}$  at analysis time  $j+1$  is given by the conditional probability mass function  $P(\mathbf{X}_{j+1} = \mathbf{s}_{i_2} | \mathbf{X}_j = \mathbf{s}_{i_1})$ , and the collection of all these transition probabilities is the transition matrix

$$\mathbf{P}_{j+1|j} = \begin{bmatrix} P(\mathbf{X}_{j+1} = \mathbf{s}_1 | \mathbf{X}_j = \mathbf{s}_1) & P(\mathbf{X}_{j+1} = \mathbf{s}_1 | \mathbf{X}_j = \mathbf{s}_2) & \dots & P(\mathbf{X}_{j+1} = \mathbf{s}_1 | \mathbf{X}_j = \mathbf{s}_N) \\ P(\mathbf{X}_{j+1} = \mathbf{s}_2 | \mathbf{X}_j = \mathbf{s}_1) & P(\mathbf{X}_{j+1} = \mathbf{s}_2 | \mathbf{X}_j = \mathbf{s}_2) & \dots & P(\mathbf{X}_{j+1} = \mathbf{s}_2 | \mathbf{X}_j = \mathbf{s}_N) \\ \vdots & \vdots & \ddots & \vdots \\ P(\mathbf{X}_{j+1} = \mathbf{s}_N | \mathbf{X}_j = \mathbf{s}_1) & P(\mathbf{X}_{j+1} = \mathbf{s}_N | \mathbf{X}_j = \mathbf{s}_2) & \dots & P(\mathbf{X}_{j+1} = \mathbf{s}_N | \mathbf{X}_j = \mathbf{s}_N) \end{bmatrix} \quad (4.2)$$

where  $j = 0, \dots, n-2$ .

The transition probability matrix and the state probability mass function at time zero are sufficient to establish the probability mass functions for states at all times because of the following relation

$$\mathbf{p}_{j+1} = \mathbf{P}_{j+1|j} \mathbf{p}_j \quad \text{for } j = 0, \dots, n-2 \quad (4.3)$$

The solar radiation random process is started on the first day of the month and  $\mathbf{p}_0$  is chosen from a uniform distribution in  $[0,1]$ .

The objective is to use measured solar radiation data to estimate the transition probability matrices of Equation 4.2. Let the data representing realizations of the system state at a particular day, and during a particular month, and the corresponding data measured during the following day be denoted by  $\mathbf{x}_j, \mathbf{y}_j$ , for  $j = 1, \dots, m$ , respectively. If data measured over a period of 10 years are used here, and the month under consideration is January, then  $m = 310$ . For example the  $\mathbf{x}_j$  might be two-element vectors; the first element represents the direct normal radiation and the second element represents the diffuse horizontal radiation on a particular day. The  $\mathbf{y}_j$  represent the same quantities one day later. (We assume that the data have been normalized prior to this analysis.) The joint probability density function (PDF) of the source of these two dependent quantities can be approximated using the kernel density estimator (KDE):

$$\hat{f}_{xy}(x, y) = \frac{1}{\sqrt{2\pi\varepsilon}} \sum_{j=1}^m \Phi\left(\frac{y-y_j}{\varepsilon}\right) \exp\left(-\frac{1}{2\varepsilon^2}(x-x_j)^2\right) \quad (4.4)$$

For details on the KDE see Silverman, et al. [16]. Likewise, the marginal PDF of the random variable that is the source of the  $\mathbf{x}_j, j = 1, \dots, m$ , can be approximated with the KDE:

$$\hat{f}_x(x) = \frac{1}{\sqrt{2\pi\varepsilon}} \sum_{j=1}^m \exp\left(-\frac{1}{2\varepsilon^2}(x-x_j)^2\right) \quad -\infty < x < \infty \quad (4.5)$$

Now, the conditional PDF of the random variable  $y$  given the random variable  $x$  is defined as:

$$f_{(y|x)}(y|x) = \frac{f_{xy}(x, y)}{f_x(x)} \quad -\infty < y < \infty \quad (4.6)$$

And the conditional cumulative distribution function (CDF) of  $y$  given  $x$  can be obtained by integrating the conditional PDF:

$$F_{(y|x)}(y|x) = \int_{-\infty}^y f_{y|x}(\theta|x) d\theta \quad -\infty < y < \infty \quad (4.7)$$

In view of this, the KDEs of Equations 4.4 and 4.5 can be used to approximate the conditional CDF of  $y$  given  $x$ . It is:

$$\hat{F}_{y|x}(y|x) = \frac{\sum_{j=1}^m \Phi\left(\frac{y-y_j}{\varepsilon}\right) \exp\left(-\frac{1}{2\varepsilon^2}(x-x_j)^2\right)}{\sum_{j=1}^m \exp\left(-\frac{1}{2\varepsilon^2}(x-x_j)^2\right)} \quad -\infty < y < \infty \quad (4.8)$$

where  $\Phi(\cdot)$  is the CDF of the standard normal random variable, and  $\varepsilon$  is the smoothing factor of the KDEs. This approach can be used, along with the definition of the state boundaries to approximate the transition probability matrices. The Markov chain model can be used in a Monte Carlo framework to generate as many daily realizations of the random process as desired.

The next step is to calculate the average radiation profile from the data to obtain a curve describing the hourly radiation profile for each day within a month. The radiation values are normalized so that the integral under the curve equals one. To generate an hourly profile, the following operations are performed:

1. Using the Markov chain model a value for the daily direct normal and diffuse horizontal radiation is obtained.
2. From the given data, the average radiation profile (for each component) is calculated; this results in a “backbone” curve describing the mean hourly radiation for each month.

- Using the daily direct normal and diffuse horizontal radiation values, the “backbone” curve’s y-values are scaled so that the integral under this curve equals the daily radiation values.
- Using a series of deterministic equations, the hourly values of direct normal and diffuse horizontal radiation are transformed to the total insolation received by a solar collector located at a particular latitude and with a certain orientation.

Using the above procedure, a numerical example was run for a location in Honolulu, Hawaii (latitude  $21^{\circ} 20' N$ ) and for a collector tilted at latitude angle. The monthly mean curves for the simulated ten years of data are compared to the actual ten years of data. Two months (August and December) are shown in Figures 4.3 and 4.4. The actual data are shown as a solid line while the simulated data are shown as a dashed line. Also the mean plus one standard deviation is shown as a plus sign (+) and the mean minus one standard deviation is shown as a circle (o).

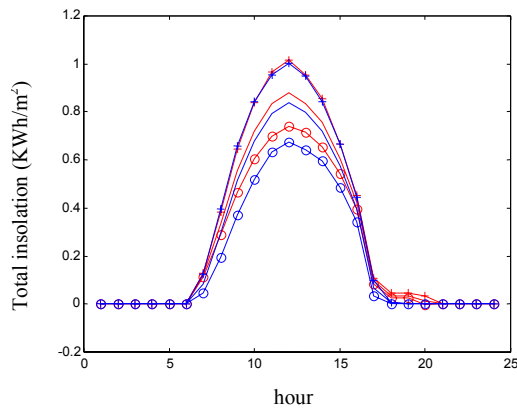


**Figure 4.3. Mean Curve Comparison for August.**

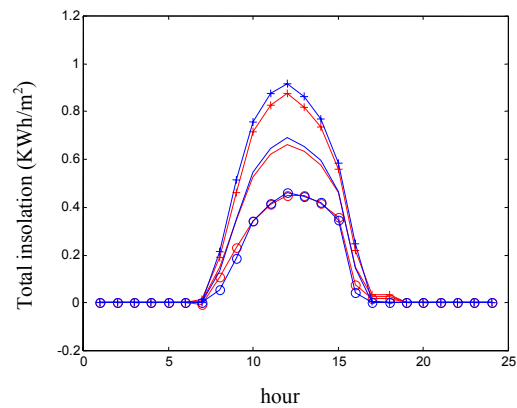


**Figure 4.4. Mean Curve Comparison for December.**

The agreement is good and with this approach, the worst error at peak values was in the range of  $\pm 6.0\%$  and the computation time was reduced from almost 8 hours to less than 10 minutes.

## 4.2 The Rechargeable Battery Model

Some enhancements have been made to the work performed in FY98. These include a comprehensive literature search of current state of the art in lead-acid battery diagnostic testing in the field of Electrochemical Impedance Spectroscopy (EIS) and the development of a test plan to be used in the experimental phase of this project. In addition, the creation of a more realistic theoretical battery damage model and the implementation of a different artificial neural network algorithm to model this damage surface were tasks completed during FY99. This work is detailed in the following paragraphs.

Common lead-acid battery failure modes are grid corrosion, lack of water, damage to the positive plates, or sulfation. In PV applications, sulfation frequently occurs when the battery remains at a low state of charge for extended time periods. If the battery is properly maintained and not

abused, most of the failures will be due to the degradation and wear out of the positive plate through either grid corrosion or active material shedding. A noninvasive technique is required to understand the system, and one such electroanalytical diagnostic tool is Electrochemical Impedance Spectroscopy (EIS). Impedance measurements can be used to provide information on transport across the electrolyte, reactions at the electrodes, and other phenomena that might affect the performance of the cell. This technique, along with battery cycle testing, and coupled with stochastic, deterministic and artificial neural network models will serve as the basis for developing enhanced software to model the behavior of a photovoltaic/rechargeable battery/load system. Ultimately, a predictive capability for the performance of the battery under the various design options is needed to optimize the system for the best trade off among cost, load requirement, battery life and reliability of the system.

Electrochemical Impedance Spectroscopy (EIS) was evaluated on the lead-acid batteries as part of the experimental phase of this study to gain an insight into the fundamental processes affecting performance, and also those leading to failure of the system. It is anticipated that EIS may be able to detect changes in battery properties with greater sensitivity and therefore allow degradation rates to be quantified at an earlier stage. This would in turn provide a better prediction of performance and end-of-life of the battery system. A literature review on previous EIS studies done on lead-acid batteries is the first step. A thorough literature search was done, and a list of the most relevant articles published during the last nine years, along with short abstracts, is presented in Appendix D.1.

A test plan, shown in Appendix D.2, was developed for the testing of the 100-Ah, GNB SUNlyte™ 12-5000X photovoltaic reserve battery [17]. The test objective was to measure the damage done to the battery, in terms of capacity loss, by deficit charging in a simulated photovoltaic application cycle. The necessary equipment to perform complex AC measurements on the GNB 12-5000X was acquired to more fully characterize the rate of battery degradation. Cycle testing of the battery followed the general pattern of the tests carried out at the Florida Solar Energy Center (FSEC) described in Reference 18. In those tests, the batteries were first cycled 25 times to a 20% DOD at rates varying from C/10 to C/60. The next step in the test was to impose 4-6 deficit charge cycles that would reduce the state-of-charge of the battery to a predetermined low voltage limit, usually 11.4 V (1.90 VPC) or higher. Once the low voltage limit was reached, a recovery period was begun using charge/load ratios from 1.0 to 1.6 in order to vary the length of time before the battery was returned to regulation within the top 20% of charge. The total number of cycles accumulated before battery capacity degraded by 20% was determined.

In the follow-on testing, the focus was on measurement of the damage caused to the battery capacity by a single period of deficit charging and recovery. The effect on the capacity degradation by changes in the low voltage limit and the charge/load ratio (which determines the length of the recovery period) were the primary parameters of interest. Since the FSEC tests did not show a recognizable trend relative to charge/discharge rate, the tests were carried out at a single rate, C/20. Only 3 initial sustaining cycles were run in order to reduce test time, and only 3 cycles were run to verify that the system has returned to regulation after recovery from the deficit charge period. For the initial set of tests, deficit charging was planned for about 5 cycles until low voltage limits corresponding to a 60% or 40% state of charge are reached. Charge/load ratios of 1.1 and 1.5 led to recovery times of between 3–4 days and 3–4 weeks. A discharge of

each unit to 1.75 V is done at the completion of the cycling to determine the available capacity and the impedance tests were also repeated. Initial capacity of the 12-5000X battery varies over a range of 24 Ah, so the results had to be individually compared back to the original measurements to determine if a loss has occurred. If required, the entire test protocol could have been repeated several times to cause a significant capacity change.

In the work performed in FY99, the revised theoretical damage surface, shown in Figure 4.5, was developed to better represent the qualitative behavior of battery damage. In addition it incorporated some available test data from the SUNlyte™ 12-5000X batteries. Experimental data was necessary to develop an accurate battery damage model (ANN or otherwise). In this phase of the project, a deterministic model was primarily used to generate data to show that an ANN could model the expected behavior of the rechargeable battery. However, the results were consistent with the limited amount of experimental data available.

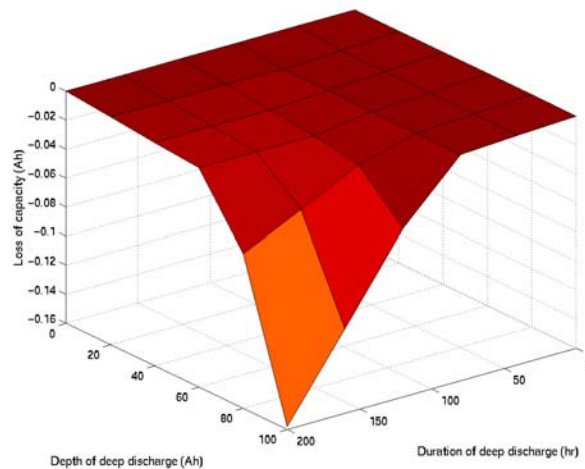


**Figure 4.5. The Battery Damage Model.**

From previous work performed in FY98, it was identified that the experimental data could potentially be highly nonlinear in certain regions of the input space. In the first phase of the project, we used a simple layer perceptron ANN to model the damage surface represented in Figure 4.5. Due to the potential presence of these nonlinearities and in order to have a robust model, a different type of ANN algorithm was implemented in FY99.

The multivariate polynomial spline (MVPS) network is an artificial neural network of the radial basis function type. The radial basis function ANN, which was developed by Moody and Darken [19], simulates mappings via the superposition of radial basis functions. The radial basis function ANN is an accurate local approximator, and although it trains rapidly, it has the potential for size difficulties as the dimension of the input space grows. A generalization of the radial basis function ANN is the connectionist normalized linear spline (CNLS) network. This was developed by Jones et al. [20] and seeks to simulate a mapping by using radial basis functions in a higher order approximation than the radial basis function network. The MVPS network generalizes the CNLS network to multiple output dimensions and higher degree local approximations. The authors introduced the use of a polynomial function (instead of a linear function) in order to enhance the network's ability to model highly nonlinear behavior. The

development of the mathematical framework behind the MVPS network is presented in the following paragraphs.

First, let  $\mathbf{X}$  be an n-dimensional input vector to the system being modeled, and let  $\mathbf{Z}$  be its corresponding m-dimensional output vector. The mapping from  $\mathbf{X}$  to  $\mathbf{Z}$  is denoted by:

$$\mathbf{Z} = g(\mathbf{X}) \quad (4.9)$$

Assume that the function  $g(\mathbf{X})$  is deterministic but that its form and parameters are unknown. Write an identity that equates  $g(\mathbf{X})$  to itself, then multiply both sides by a weighting function (radial basis function) that is centered at  $\mathbf{C}_j$ :

$$g(\mathbf{X}) w(\mathbf{X}, \mathbf{C}_j, \beta) = g(\mathbf{X}) w(\mathbf{X}, \mathbf{C}_j, \beta) \quad (4.10)$$

$$j = 1, \dots, N$$

Expand the function  $g(\mathbf{X})$  on the right hand side of Equation 4.10 using the first three terms in the Taylor series:

$$g(\mathbf{X}) w(\mathbf{X}, \mathbf{C}_j, \beta) \cong [A_{0j} + A_{1j}(\mathbf{X} - \mathbf{C}_j) + A_{2j}\zeta] w(\mathbf{X}, \mathbf{C}_j, \beta) \quad (4.11)$$

where  $A_0$ ,  $A_1$  and  $A_2$  are the coefficients of the local models,  $\mathbf{C}_j$  is the “center” of the  $j^{\text{th}}$  local approximation (also referred to as center vector or center),  $\zeta$  contains the quadratic and cross terms obtained from the elements in  $\mathbf{X}$ ,  $\beta$  is a parameter related to the width of the radial basis function and  $w(\mathbf{X}, \mathbf{C}_j, \beta)$  are the weights attached to the local models (in this case a multivariate Gaussian probability density function is chosen as the weighting expression).

This approximation can be optimized in the neighborhood of  $\mathbf{C}_j$  using least squares or weighted least squares and is accurate in the vicinity of the data used to develop it as long as the behavior of the mapping in the neighborhood is closely represented by the Taylor series. Approximations can be developed in all neighborhoods of the input vector space. The subscript  $j$  (where  $j = 0, 1, \dots, N$ , and  $N$  is the number of regions of approximation) accounts for this in Equations 4.10 and 4.11.

The local approximations of the  $\mathbf{X}$  to  $\mathbf{Z}$  mapping can now be combined to create an approximate, global map. To accomplish this, several of the approximations are superimposed in a series. Each component in the series is weighted according to its distance from the input vector  $\mathbf{X}$ . Local models that are near  $\mathbf{X}$  are weighted heavily, whereas those that are further away are weighted less. The series is obtained by summing the terms in Equation 4.11 as follows:

$$\sum_j g(\mathbf{X}) w(\mathbf{X}, \mathbf{C}_j, \beta) \cong \sum_j [A_{0j} + A_{1j}(\mathbf{X} - \mathbf{C}_j) + A_{2j}\zeta] w(\mathbf{X}, \mathbf{C}_j, \beta) \quad (4.12)$$

Since  $g(\mathbf{X})$  on the left-hand side of Equation 4.12 is independent of the index  $j$ , it can be removed from the summation. The resulting expression can be normalized to obtain:

$$g(\mathbf{X}) \cong \frac{\sum_j [A_{0j} + A_{1j}(\mathbf{X} - \mathbf{C}_j) + A_{2j}\zeta] w(\mathbf{X}, \mathbf{C}_j, \beta)}{\sum_j w(\mathbf{X}, \mathbf{C}_j, \beta)} \quad (4.13)$$

Equation 4.13 represents the parametric form of the MVPS network. Figure 4.6 shows a single input/single output example of local polynomial models fitted to arbitrary input/output data. It can be seen from the figure that for a highly nonlinear response, the local polynomial modeling is quite appropriate. Ultimately, and as described in the above paragraphs, the local models are splined together to form a global model.

The MVPS network is used in feed forward operation by specifying the input vector  $\mathbf{X}$ , evaluating the weights  $w$ , calculating  $\zeta$ , substituting the weights and  $\zeta$  into Equation 4.13, and evaluating the output  $g(\mathbf{X})$ . This output is an interpolation among the training outputs. Note that the range of the summation index  $j$  is not specified in Equation 4.13. It is clear that the summation should be carried out over those local models nearest the input vector  $\mathbf{X}$ . The ANN computer code used in the present investigation accepts a user-defined number of local models and the ones nearest, in Cartesian space, to the input vector are chosen to make each prediction. Using this ANN algorithm, the surface shown in Figure 4.6 was modeled with a high degree of accuracy and with the ability to capture any potential nonlinearity in the data even in the presence of noisy input data.

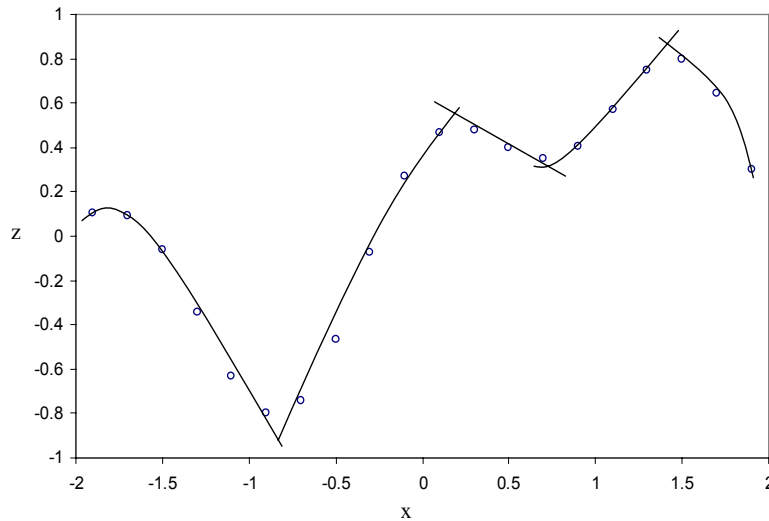


**Figure 4.6. Local Polynomial Models.**

### 4.3 Reliability Analysis

Because the current analyses are being run in the Monte Carlo framework, any of a number of probabilistic characterizations of system behavior could have been developed. Since a reliability analysis was ultimately desired, a first passage probability analysis on the response was performed. Before the results of this analysis are presented, a brief summary of the theory behind the technique is given (from Urbina et al. [21]).

The first passage probability distribution of a random process is the chance that the random process passes beyond a barrier of interest for the first time, at or before a time  $t$ . An estimation is made of the first passage probability of  $M_c(t)$ , the maximum potential capacity, below a barrier that is a fraction of its initial value. The first passage problem is defined as follows. Let  $\{Y_j, j = 0, \dots, n-1\}$  be a random process, with discrete time index  $j$ , and let  $T_S$  be a random variable denoting the first time index at which the state of the random process passes into the set  $S$ . Then the CDF of the random variable  $T_S$  is the first passage probability distribution of the random process  $\{Y_j, j = 0, \dots, n-1\}$ , with reference to the set of states  $S$ .

The CDF of the random variable  $T_S$  is estimated using the realizations of  $\{Y_j, j = 0, \dots, n-1\}$  generated during the Monte Carlo analysis. Denote these realizations  $y_j^{(k)}, j = 0, \dots, n-1, k = 1, \dots, M$ , where  $M$  is the total number of realizations generated during the Monte Carlo analysis. For each realization, the time at which the signal first passes into the set  $S$  is estimated. (This is accomplished, for example, simply by tracking the response time history.) Denote by  $t^{(k)}, k = 1, \dots, M$ , the time at which the  $(k)^{\text{th}}$  realization passes into the state  $S$ . (Some realizations may not pass into the state  $S$  within the time indices  $j = 0, \dots, n-1$ . For these, the quantity  $t^{(k)}$  might be set to some value that is large relative to the time index  $j = n$ . For such a case, the first passage probability distribution will not reach a value of one by  $j = n-1$ .) The ensemble of values  $t^{(k)}, k = 1, \dots, M$ , can now be used in the kernel cumulative distribution function estimator to approximate the CDF of the random variable  $T_S$ . This is:

$$F_{T_S}(t) = \frac{1}{M} \sum_{k=1}^M \Phi\left(\frac{t - t^{(k)}}{\varepsilon}\right) \quad (4.14)$$

where  $\Phi(\cdot)$  is the standard normal CDF, and  $\varepsilon$  is the smoothing factor of the kernel CDF estimator. Using this approach, a reliability analysis of the simulated and the actual data was performed for several levels of maximum potential capacity for the Honolulu example. Values of 99, 95 and 90 percent of the initial capacity of the battery were investigated and the results shown in the following figure. This figure contrasts the results obtained from the 10 Monte Carlo simulated data and from the actual data for a system subjected to a random load during the day and a constant load during the night. In this figure the analysis performed using actual solar data is shown as a solid line while the analysis using simulated solar data is shown as a dashed line.

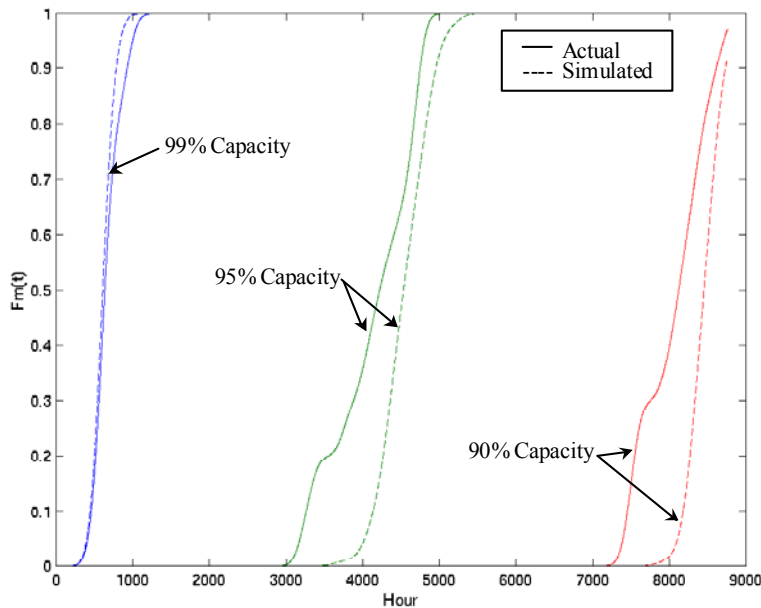


**Figure 4.7. First Passage Probability of  $M_c(t)$  (tilt angle = 21°).**

From Figure 4.7 it can be seen that the load profile causes most of the batteries to drop to the 90% capacity level within one year's time. It can also be observed from the figures that the first passage probability distributions of the maximum potential capacity data derived from the simulated and actual solar data are not exactly the same. While the 99% capacity level distribution is very similar for the actual and the simulated data, the distributions at the remaining lower capacity levels are slightly different. The reason for this can be attributed to a slight over-prediction of the solar resource available to recharge the batteries, particularly in the early months of the year.

From this example, it is possible to draw some conclusions about the behavior of the photovoltaic power supply system. The majority of the batteries suffer a drop in capacity of roughly 1% of the initial capacity by the end of the first two months of the year. By around the end of July, the maximum potential capacity is at 95% of the initial value and by the end of the year the maximum potential capacity drops by 10% from the initial capacity.

Changing some of the operational parameters of the system can modify the reliability of the system. These parameters include:

1. The number of amperes produced by the photovoltaic array – i.e., increase the size of the array.
2. The array's tilt angle and azimuth angle (to optimize energy production year-round).
3. The storage capacity of the system – i.e., the number of batteries.

## 4.4 C++ Code Translation

Because of the need to integrate the analysis software developed in this study into a comprehensive power grid analysis software, efforts were under way at the end of this study to convert the current MATLAB<sup>®</sup> code into C++ code. An initial attempt using a commercially available translator was successful in converting the bulk of the MATLAB<sup>®</sup> code into C++ code. Some additional work was needed to verify and optimize the converted code. One benefit from converting the code into C++ code and subsequently into a compiled executable file, is the improvement in the performance of the software. MATLAB<sup>®</sup> provides a good development and testing environment, but it is inefficient in the performance of iterative calculations. A C++ executable is much more efficient in this type of calculations, which are an integral part of a statistical analysis. Execution of the converted C++ software has shown a reduction in the processing time of about one-half versus running it within the MATLAB<sup>®</sup> environment. An additional benefit comes from the portability of the C++ executable (no C++ compiler or other software is needed to run the program). Once the program is translated into C++, the code can be integrated into the power flow model either via an object file (to be linked to the rest of the code) or through a dynamic linked library (DLL) which can be called by the power flow code. (The power flow model is presented in Appendix B.)

## 5.0 Summary of Work for Fiscal Year 2000

In previous work, we used a bivariate Markov process to simulate the direct normal and diffuse horizontal solar radiation data. This technique yields accurate realizations of the random process but it is very CPU intensive. In light of this, we sought a faster method that will be as accurate as, or more accurate than our current technique.

One focus of this investigation was therefore to implement a canonical variate analysis (CVA) approach to modeling the daily direct normal and diffuse horizontal radiation components. CVA has been successfully used to model random processes, such as the dynamic response of a nonlinear mechanical system (see Paez and Hunter [22]).

Another important goal for FY00 was the implementation of the PV generator code into a power flow model. This was done with the help of a commercially available translator that takes MATLAB<sup>®</sup> code and converts it into C++ code. The converted code was then integrated into a main power flow program and a sample calculation was performed.

Additionally, EIS measurements were performed on two different lead-acid batteries to evaluate the use of this technique for determining the capacity degradation. The results in the above areas of work are documented in the following sections.

### 5.1 Canonical Variate Analysis

Canonical variate analysis is an extension of the auto-regressive moving average (ARMA) modeling technique. Originally developed by Hotelling [23], CVA was improved by Larimore [24]. Larimore's implementation of CVA permits accurate and efficient simulation of random processes. CVA is described in detail in several references (see Larimore [24], Hunter [25]).

CVA involves three critical transformations, namely, the measurement to state transformation, the evolution of past states to future states, and the future state to estimated measurement transformation. Equations 5.1 through 5.4, below, implement these steps.

Let  $x(t_j), j = \dots, -1, 0, 1, \dots$ , denote a (possibly multivariate) measured excitation, at times  $t_j = j\tau, j = \dots, -1, 0, 1, \dots$ , and let  $y(t_j), j = \dots, -1, 0, 1, \dots$ , denote the corresponding (possibly multivariate) measured response. The first operation of CVA transforms measurements of the system “past”,  $\mathbf{p}$ , into a state space  $\mathbf{s}$ ,

$$\mathbf{s}(t_j) = \mathbf{J}\mathbf{p}(t_j) \quad (5.1)$$

where the system past, relative to time  $t_1$ , is defined:

$$\begin{aligned} \mathbf{p}(t_1) = & \dots \\ & [y(t_1 - \tau) \ \dots \ y(t_1 - l\tau) \ x(t_1) \ \dots \ x(t_1 - j\tau)]^T \end{aligned} \quad (5.1a)$$

The transformation matrix,  $\mathbf{J}$ , will be defined below. The ensemble of past signals,  $\mathbf{P}$ , and the ensemble of future signals,  $\mathbf{F}$ , of the system are defined as follows, relative to time  $t_1$ , in terms of measured excitation and response.

$$\mathbf{P} = \begin{bmatrix} y(t_1 - \tau) \cdots y(t_1 - l\tau) x(t_1) \cdots x(t_1 - j\tau) \\ y(t_2 - \tau) \cdots y(t_2 - l\tau) x(t_2) \cdots x(t_2 - j\tau) \\ \vdots \quad \quad \quad \vdots \quad \quad \quad \vdots \quad \quad \quad \vdots \\ y(t_k - \tau) \cdots y(t_k - l\tau) x(t_k) \cdots x(t_k - j\tau) \end{bmatrix} \quad (5.2)$$

$$\mathbf{F} = \begin{bmatrix} y(t_1) \cdots y(t_1 + l\tau) \\ y(t_2) \cdots y(t_2 + l\tau) \\ \vdots \quad \quad \quad \vdots \\ y(t_k) \cdots y(t_k + l\tau) \end{bmatrix} \quad (5.2a)$$

Past states are evolved into future states, and future states are inverse transformed into the measured response space using the standard modal analysis framework. That framework is characterized by the equations

$$\begin{aligned} \mathbf{s}(t + \tau) &= \mathbf{A}\mathbf{s}(t) + \mathbf{B}\mathbf{x}(t) + \mathbf{e}(t) \\ \mathbf{y}(t) &= \mathbf{C}\mathbf{s}(t) + \mathbf{D}\mathbf{x}(t) + \mathbf{E}\mathbf{e}(t) + \mathbf{w}(t) \end{aligned} \quad (5.3)$$

where  $\mathbf{A}$ ,  $\mathbf{B}$ ,  $\mathbf{C}$ , and  $\mathbf{D}$ , are system matrices,  $\mathbf{e}(t)$  and  $\mathbf{w}(t)$  are noise vectors, and  $\mathbf{E}$  accounts for state model noise in the state to measurement transformation. The measurement to state transform defined by the matrix  $\mathbf{J}$  in Equation 5.1 is developed as follows:

$$\begin{aligned} \mathbf{J} &= \mathbf{U}^T [\mathbf{P}^T \mathbf{P}]^{-1/2} \\ \text{SVD} \left[ [\mathbf{P}^T \mathbf{P}]^{-1/2} [\mathbf{P}^T \mathbf{F}] [\mathbf{F}^T \mathbf{F}]^{-1/2} \right] &= \mathbf{U} \mathbf{W} \mathbf{V}^T \end{aligned} \quad (5.4)$$

where  $\text{SVD}[\cdot]$  indicates the singular value decomposition. The gist of the operations carried out in these equations is to, first, establish the autocorrelation matrices of the system past,  $\mathbf{P}$ , and future,  $\mathbf{F}$ , using ensembles of segments of the measured excitation and response. These autocorrelations are decomposed using the Karhunen-Loeve expansion (see Ghanem and Spanos [26]). The principal components are retained, and their cross correlations are orthogonalized. This yields the transformation matrix,  $\mathbf{J}$ , a measurement to state space transformation that yields an optimal relation between past and future principal components. Next all measured data segments are transformed into the state space using  $\mathbf{J}$ . The state transition and other state space matrices,  $\mathbf{A}$ ,  $\mathbf{B}$ ,  $\mathbf{C}$ , and  $\mathbf{D}$ , are identified using linear least squares. The transformation and state space parameters are identified using  $\mathbf{P}$  and  $\mathbf{F}$ , ensembles of signals. Response predictions operate on  $\mathbf{p}$  to predict  $\mathbf{f}$ .

A global model can be created using all the data, or a local model can be created using data in the neighborhood of a particular past,  $\mathbf{p}$ . In this way, we create global and local linear models. In this investigation, local linear models are used to characterize the joint behavior of direct normal and diffuse horizontal insolation. Further, we take the excitation,  $\mathbf{y}$ , to be zero in this application. Equation 5.4 results from minimizing the mean square error in the prediction of the future  $\mathbf{f}$  from the past  $\mathbf{p}$ . The process of transforming the measurements  $\mathbf{p}$  to critical waveforms  $\mathbf{s}$ , transforming past states  $\mathbf{s}$  to future states, and finally returning to the measurement domain for  $\mathbf{f}$  may seem awkward, but in fact is considerably more stable than directly predicting  $\mathbf{f}$  from  $\mathbf{p}$ . Intuitively, the gain comes from minimizing the number of parameters necessary in the past to future prediction process. With the approach outlined above, we generate realizations of daily direct normal and diffuse horizontal radiation and subsequently use them to calculate total hourly insolation at any given location.

## 5.2 Test Case and Results

A test case was set up to exercise the PV/rechargeable battery/load model. The model was operated on the Monte Carlo principle to yield realizations of the hourly solar insolation data, using the CVA technique described earlier. The solar insolation along with the load profile was input to the lead-acid battery model and hourly capacity cycling data were produced.

The specific test case consisted of a PV array located in Albuquerque, NM (latitude 35° 03'). The tilt angle was set at 50° (which enhances power generation in the winter months) and the azimuth angle was set to 0° (which means that the array is facing due South). The PV array is rated at 2.1 amps at standard test conditions (i.e., 1000 w/m<sup>2</sup> and 25°C temperature) and has a nominal voltage of 12 volts. Three PV modules were connected in parallel to give a current of 6.3 amps. An 105 Ah lead-acid battery served as the energy storage device for this example. It was assumed that the capacity threshold,  $C_d$ , below which a discharge started to cause damage, was 52 Ah (50% of initial capacity). The battery damage surface was simulated via the MVPS ANN. The applied load consisted of a constant load during nighttime and a randomly applied load during the daytime. This load profile required an average of 30 Ah per day/night.

The following results were obtained using simulated PV data based on 10 years of actual insolation measurements for the Albuquerque, New Mexico, area. Figure 5.1 shows measured hourly insolation data for the month of January 1978. Figure 5.2 shows a realization of hourly insolation data for a simulated January as obtained with our PV simulator software. It is important to note that these realizations will not be identical because they are random process realizations, but their characters should be similar because the random process source of Figure 5.2 is meant to simulate the random process source of Figure 5.1. That is, there are days in which the insolation is low and others in which it is high.

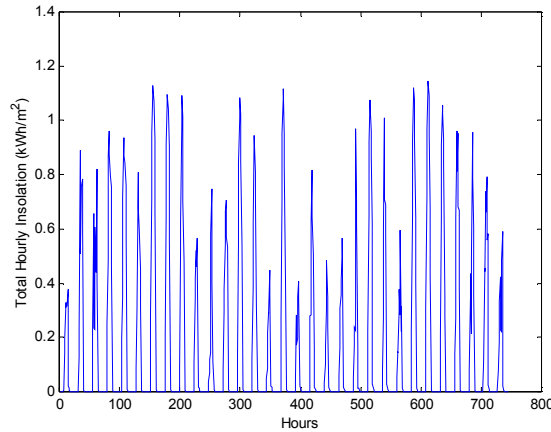


**Figure 5.1. Measured Total Hourly Insolation for January 1978.**

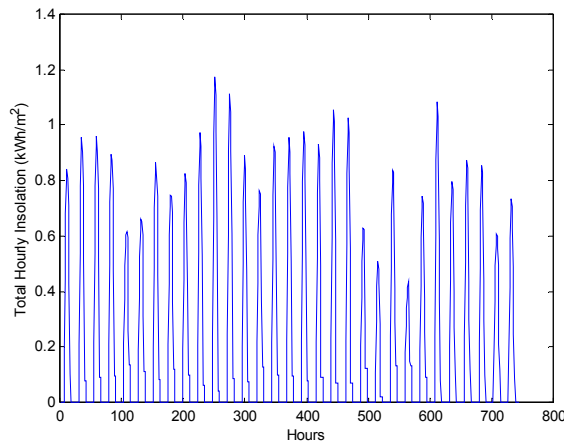


**Figure 5.2. Simulated Total Hourly Insolation for 31 January Days.**

### 5.3 Code Integration into Power-Flow Model

One of the major tasks in this LDRD project was the integration of our code into a power-flow model. Literature on the development of the power-flow model, provided by Dr. Satish Ranade at New Mexico State University (NMSU), served as a starting point to understand the interaction of the codes [27]. The first challenge was to convert our MATLAB<sup>®</sup> software into C<sup>++</sup> so that it could be incorporated into the existing C<sup>++</sup> power flow code (presented in Appendix B). Our

code was translated using a commercially available translator, which generated a C<sup>++</sup> function that was ultimately compiled with the existing power flow code. This translation provided a seamless integration of the codes and allowed our code to run more efficiently (MATLAB<sup>®</sup> code does not run iterative calculations as efficiently as C<sup>++</sup>). Figure 5.3 shows the flow diagram for the interface of our PV/rechargeable battery generator and the power flow software.

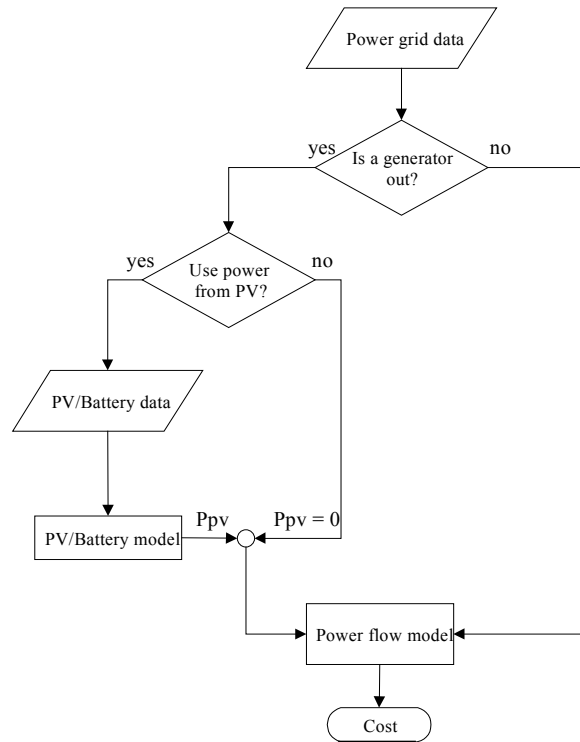


**Figure 5.3. PV Generator Interface Diagram.**

The power grid data is stored in a text file and is used by the power flow program to assess the initial state of the grid. Using a stochastic approach, a generator is outaged at random times. When this is the case, a decision is made to either use the PV generator or not. If it is desired to use the PV model, the software calculates the insolation for the given day and time and calculates the available power ( $P_{pv}$ ) supplied by the PV generator, using the given PV input data. If not,  $P_{pv}$  will be equal to zero. This additional power (or lack thereof) is passed to the power flow model and a cost is calculated. The cost represents the fuel cost associated with producing power plus any penalties associated with exceeding generators', transformers', and transmission lines' thresholds [27]. To exercise the interface between the two codes the simple power grid shown in Figure 5.4 was used.

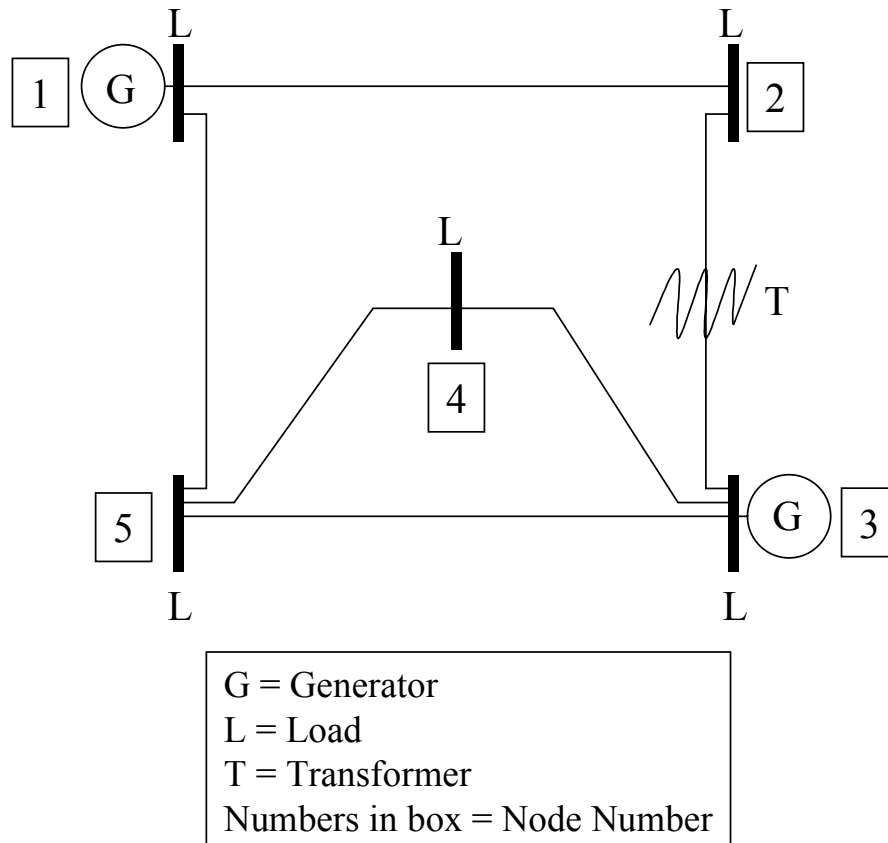


**Figure 5.4. Sample Power Grid.**

This example grid consisted of the following components:

Component (at node)	Power Used	Power Produced	
		(min)	(max)
Generator at node 1	N/A	20 MW	300 MW
Generator at node 3	N/A	20 MW	300 MW
Load at node 1	65 MW	N/A	N/A
Load at node 2	115 MW	N/A	N/A
Load at node 3	70 MW	N/A	N/A
Load at node 4	70 MW	N/A	N/A
Load at node 5	85 MW	N/A	N/A
Transformer	N/A	N/A	N/A

The photovoltaic model consisted of a PV array located in Albuquerque, New Mexico, tilted at latitude angle plus 15° and with an azimuth angle of 0°. The maximum rated array current for one module is 6.3 amps (at standard test conditions, STC, of 1000 W/m<sup>2</sup> solar insolation and 25°C) and the rated current is 17.5 volts. It was assumed that there are 3 modules connected in parallel and 712 modules connected in series; this yields a 20 amps/12470 volt string that should

supply a maximum power of 249.4 kW (at STC). It was assumed that a PV generator was connected to the grid at node 3 and was only used as a backup (i.e., when the generator went out of service).

The combined power flow/PV generator model was exercised to simulate regular operation (i.e., all components, excluding PV generator, are operating) and random-occurring outages of generator #3. During these outages, the PV generator was activated and supplied whatever power it had available at the time of the outage. As expected, the cost associated with operating with PV backup was lower than if no PV backup was available. This demonstrates the benefits of PV as a backup power source to the grid.

#### **5.4 EIS Measurements on Lead-Acid Batteries**

The feasibility of using electrochemical impedance spectroscopy (EIS) as a diagnostic tool to follow damage accumulating in lead-acid batteries because of deficit charging was investigated. Full frequency EIS measurements are able to separate ohmic and interfacial contributions to the impedance and can also identify specific components responsible for battery performance degradation in many cases. This type of measurement has been applied to a variety of primary and secondary battery chemistries for both state-of-charge (SOC) and state-of-health determinations. Several recent papers and reviews have been published on this topic [28,29,30]. Field evaluations of lead-acid batteries are normally carried out with a single frequency impedance or conductance meter. However, a few full frequency impedance studies of small lead-acid batteries or electrodes have appeared.

Due to the 6-V limit of the potentiostat in the impedance measuring apparatus, initial impedance data were recorded on small batteries in the 5 – 10 Ah range where access could be made to short series strings of three cells or less. In the case of the 3-cell string, the state-of-charge was reduced slightly below 100% to keep the voltage under 6V. The first batteries studied were prismatic 4-V sealed lead-acid batteries with a 10-Ah rated capacity (Power Sonic model PS-4100). Impedance spectra were recorded from 65 kHz to 0.1 Hz at a 500 microvolt AC amplitude. A total of six identical batteries was measured at full charge, approximately 50% SOC, and about 0% SOC. Nyquist plots of the data are shown in Figures 5.5 through 5.7 respectively.

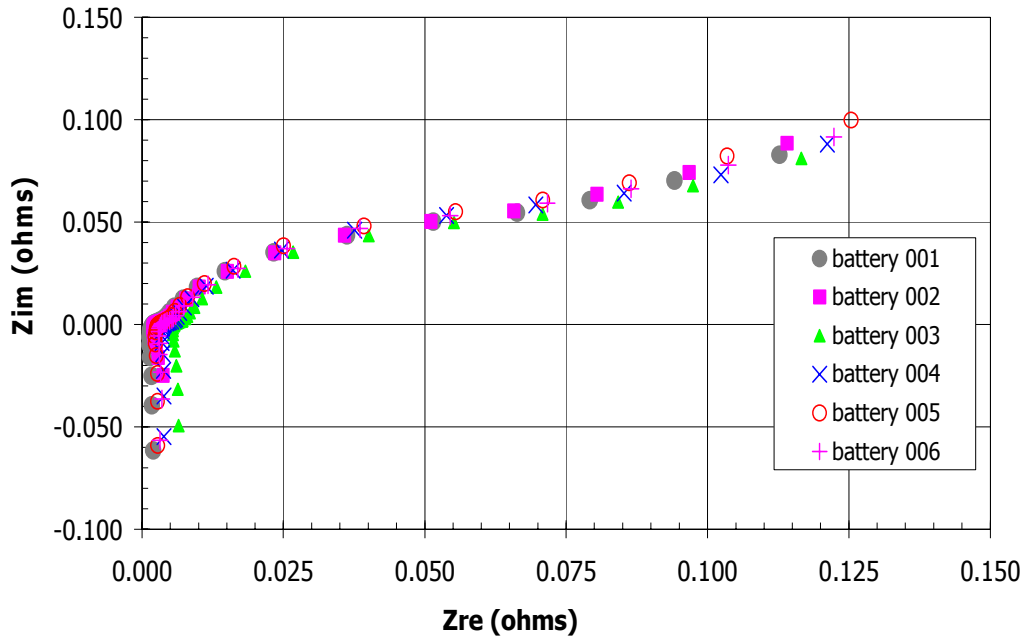


Figure 5.5. Impedance of Power Sonic PS-4100 Batteries Fully Charged at 4.3 V.

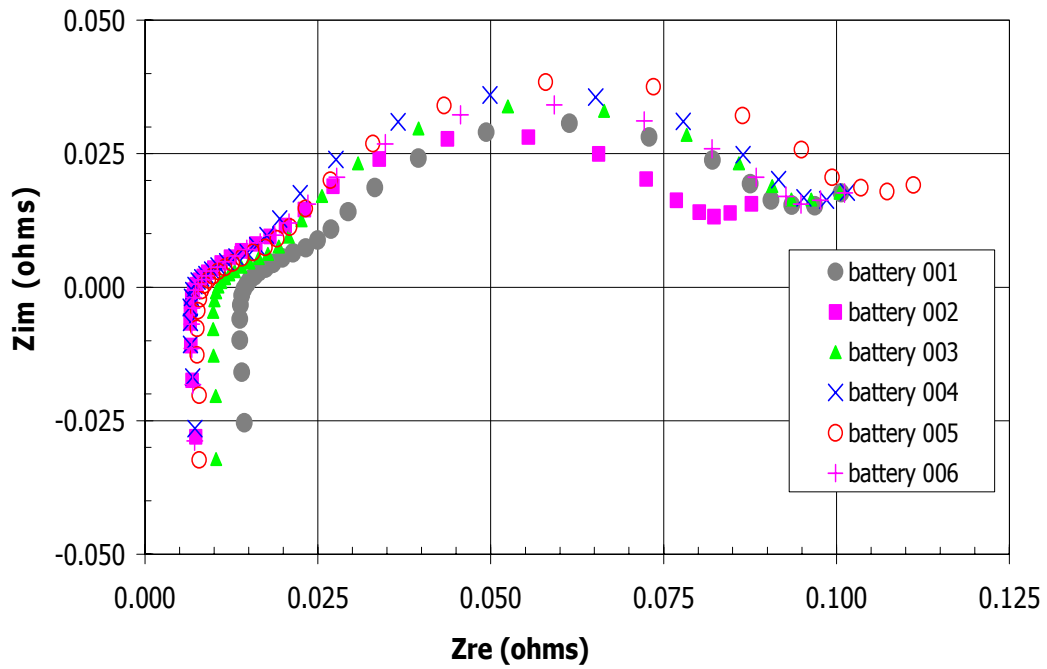
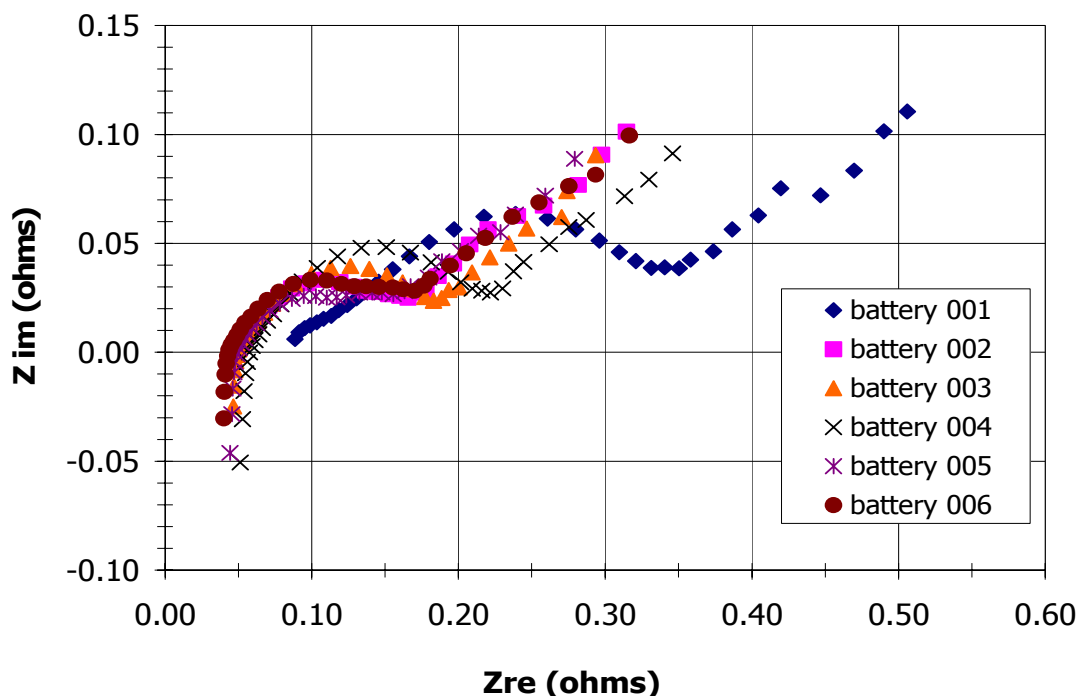


Figure 5.6. Impedance of Power Sonic PS-4100 Batteries at About 50% SOC.



**Figure 5.7. Impedance of Power Sonic PS-4100 Batteries at About 0% SOC.**

The fully charged batteries showed a low ohmic resistance near 5 mΩ and a relatively small interfacial impedance loop that is dominated by the diffusion tail. When the SOC is lowered to about 50%, the ohmic crossing point increases to the range of 7–15 mΩ and the interfacial loop becomes more pronounced (75 mΩ or more). At 0% SOC, the ohmic crossing point is near 50 mΩ and the interfacial loop has grown to more than 150 mΩ. These changes reflect the reduced electrolyte acid concentration on discharge (higher ohmic resistance) and the formation of a surface film on the electrodes (most likely lead sulfate). One of the cells showed a larger interfacial loop than the other five, both in terms of its impedance and capacitance. This indicates the presence of surface deposits on the electrodes that are different from the others both in terms of type and quantity. This difference did not show up at higher SOC.

The second battery type studied was a three-cell pack of cylindrical sealed lead acid cells in series (Hawker Energy Cyclon). The pack has a rated capacity of 5.0 Ah. Impedance spectra were recorded from 60 kHz to 0.01 Hz at a 100 microvolt AC amplitude in this case. Results were recorded for three batteries near full charge (5.92 V), with 2.5 Ah of capacity removed, 3.75 Ah of capacity removed and with 5.0 Ah of capacity taken out (near complete discharge). Results are shown in Figures 5.8 through 5.11.

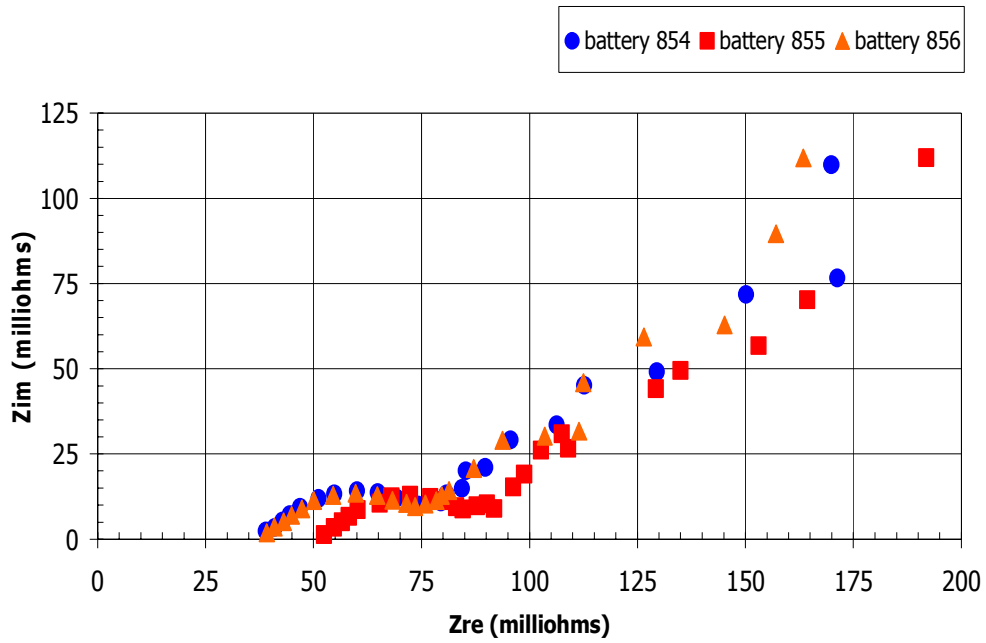


Figure 5.8. Impedance of Hawker Cyclon Batteries near Full Charge (11.83 V).

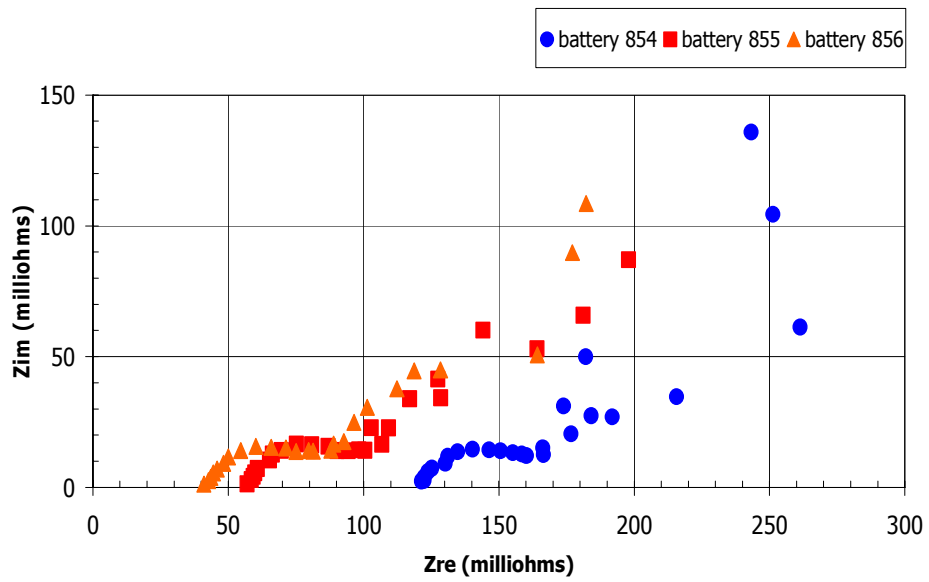


Figure 5.9. Impedance of Hawker Cyclon Batteries at About 50% SOC.

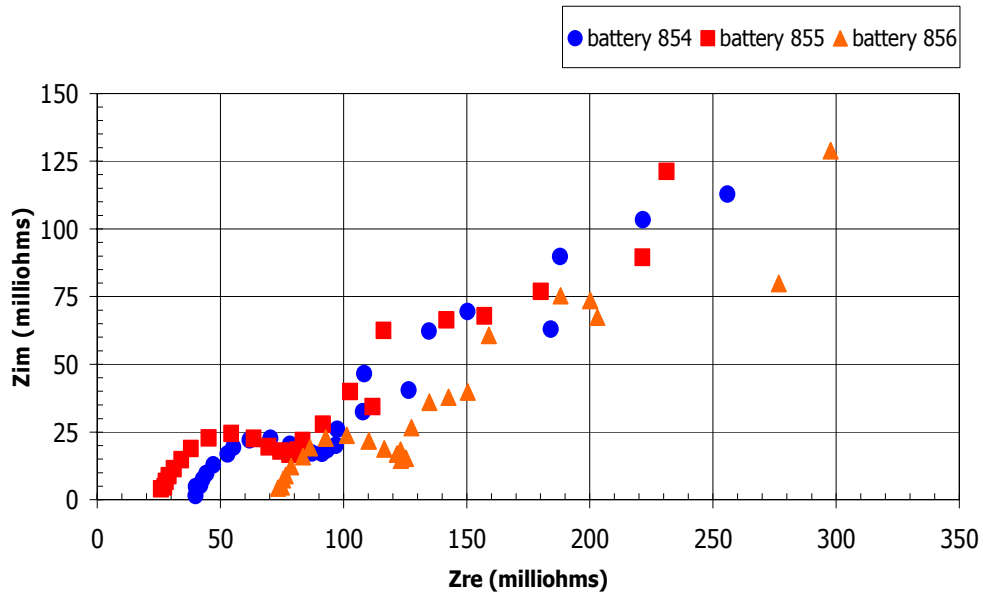
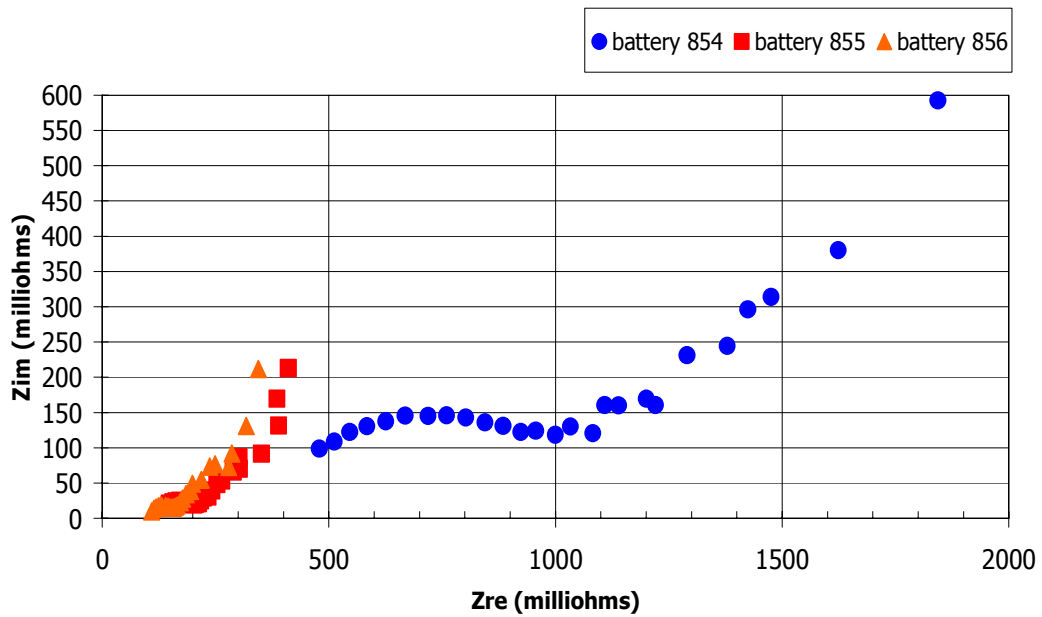


Figure 5.10. Impedance of Hawker Cyclon Batteries at About 25% SOC.



The ohmic resistance at near full charge ranged from 40 to 70 m $\Omega$  and the interfacial loop was again small. After 2.5 Ah was removed, the ohmic resistance was 40 – 120 m $\Omega$  and the interfacial loop was mostly unaffected. With 3.75 Ah removed, the ohmic value was 25 – 75 m $\Omega$  and the interfacial impedance was still around 50 m $\Omega$ , although the capacitance of the loop had increased somewhat. With 5 Ah removed the ohmic impedance increased to 100 m $\Omega$  while the interfacial loop was again fairly constant. The overall range of impedance was similar to the 10 Ah prismatic batteries, but the change during a discharge was slightly less. One of the packs showed much larger impedance, which at this point is considered an anomaly.

These batteries showed significant changes in impedance at different SOCs, which may mask the effects of damage due to periods of deficit charging. In addition, the GNB 12-5000X batteries that are the main focus of this study are much larger in capacity (100 Ah) than the two units studied here. The consequence of the larger electrode surface area is that the impedance will be significantly smaller than the values found for 5 and 10 Ah batteries. Another difficulty is that the 12-5000X battery is a 12-V unit, which exceeds the range of the potentiostat. Individual cells are not accessible without physical penetration of the battery jar. For all of these reasons, the complexity of the impedance measurements on the 12-5000X batteries was deemed to be beyond the scope of the present LDRD study. Smaller batteries would be a better test vehicle for the initial study of the effect of deficit charge periods on the battery impedance. Once the general nature of the expected changes is identified, it may prove possible to extend the measurements to the lower impedance regime of larger sealed lead-acid batteries.

## 6.0 Conclusions

The objective of this investigation was to develop a framework for simulating the power output from a photovoltaic system, including an energy storage device. The model has also been demonstrated to be capable of assessing the reliability and life of rechargeable batteries in the PV use environment. This information can be applied to optimize PV system designs and establish more cost-effective battery replacement schedules. A means for simulating the solar insolation random process was required, and we sought an efficient technique for the generation of random process realizations, where historical records of the phenomenon only characterize the random process. Several approaches to model the solar insolation were investigated: 1) a Markov-chain based method to calculate *hourly* insolation values; 2) a Markov-chain based method to calculate *daily* insolation values and then using a backbone curve approach to yield hourly insolation values and 3) a canonical variate analysis approach to calculate hourly radiation values.

The current system uses lead-acid batteries for energy storage. It is acknowledged that damage can accumulate in rechargeable batteries when they are used in a deficit charge environment, such as PV. Damage modeling was performed using a multivariate polynomial spline artificial neural network. Impedance testing on lead-acid batteries was evaluated for measuring capacity degradation. Change due to state-of-charge appeared to dominate the impedance results so that small changes due to battery aging/damage were difficult to observe. The system load was modeled as a combined deterministic/stationary random process.

The results of the investigation and numerical examples indicate that plausible simulations of available battery capacity and maximum potential capacity,  $M$ , can be generated. Indeed, the

important measure of model performance embodied in the first passage probability distributions for M shows that the system performance simulations are accurate. Calculations for a test case predicted good retention of battery capacity for at least one year. It remains to investigate more metrics of system performance to assure that system simulations are accurate in all details.

The integration of the PV generator code with a the power flow model was also accomplished. This was done via the translation of MATLAB<sup>®</sup> code to C<sup>++</sup> code and subsequent integration of the PV generator into the main body of the power flow code. Preliminary results, using a simple power grid, clearly indicate the benefits of using PV power as backup to the main grid.

## References

1. National Renewable Energy Laboratory, *National Solar Radiation Database User's Manual (1961-1990)*, version 1.1, 1994.
2. National Renewable Energy Laboratory's Analytic Studies Division, *Solar Radiation Data Manual for Flat-Plate and Concentrating Collectors*, 1994.
3. J. F. Kreider and F. Kreith, *Solar Energy Handbook*, pp. 2-1–2-18 and 2-72–2-73, McGraw Hill, New York, 1981.
4. R. Perez, P. Ineichen, R. Seals, J. Michalsky and R. Stewart, "Modeling Daylight Availability and Irradiance Components from Direct and Global Irradiance," *Solar Energy*, Vol. 44, No. 5, pp. 271–289, 1990.
5. Photovoltaic Design Assistance Center, *Stand-Alone Photovoltaic Systems: A Handbook of Recommended Design Practices*, SAND87-7023, Sandia National Laboratories, 1991.
6. R. J. Aguiar, M. Collares-Pereira and J. P. Conde, "Simple Procedure for Generating Sequences of Daily Radiation Values Using a Library of Markov Transition Matrices," *Solar Energy*, Vol. 40, No. 3, pp. 269–279, 1988.
7. K. M. Knight, S. A. Kline, and J. A. Duffie, "A Methodology for the Synthesis of Hourly Weather Data," *Solar Energy*, Vol. 46, No. 2, pp. 109–120, 1991.
8. R. Aguiar and M. Collares-Pereira, "TAG: A Time-Dependent, Autoregressive, Gaussian Model for Generating Synthetic Hourly Radiation," *Solar Energy*, Vol. 49, No. 3, pp. 167–174, 1992.
9. J. Remund, E. Salvisberg and S. Kunz, "On the Generation of Hourly Shortwave Radiation Data on Tilted Surfaces," *Solar Energy*, Vol. 62, No. 5, pp. 331–344, 1998.
10. *MATLAB® Reference Manual*, The MathWorks, Inc., Natick, Massachusetts, 1995.
11. C. C. O'Gorman, D. Ingersoll, R. G. Jungst and T. L. Paez, "Artificial Neural Network Simulation of Battery Performance," Proceedings of the 31<sup>st</sup> Hawaii International Conference on System Sciences, IEEE, The University of Hawaii, Hawaii, Hawaii, 1998.
12. T. L. Paez and N. Hunter, "Dynamical System Modeling Via Signal Reduction and Neural Network Simulation," Proceedings of the 67<sup>th</sup> Shock and Vibration Symposium, Baltimore, MD, 1997.

13. J. A. Freeman and D. M. Skapura, *Neural Networks, Algorithms, Applications, and Programming Techniques*, Addison-Wesley Publishing Company, Reading, Massachusetts, 1991.
14. A. Urbina, R. G. Jungst, D. Ingersoll, T. L. Paez, C. C. O’Gorman and P. Barney, “Probabilistic Analysis of Rechargeable Batteries in a Photovoltaic Power Supply System,” Proceedings of the 194<sup>th</sup> Electrochemical Society, Boston, Massachusetts, 1998.
15. D. Isaacson and R. Madsen, *Markov Chains: Theory and Applications*, Wiley, New York, 1976.
16. B. Silverman, *Density Estimation for Statistics and Data Analysis*, Chapman & Hall, Monographs on Statistics and Applied Probability 26, London, 1986.
17. GNB Technologies, GNB SUNlyte™ 12-5000X Photovoltaic Reserve Battery Technical Brochure, GNB Technologies, Lombard, Illinois, 1998.
18. “Preliminary Test Results From the FSEC/Sandia PV Battery Cycle-Life Test Procedure,” Tom Hund, Ramu Swamy, and Jim Dunlop, Draft dated 3/31/98
19. J. Moody and C. Darken, “Fast Learning in Networks of Locally Tuned Processing Units,” *Neural Computation*, (1) 2, 281-294, 1989.
20. R. D. Jones et al., “Nonlinear Adaptive Networks: A Little Theory, A Few Applications,” Cognitive Modeling in System Control, The Santa Fe Institute, 1990.
21. A. Urbina, T. L. Paez, C. C. O’Gorman, P. Barney, R. G. Jungst and D. Ingersoll, “Reliability of Rechargeable Batteries in a Photovoltaic Power Supply System,” Proceedings of the 21<sup>st</sup> International Power Sources Symposium, Brighton, England, 1999.
22. Paez, T. and N. Hunter, “Dynamical System Modeling Via Signal Reduction and Neural Network Modeling,” Proceedings of the 70<sup>th</sup> Shock and Vibration Symposium, 1999.
23. Hotelling, H., “Relations Between Two Sets of Variates,” *Biometrika*, V. 28, pp. 321–377, 1936.
24. Larimore, W., “System Identification, reduced Order Filtering, and Modeling Via Canonical Variate Analysis,” Proceedings of the American Control Conference, H. Rao, P. Dorato, eds, 1983.
25. Hunter, N., “State Analysis of Nonlinear Systems Using Local Canonical Variate Analysis,” Proceedings of the 30<sup>th</sup> Hawaii International Conference on System Science, 1997.
26. Ghanem, R., Spanos, P., *Stochastic Finite Elements: A Spectral Approach*, Springer-Verlag, New York, 1991.

27. Ranade, S., et al, "Optimal Power Flow Using SGOPT – An Experiment," draft report submitted to Sandia National Laboratories, April 1999.
28. F. Huet, "A Review of Impedance Measurements for Determination of the State-of-Charge or State-of-Health of Secondary Batteries," *Journal of Power Sources*, **70** 59, 1998.
29. M. Kniveton and A. I. Harrison, "Impedance/Conductance Measurements as an Aid to Determining Replacement Strategies," Proceedings of the 20<sup>th</sup> International Telecommunications Energy Conference (INTELEC '98), Oct. 4–8, 1998.
30. K. Takano, K. Nozaki, Y. Saito, K. Kato, and A. Negishi, "Impedance Spectroscopy by Voltage-Step Chronoamperometry Using the Laplace Transform Method in a Lithium-Ion Battery," *Journal of the Electrochemical Society*, 147 (3), 2000.
31. A. K. Shukla, V. G. Kumar, N. Munichandraiah and T. S. Srinath, "A Method To Monitor Valve-Regulated Lead Acid Cells," *Journal of Power Sources*, Vol. 74, No. 2, 234–239, 1998.
32. J. Diard, B. Le Gorrec and C. Montella, "EIS Study of Electrochemical Battery Discharge On Constant Load," *Journal of Power Sources*, Vol. 70, No. 1, 78-84, 1998.
33. G. Lindbergh, "Experimental Determination of the Effective Electrolyte Conductivity in Porous Lead Electrodes in the Lead-Acid Battery," *Electrochimica Acta*, Vol, 42, No. 8, 1239–46, 1997.
34. J.M. Charlesworth, "Determination of the State-of-Charge of a Lead-Acid Battery Using Impedance of the Quartz Crystal Oscillator," *Electrochimica Acta*, Vol, 41, No. 10, 1721–26, 1996.
35. V.V. Viswanathan, A. J. Salkind, J. J. Kelley and J. B. Ockerman, "Effect of State of Charge on Impedance Spectrum of Sealed Cells .2. Lead-Acid-Batteries," *Journal of Applied Electrochemistry*, Vol. 25, No. 8, 729–739, 1995.
36. B. Szczesniak, J. Kwasnik, J. D. Milewski and T. Pukacka, "Performance of Valve-Regulated Lead Acid Test Cells for Float Operation Using Modified Positive Active Materials," *Journal of Power Sources*, Vol. 53, No. 1, 119–125, 1995.
37. K.V. Rybalka and L. A. Beketaeva, "Impedance Studies of Electrochemical-Behavior of the Active Mass of Lead-Acid-Battery Electrodes," *Russian Electrochemistry*, Vol. 29, No. 2, 279–287, 1993.
38. S.A. Ilangovan and S. Sathyanarayana, "Impedance Parameters of Individual Electrodes and Internal Resistance of Sealed Batteries by a New Nondestructive Technique," *Journal of Applied Electrochemistry*, Vol. 22, No. 5, 456–463, 1992.

39. J. Jindra, M. Musilova, J. Mrha and A. A. Taganova, "Impedance Characteristics of Sealed Lead Acid Cells During Galvanostatic Charge," *Journal of Power Sources*, Vol. 37, No. 3, 403–409, 1992.
40. P.R. Roberge, E. Halliop, G. Verville and J. Smit, "Nondestructive Characterization of Sealed Lead-Acid-Battery Cells With Electrochemical Impedance Spectroscopy," *Journal of Power Sources*, Vol. 32, No. 3, 261–270, 1990.
41. J.P. Diard, B. LeGorrec, C. Montella and P. Landaud, "Constant Load Vs Constant Current EIS Study of Electrochemical Battery Discharge," *Electrochimica Acta*, Vol, 42, No. 23-24, 3417–20, 1997.
42. J. R. Vilche and F. E. Varela, "Reaction Model Development for the Pb/Pbso<sub>4</sub> System," *Journal of Power Sources*, Vol. 64, No. 1-2, 39–45, 1997.
43. K.V. Rybalka, L. A. Beketaeva and E. L. Protasova, "Application of the Operational Impedance Method to Estimation of the State of Charge of Chemical Power Sources: A Lead-Acid Battery," *Russian Journal of Electrochemistry*, Vol. 32, No. 6, 632–636, 1996.
44. K. Yamamoto, T. Ogata, K. Takano and Y. Konya, "Deterioration Estimation Method for 200-Ah Sealed Lead-Acid-Batteries," *NTT Review*, Vol. 7, No. 4, 65–69, 1995.

**Appendix C.1:  
Lead-Acid Battery Diagnostics –  
Literature Search on Electrochemical Impedance Spectroscopy**

## **A METHOD TO MONITOR VALVE-REGULATED LEAD ACID CELLS**

Shukla AK, Kumar VG, Munichandraiah N, Srinath TS  
JOURNAL OF POWER SOURCES  
74: (2) 234-239 AUG 1 1998

### **Abstract:**

The individual electrode impedance parameters and internal resistance of industrial type 120-Ah valve-regulated lead acid (VRLA) cells are obtained from a galvanostatic nondestructive technique. The resistive components of the cells are found to be minimum at a state-of-charge (SOC) value of 0.5. The study reflects that the optimum performance of the VRLA cells is achieved at SOC values between 0.2 and 0.8.

## **EIS STUDY OF ELECTROCHEMICAL BATTERY DISCHARGE ON CONSTANT LOAD**

Diard JP, Le Gorrec B, Montella C  
JOURNAL OF POWER SOURCES  
70: (1) 78-84 JAN 30 1998

### **Abstract:**

The impedance of electrochemical battery has been measured using a classical impedance-measurement apparatus to control the battery discharging into a constant load under current perturbation. This new method can be used even when the discharge current is greater than the maximum current that could be supplied by the regulation of the impedance-measurement apparatus used. Impedance measurements were first carried out on sealed Ni-Cd cells with a capacity of 0.65 Ah using the classical modulated current method and the new proposed method. The results show that the impedance diagrams, obtained during battery discharge through a constant load  $R$ , are identical to those obtained during discharges at a constant current with value  $U_{\text{mean}}/R$  where  $U_{\text{mean}}$  is the mean voltage of the battery during its natural discharge. These comparative measurements validate the proposed impedance-measurement method, which can be used to test all types of batteries or fuel cells. Impedance measurements are presented for sealed lead/acid cells with a capacity of 25 Ah and battery discharge currents greater than the maximum current that the regulation system could supply. These measurements show that the proposed method may be used with classical impedance-measurement set to test high-capacity and low-impedance batteries during discharge into a constant load.

## **EXPERIMENTAL DETERMINATION OF THE EFFECTIVE ELECTROLYTE CONDUCTIVITY IN POROUS LEAD ELECTRODES IN THE LEAD-ACID BATTERY**

Lindbergh G  
ELECTROCHIMICA ACTA  
42: (8) 1239-1246 1997

### **Abstract:**

An electrochemical impedance technique which measures the impedance between two reference electrodes placed on opposite sides of the working electrode, and which can be used for the

determination of the effective conductivity in the pore electrolyte in a porous electrode is presented. Information about the electroactive surface area and kinetic parameters can also be obtained from these measurements. A theoretical expression for the evaluation of the experimental results has been derived and analyzed. The high frequency intercept of the impedance curve with the real axis will give the external ohmic resistance for electrode materials with an infinitely high conductivity. Even at very low frequencies, some of the current passing through the electrode will pass through the electrode in the solid material. The relative importance of this transfer of current in the solid phase through the electrode can be determined for the general case by the dimensionless quantity  $\lambda$ , which depends on the electrode thickness, the effective conductivity of the pore electrolyte and the local impedance. Two limiting cases can be observed. A comparison between this type of measurement and conventional electrochemical impedance spectroscopy measured between the working electrode and a reference electrode shows that the difference between the two methods depends on the relative magnitude of the local impedance. The method has been used for the evaluation of data for a porous lead electrode in the lead-acid battery system. The experimental data obtained at different states of discharge have been analyzed by means of an impedance model, which takes into account the distribution of the local impedance in the porous structure, as well as the electrochemical reaction and mass transfer limitations in the electrode. Good agreement between the experimental data and the model has been obtained.

#### **DETERMINATION OF THE STATE-OF-CHARGE OF A LEAD-ACID BATTERY USING IMPEDANCE OF THE QUARTZ CRYSTAL OSCILLATOR**

Charlesworth JM  
ELECTROCHIMICA ACTA  
41: (10) 1721-1726 JUN 1996

##### **Abstract:**

Electrolyte density in a lead-acid battery may vary by up to 20% during the discharge-charge cycle and this property can be used as an indication of the amount of stored energy. We describe the application of impedance measurements on a 10 MHz AT cut quartz crystal immersed in solutions of 0-59 wt% sulfuric acid for the purpose of determining the state-of-charge during battery operation. Changes in impedance magnitude, phase angle and equivalent circuit resistance were followed, all of which showed strong dependency on viscosity and density. Good agreement with the theoretically predicted behavior of the motional resistance of thickness shear mode oscillators immersed in liquids was observed. These passive measurements of the crystal properties gave reproducible values, in contrast to active measurements involving determination of the frequency of a resonating circuit incorporating the crystal, which we have previously found to suffer from instability. Combining computer data acquisition and processing with appropriate calibration curves enabled direct monitoring of the discharge of a lead-acid battery.

#### **EFFECT OF STATE OF CHARGE ON IMPEDANCE SPECTRUM OF SEALED CELLS .2. LEAD-ACID-BATTERIES**

Viswanathan VV, Salkind AJ, Kelley JJ, Ockerman JB.  
JOURNAL OF APPLIED ELECTROCHEMISTRY  
25: (8) 729-739 AUG 1995

**Abstract:**

Alternating current impedance spectroscopy (ACIS) was performed on commercial sealed lead acid batteries. A method previously developed in the literature was modified to determine the state of charge of sealed lead acid cells by obtaining the impedance spectrum in a wide frequency range. The data were sensitive to state of charge at low frequencies. A modified Randles' circuit was used to fit the impedance data. The effect of the state of charge on the equivalent circuit parameters was determined.

**PERFORMANCE OF VALVE-REGULATED LEAD ACID TEST CELLS FOR FLOAT OPERATION USING MODIFIED POSITIVE ACTIVE MATERIALS**

Szczesniak B, Kwasnik J, Milewski JD, Pukacka T  
JOURNAL OF POWER SOURCES  
53: (1) 119-125 JAN 1995

**Abstract:**

Three types of valve-regulated lead/acid cells have been made with positive active material prepared from: (i) tribasic lead sulfate; (ii) tetrabasic lead sulfate; (iii) tetrabasic lead sulfate with graphite added. The cells have been subjected to float operation. They undergo premature capacity loss. The circumstances of this effect, the possibility of recovery of the capacity, the role of the graphite, and the impedance spectra of the cells are discussed.

**IMPEDANCE STUDIES OF ELECTROCHEMICAL-BEHAVIOR OF THE ACTIVE MASS OF LEAD-ACID-BATTERY ELECTRODES**

Rybalka KV, Beketaeva LA  
RUSSIAN ELECTROCHEMISTRY  
29: (2) 279-287 FEB 1993

**Abstract:**

The potential of impedance measurements in studies of porous electrochemical systems was discussed. Results were presented which were obtained when investigating the active mass of lead-acid battery negatives, both under equilibrium conditions and under polarization. It was shown that by impedance measurements it is possible to determine the parameters of porous structure of the electrodes without adding additional data from other techniques. The potential of impedance measurements in the scanning of porous electrodes was discussed.

**IMPEDANCE PARAMETERS OF INDIVIDUAL ELECTRODES AND INTERNAL RESISTANCE OF SEALED BATTERIES BY A NEW NONDESTRUCTIVE TECHNIQUE**

Ilangovan SA, Sathyanarayana S  
JOURNAL OF APPLIED ELECTROCHEMISTRY  
22: (5) 456-463 MAY 1992

**Abstract:**

A new robust method for the nondestructive determination of impedance parameters of the individual electrodes of sealed batteries has been developed. In this method, a battery is discharged at a constant current of about 2000 h (or less) rate for a few seconds only. The

discharge transient of voltage against time is analyzed theoretically to give effective double layer capacitances and charge transfer resistances of battery cathode and anode separately, as well as the internal resistance of the battery. Experimental data from discharge transients are processed with a new procedure which is immune to normal measurement errors and which permits a resolution of the parameters of the anodic and cathodic relaxation processes even if their time constants are not far apart. The correctness of the method is verified by simulation studies, and applied to sealed recombinant type lead-acid batteries. Diffusion resistance is shown to be negligible under the test conditions. The effects of switching transients and any series inductance are eliminated by the method. The results are directly relevant to improved battery design and failure analysis.

### **IMPEDANCE CHARACTERISTICS OF SEALED LEAD ACID CELLS DURING GALVANOSTATIC CHARGE**

Jindra J, Musilova M, Mrha J, Taganova AA  
JOURNAL OF POWER SOURCES  
37: (3) 403-409 FEB 1992

#### **Abstract:**

The electrochemical impedance of a model hermetic lead accumulator and its electrodes was measured during continuous or interrupted charging either in potentiostatic (at 10(4)-10(-3) Hz) or in galvanostatic (at 0.1 Hz) mode. The impedance characteristics of the negative electrode changed considerably during the second half of charging and during overcharging. The impedance curve at 0.1 Hz measured during continuous galvanostatic charging can be used to indicate the state of full charge of the cell.

### **NONDESTRUCTIVE CHARACTERIZATION OF SEALED LEAD-ACID-BATTERY CELLS WITH ELECTROCHEMICAL IMPEDANCE SPECTROSCOPY**

Roberge PR, Halliop E, Verville G, Smit J  
JOURNAL OF POWER SOURCES  
32: (3) 261-270 SEP 1990

#### **No Abstract**

### **CONSTANT LOAD VS CONSTANT CURRENT EIS STUDY OF ELECTROCHEMICAL BATTERY DISCHARGE**

Diard JP, LeGorrec B, Montella C, Landaud P  
ELECTROCHIMICA ACTA  
42: (23-24) 3417-3420 1997

#### **Abstract:**

An experimental method to measure the impedance of electrochemical batteries during discharge has been developed. The method uses classical impedance-measurement apparatus and current

perturbation to control a battery discharging into a constant load. Impedance measurements were carried out on sealed Ni-Cd cells with a capacity of 0.65 Ah using the classical modulated-current method and the new proposed method. The results are compared for cases in which both methods may be used. Impedance measurements carried out using the new method are also presented for sealed lead-acid cells with a capacity of 25 Ah and battery discharge currents greater than the maximum current that the regulation system could supply. These measurements show that the proposed method may be used with classical impedance-measurement set to test high-capacity and low impedance batteries during discharge into a constant load.

### **REACTION MODEL DEVELOPMENT FOR THE PB/PBSO<sub>4</sub> SYSTEM**

Vilche JR, Varela FE  
JOURNAL OF POWER SOURCES  
64: (1-2) 39-45 JAN-FEB 1997

#### **Abstract:**

Metal dissolution, active-passive transition and passive layer electroreduction reactions taking place during discharge/charge processes in the lead/sulfuric acid system are discussed on basis of data obtained from steady-state polarizations, potentiostatic pulses, single (STPS) and repetitive (RTPS) triangular potential sweeps, modulated voltammetry, complex voltammetry combined with potentiostatic steps, and electrochemical impedance spectroscopy, using rotating ring (Pb)-disc (Pb) electrode assembly, as well as scanning electron microscopy (SEM). Data analyses derived from transient electrochemical techniques employing parametric identification procedures, non-linear fit routines and computer simulations have been interpreted in terms of appropriate nucleation and growth models for the formation of new phases, in which the characteristics and properties of the compounds generated on the Pb electrode surface exhibit a remarkable dependence on the operational potential.

### **APPLICATION OF THE OPERATIONAL IMPEDANCE METHOD TO ESTIMATION OF THE STATE OF CHARGE OF CHEMICAL POWER SOURCES: A LEAD-ACID BATTERY**

Rybalka KV, Beketaeva LA, Protasova EL  
RUSSIAN JOURNAL OF ELECTROCHEMISTRY  
32: (6) 632-636 JUN 1996

#### **Abstract:**

Potentialities of the operational impedance method for estimation of the performance of chemical power sources are considered. It is shown that the operational impedance of a lead-acid battery distinctly depends on the stages of charge (at level of charges from 0 to 50%). This fact can serve as a basis for the development of a device for battery fast testing.

### **DETERIORATION ESTIMATION METHOD FOR 200-AH SEALED LEAD-ACID-BATTERIES**

Yamamoto K, Ogata T, Takano K, Konya Y  
NTT REVIEW  
7: (4) 65-69 JUL 1995

**Abstract:**

Sealed lead-acid batteries are widely used in the telecommunications network for stand-by power systems. Their capacity must be checked periodically because deteriorates with age. But this takes considerable manpower. This paper discusses evaluation of the deterioration of 200-Ah sealed lead-acid batteries by the pulse-discharging method. The results indicate that battery deterioration is reflected in its impedance characteristics. Equipment for estimating the battery deterioration has been developed. This equipment can test batteries without disconnecting them from the load and can greatly reduce the manpower requirement.

**Appendix C.2:**  
**GNB Sunlyte™ 12-5000× Battery Test Plan**

**TEST PLAN:**  
**GNB SUNlyte™ 12-5000X**  
**Photovoltaic Reserve Battery**

Test Plan Revision: Revision 0.1, January 22, 1999

Test Unit ID:

Developer: GNB Technologies

Test Organization: Sandia National Laboratories Energy Storage Systems Department (2525)

Test Plan Author: Rudy Jungst

### **1.0 Purpose/Overview**

This document specifies the test and monitoring procedures for the 100-Ah, GNB SUNlyte™ 12-5000X photovoltaic reserve battery. The test objective is to measure the damage done to the battery, in terms of capacity loss, by deficit charging in a simulated photovoltaic application cycle. A damage surface for the battery will be determined as a function of depth of discharge and length of time spent at a low state of charge. The intent is to incorporate this experimentally measured damage profile into a model for the operation of a stand-alone photovoltaic system that contains battery energy storage. These tests are an extension of work that was carried out at the Florida Solar Energy Center (FSEC) under Sandia auspices from 1996 to 1998. The current tests are being performed for Rudy Jungst of the Sandia Lithium Battery Research and Development Department (2521). Four SUNlyte™ 12-5000X batteries were received by SNL in September 1998, for the initial phase of this test.

### **2.0 References**

1. ES&H SOP, Chemical Handling in Battery Analysis & Evaluation Department Laboratories, SP471735, Author: Catherine Hayes.
2. "Preliminary Test Results From the FSEC/Sandia PV Battery Cycle-Life Test Procedure", Tom Hund, Ramu Swamy, and Jim Dunlop, Draft dated 3/31/98.
3. GNB Technologies product data section 62.26, "SUNlyte™ Photovoltaic Reserve Battery", RPT 4/98.
4. GNB Technologies preliminary performance curves for the SUNlyte™ 12-5000, dated 10/12/98.

### **3.0 GNB SUNlyte™ 5000X Battery Specifications**

Battery Ratings:

8-h Rate Capacity: 85 Ah to 1.75 VPC at 25°C

20-h Rate Capacity: ~92 Ah to 1.75 VPC at 25°C

100-h Rate Capacity: 100 Ah to 1.75 VPC at 25°C

Nominal Open Circuit Voltage: 12 V

Max. Peak Current, Max. Continuous Current (Charge and Discharge): 500 A

Estimated Cycle Life (8 h rate to 1.75 VPC @ 25°C)

300 cycles at 80% DOD

600 cycles at 50% DOD

1,000 cycles at 20% DOD

Physical Measurements:

Overall Dimensions: 12.07 in. long X 6.87 in. wide X 8.69 in. high  
Battery Weight: 59 lbs.

Charge/Discharge Termination Conditions:

Charge:

Maximum Normal Charge Voltage: 14.22 V (2.37 VPC)

Maximum Float Charge Voltage: 15.3 V

Maximum Charge Return: 120%

Maximum Temperature at Start of Charge: 35°C

Maximum Temperature during Charge: 45°C

Discharge:

Minimum Discharge Voltage: 10.5 V at 20-h rate

Minimum Cell Voltage: 1.75 V at 20-h rate

Maximum Temperature at Start of Discharge: 45°C

Maximum Temperature during Discharge: 45°C

**4.0 Parameters to Monitor During Test**

Monitor battery voltage, current, and temperature (at the negative terminal) versus time. Also monitor room temperature.

Set Tmax to 45°C. If Tmax is reached during charge, allow the battery to cool to 35°C before resuming charge.

Data collection rate will be initially set at one point every 30 s or on detection of a 2% change in a parameter.

**5.0 Test Procedure**

Baseline Evaluation

Each SUNlyte™ 5000X batteries evaluated will initially be capacity tested at a C/20 rate (charge and discharge) and ambient temperature for a minimum of 5 cycles to verify that its capacity is stable and up to the manufacturer's nominal specifications. The discharge curves from this characterization will also serve to define the cutoff voltage at different states of charge for the C/20 rate. Discharges will be terminated at a 10.5 V cutoff (1.75 VPC). Charging voltage will be capped at 14.22 V (2.37 VPC). Charge termination will occur after 115% capacity overcharge or 5 hours after the current has tapered to a stable value (less than 10% change in 1 hour), whichever occurs first. After the first two discharges, the discharge/charge rates will be reset using the actual measured capacity values. Following the initial capacity tests, a complex AC impedance spectrum will be obtained at full charge and at 100% discharge to document the baseline condition of the unit. Mani Nagasubramanian of Dept. 2521 will assist in the collection of the impedance data.

Deficit Charge Cycle Tests

Cycle testing of the battery will follow the general pattern of the tests carried out at the Florida Solar Energy Center (FSEC) described in Reference 2. In those tests, the

batteries were first cycled 25 times to a 20% DOD at rates varying from C/10 to C/60. The next step in the test was to impose 4-6 deficit charge cycles that would reduce the state-of-charge of the battery to a predetermined low voltage limit, usually 11.4 V (1.90 VPC) or higher. Once the low voltage limit was reached, a recovery period was begun using charge/load ratios from 1.0 to 1.6 in order to vary the length of time before the battery was returned to regulation within the top 20% of charge. The total number of cycles accumulated before battery capacity degraded by 20% was determined.

In the present testing, the focus is to be on measurement of the damage caused to the battery capacity by a single period of deficit charging and recovery. The effect on the capacity degradation by changes in the low voltage limit and the charge/load ratio (which determines the length of the recovery period) are the primary parameters of interest. Since the FSEC tests did not show a recognizable trend relative to charge/discharge rate, the tests will be carried out at a single rate, C/20. Only 3 initial sustaining cycles will be run in order to reduce test time, and only 3 cycles will be run to verify that the system has returned to regulation after recovery from the deficit charge period. For the initial set of tests, deficit charging will be carried out for about 5 cycles until low voltage limits corresponding to a 60% or 40% state of charge are reached. Charge/load ratios of 1.1 and 1.5 will be tested, which should lead to recovery times of between 3-4 days and 3-4 weeks. Since we do not know at this point how successful we will be at reversing the damage caused by these tests with an extended boost charge, each test in the 2X2 matrix should be run on a different battery the first time through. A discharge of each unit to 1.75 V will be done at the completion of the cycling to determine the available capacity and the impedance tests will also be repeated. Initial capacity of the 12-5000X battery is reported to vary over a range of 24 Ah, so the results must be individually compared back to the original measurements to determine if a loss has occurred. The entire test protocol may be repeated several times or until a significant capacity change has been found.

## **6.0 Contingencies**

If the battery voltage falls below the cutoff for a C/20 discharge rate (10.5 V, 1.75 VPC), then the test shall be terminated.

If a tester failure occurs during the course of a cycle test, the following shall be observed:

Restart the test at the point it was halted if the interruption was less than 12 hours

Restart the test at the point it was halted if the interruption was between 12 and 72 hours and the battery state of charge was not below 70%.

Terminate the test if the interruption was longer than 72 hours or if the battery state of charge was below 40% for more than 24 hours or below 60% for more than 48 hours.

## **7.0 Data Collection**

Plot the voltage curves for the initial capacity tests versus state of charge.

Plot the battery voltage versus cycle number and the Amp-hour capacity in and out for each cycle.

Record the final capacity obtained after the cycling is done.

## **8.0 Data Retention**

All measurements will be retained permanently in the SNL battery test database, which is located in Building 894, Room 138C. The SNL test technician will be responsible for maintaining a test notebook that contains tester setup worksheets, plotted data, tabular summary information of all tests performed, and other relevant information regarding any unusual events that were noted during the course of the work.

## **9.0 Data reporting**

Reporting of the data will be accomplished through periodic updates given to the test manager and test consultant during performance of the tests. The results will be documented as part of the final report on the LDRD project.

## **10.0 Safety Concerns and Precautions**

Anyone who is assigned by the Department Manager to conduct the testing covered by this test plan and anyone required to come in contact with the unit for whatever reason must read and understand the following documentation before testing commences. This document specifies the safety concerns and precautions needed when dealing with this technology:

ES&H SOP, Chemical Handling in Battery Analysis and Evaluation Department Laboratories, SP471735, Author: Catherine Hayes

# Appendix D

## Cassandra Parallel Coding, Porting, and Usage

### Introduction

Cassandra is a C++ code used in conjunction with the CRAX (**C**assandra **E**xoskeleton) graphical user interface and a physical model such as Spice, Quicksilver, Astros, or some CFD code. Cassandra is used as the uncertainty analysis engine, while CRAX is the user interface.

For this project, Cassandra was parallelized using the Message Passing Interface (MPI). Then, the code was ported onto various parallel systems such as the DEC 8400, Janus, and the C-Plant. The makefile was upgraded so that the code could be compiled and executed in parallel systems. Finally, the code output was compared with the serial output to ensure that the parallel code worked as intended and that it was robust.

### Massive Parallel Computing

Before proceeding to the discussion of the CRAX/Cassandra implementation, we present a brief introduction to massively parallel computing. The discussion below first provides terminology for the subject and then presents a framework for the discussion of massively parallel implementation that follows.

#### Definitions

***Multiprocessing parallel machine:*** A machine or group of machines with more than one processor. Each processor can be utilized to compute or solve separate parts of the same program in parallel (i.e., each processor is computing its part of the program at the same time the other processors are computing theirs).

***Nodes:*** There are two main types of nodes in a parallel-processing machine: ***Service*** nodes and ***computational*** nodes. A single node can be either a single processor or a group of processors depending on the specific parallel machine being used.

***Service nodes:*** Service nodes are the nodes in which administrative computing takes place. For example, the Unix shell itself, editing programs, compilers, or any other program that is not specifically started with the designated program that initiates computational node execution using a protocol such as MPI.

***Computational nodes:*** Computational or compute nodes are where the actual parallel computation is taking place. These nodes can be accessed by first running the program that starts the MPI protocol program or other parallel processing communication protocol program. In the case of the DEC 8400 the program is called *dmpirun*. The *dmpirun* program then assigns one or more compute nodes that the parallel program will use and starts the parallel program on each of those CPUs.

**MPI:** Communication protocol interface for running on a multiparallel machine.

### Parallel Processing

In general, parallel processing is accomplished in the following way. To execute a program *myprog* using five processors, call the *dmpirun* program with the number of processors and the name of the program as arguments as follows:

```
%dmpirun 5 myprog
```

The *dmpirun* program would then initiate the *myprog* program on five different CPU compute nodes. Essentially, this means that each line of the *myprog* program will be executed five times, once for each CPU. Therefore, if *myprog* outputs “Hello World,” the following would appear as output:

```
%Hello World
%Hello World
%Hello World
%Hello World
%Hello World
```

The DEC 8400 uses the MPI communication protocol. This protocol assigns a number to each CPU being used, starting at 0. This number is often referred to as the CPU’s rank. If, in addition to “Hello World,” the CPU number associated with each CPU were also output, the following would appear as output:

```
%Hello World I am CPU #2
%Hello World I am CPU #0
%Hello World I am CPU #1
%Hello World I am CPU #4
%Hello World I am CPU #3
```

Note that:

1. The order is mixed. There is no guarantee which CPU will finish before another.
2. All output from any CPU goes to the same device (i.e., screen or directory structure).
3. Although the CPUs share the same file structure, each CPU has its own memory space.

Control of the parallel processing is done through use of **if** statements where the rank of a particular CPU can be used to identify which node is used to run a particular code segment. If the **if** statement fails for a particular CPU, then that CPU will not execute that line or lines of code. For example:

```
if (my_rank == 0)
{
do something
} else {
```

```
do something else
}
```

Since the memory of each CPU is separate from all the others, the variable *my\_rank* can then be set to the CPU number using the MPI commands. Therefore *my\_rank* for CPU 3 is 3, but for CPU 0 *my\_rank* will be seen as being equal to 0, and so on. The MPI commands can be used to send particular logical operations to a unique CPU. For example, if a variable called *x* exists in the program, MPI commands can be made to set *x* to a different value in each CPU's memory space. One CPU can also inquire as to the value stored in another CPU's memory area for any variable that exists in the program. Using these tools, a program can be developed that can take an array of five numbers and compute five different square roots at the same time (in parallel).

This would be done first by sending each CPU a different element from the array and setting it as the value of *x* (*x* will be different for each CPU). Then all five CPUs will compute a line similar to the following:

```
answer = sqrt(x);
```

Now, since *x* is different for each CPU and because each CPU has an independent and separate memory area, each CPU will use a different *x* and compute a different *answer*. Again, because each CPU has an independent and separate memory area, the value stored in *answer* will be different for each CPU. One could now designate one CPU (e.g., *root*) to inquire of each of the other CPUs what their stored value in *answer* is. *Root* could then store them in an array (including its own *answer*) and then print them to a file. This new array would be defined in each CPU's memory area, but the values would be valid only in the CPU memory, which is now called *root*.

We used the standard practice in naming *root* the processor (CPU) with rank 0. In the example above, the root processor was performing computations (the square root command). On some multiprocessing parallel machines it is required that root not perform any computations and that *root* is the only processor permitted to do any input/output. We adhere to both of these practices in order to keep the software compatible with all multiprocessing parallel machines.

## Approach for Generic CRAX/Cassandra Implementation

Since none of previous versions of the uncertainty software (CRAX/Cassandra) required a command line interface, unique software modifications were required. Two distinct efforts were involved with getting the CRAX/Cassandra analysis code to execute in a parallel-processing environment:

1. Adding MPI coding to the LHS code to cause the *root* CPU to load each other CPU with a different set of input parameters in their own memory space and then to run the *g*-function on every CPU except *root*. *Root* then inquired each other CPU as to the results. *Root* then stores the results in an array and then continues performing all output file generation.

2. Changing the communication interface between the three parts of the CRAX/Cassandra analysis code to work in the multiprocessing parallel machine environment.

Due to the accessibility, the DEC 8400 was chosen for the initial implementation. However, this multiprocessor platform has two limitations:

1. The Tcl/Tk library can be compiled to run on the compute nodes, but because of the way Tcl/Tk coded the event loop, if a Tcl/Tk script is running on the compute nodes then there will be  $x$  number of windows generated ( $x$  is the number of CPUs specified to be used in the MPI program command arguments). In general we would want everything that happens in the Tcl/Tk GUI to only happen once (i.e., button pushes, window generation or redraws, call backs, etc.). To make Tcl/Tk operate this way in a parallel environment (if it is even possible) would require the Tcl/Tk code to be completely rewritten.
2. The Common Object Request Broker Architecture (CORBA) was not implemented even though more than 400 commercial software vendors (e.g., Hewlett Packard) have adopted its interface standards, since a version compatible with a multiprocessing parallel platform was not available.

Therefore, Tcl/Tk could run only on the service nodes and communication between parts had to use system call commands and file I/O instead of being directly linked.

CRAX/Cassandra code has the following characteristics on the DEC 8400:

1. Each of the three parts is a separate program: CRAX, Cassandra, and the g-function (in this case, power flow).
2. CRAX is started on the service nodes. It handles all window creation and interaction with the user. Since it is running on a service node, it responds the same as if it were running on a non-multiprocessing parallel machine. CRAX still uses embedded C++ commands, but now these commands are stubs that only make a system call to start Cassandra running in parallel on the compute nodes. The system call incorporates the MPI program as follows:

*dmpirun X cassandra method.dat*

where: *dmpirun* is the name of the program that starts Cassandra running on  $X$  number of processors.

$X$  is any integer greater than 0 but equal to or less than the maximum usable processors (CPU nodes) on the DEC 8400 (the maximum number of compute nodes is dependent on the platform you are running on).

*cassandra* is the command line version of Cassandra.

*method.dat* is a file name that the program Cassandra uses for input from the CRAX program.

3. Cassandra had to be modified so that it could execute from the command line, i.e., without the CRAX GUI front end. The program Cassandra takes the *method.dat* file as an argument. The file provides Cassandra all the information needed to run the analysis (method type, random variables, etc.). Note that Cassandra has to run on the compute nodes because it makes the call to the g-function, which is equivalent to the square root function call in the example above. All MPI commands are made in Cassandra to give each CPU a different set of random variables values. After the g-function call returns, MPI calls are made from the *root* CPU to gather the results from all the other CPU nodes. MPI commands can be made only on compute nodes; therefore, Cassandra must be on the compute nodes. The root CPU then uses the results to generate the normal plot and report files.
4. When Cassandra makes a call to the g-function, it is actually making a call to a g-function stub. All the g-function stub does is make a system call to start the g-function program. The system call is of the following form:

*gsrun infile outfile pid#*

At this time, whether the user wishes to run solder, cbeam, power flow or some other problem, the program executable name must be renamed to “*gsrun*.” The arguments *infile* and *outfile* are file names telling the g-function (*gsrun*) where to find its input values (from Cassandra) and where to print its output results (to be read by Cassandra). The *pid#* must be distinct for each different CPU (in this case we use the number designating the CPU itself). The *pid#* must be attached to the name of any file that the g-function program creates while running. This is because the physical file structure for all CPU nodes is the same. If each CPU running a g-function program cannot distinguish its own temporary files, then it will overwrite other temporary files of the same name. This may require that the code of the third-party g-function be available to edit in order to port the g-function program to the DEC 8400. This was the case for the power-flow program. Note also the *infile* and *outfile* also must contain the *pid#* in order to distinguish them from the other files being generated by the other Cassandra programs running on other CPUs.

5. Currently, only the LHS and quasi-Monte Carlo sampling methods can take advantage of parallel processing benefits. For all other methods, Cassandra is called by CRAX with the number of CPU nodes to be used set to 1. LHS and the Quasi-Random Sampling method generate two cases for the value of *X* when dealing with the number of CPUs in the following system call made by CRAX:

*dmpirun X cassandra method.dat*

The use of LHS and the quasi-Monte Carlo sampling methods result in two situations dependent on the value of *X* (the number of CPU nodes) in the system call made by CRAX above. First, if the number of sample vectors required is equal to or less than the maximum number of CPUs minus 1 then CRAX will set the value of the *X* (shown above) to the number of sample vectors plus 1. In this case, one CPU will do each g-function evaluation.

The second case occurs if the number of sample vectors is greater than the maximum number of CPU nodes minus 1. In this case, *X* will be set to the maximum. Each CPU will handle one g-

function call until all the CPUs capable of doing calculations have made one g-function evaluation. Then a second g-function evaluation will be given to each CPU starting with the lowest rank (1) and giving each preceding rank CPU a second g-function evaluation. This will continue until all g-function evaluations have been made or until each CPU has done two evaluations. At this point, a third evaluation will be given to each CPU in the same way the second iteration was given, and so on until no more evaluations are required.

## Algorithm

Three cases are considered, based on the number of observations ( $n_{obv}$ ) and the number of processors  $- 1$  ( $n_{proc} - 1$ ) used.

Case 1:  $n_{obv} < n_{proc} - 1$

Case 2:  $n_{obv} = n_{proc} - 1$

Case 3:  $n_{obv} \bullet n_{proc} - 1$

For Case 1, the code does a parallel calculation on each work processor for each of the observations. However, the remaining work processors ( $n_{proc} - 1 - n_{obv}$ ) remain idle.

For Case 2, the code does a parallel calculation on each work processor for each of the observations. No processors remain idle.

For Case 3, the code does a parallel calculation on a total of  $n_{proc} - 1$  processors, for as many times (loops) as are necessary to achieve  $m_{max} = [n_{obv}/(n_{proc}-1)]$  number of passes. Then, if there are any observations left (i.e.,  $\text{modulus}[n_{obv}/(n_{proc}-1) \bullet 0]$ ), the remainder of the observations run on the “ $\text{modulus} \bullet 0$  portion of the code” in the final loop, with some processors necessarily remaining idle. By that point, all observations have been processed.

## Coding

The C++ coding uses the Message Passing Interface (MPI). The basic premise uses if-tests to determine which processors do what. For example, if the processor is root, then some task is done; otherwise, the work processors do some other tasks. To help increase the code's portability, root is not allowed to generate messages; some parallel systems prohibit root from doing so. The basic coding resembles the following code fragment:

```
if (my_rank = root)
{
    MPI_Send(&answer[1], 1, MPI_DOUBLE, root, my_rank, MPI_COMM_WORLD);
}
```

```

else
{
    MPI_Recv(v, _nvar+1, MPI_DOUBLE, root, my_rank, MPI_COMM_WORLD, &status);
}

```

where the first path is computed uniquely by the root processor, and the second path is computed by the work processors. This technique is otherwise known as the single-program multiple-data (SPMD) approach. The SPMD technique is quite effective for multiple-instruction multiple-data (MIMD) parallel systems such as Janus and C-Plant. In essence, a MIMD system is capable of both accessing multiple data streams and executing multiple instruction streams.

Blocking vs. nonblocking:

A blocking statement causes a processor to not surrender control to the user program until the statement has been completed via the exchange of message tags. On the other hand, a nonblocking statement will be processed immediately, without waiting for the message tag. For example, if the message tag for MPI\_Send is not available, then the processor will remain idle, waiting for the message to become available; if the message never gets generated, then the program will remain idle indefinitely. Although blocking and nonblocking MPI data exchange statements exist, we chose to use blocking statements; for most applications, the additional complexity added to the program by using nonblocking statements is not worth the potential increased robustness (assuming any is gained at all). For this coding, part of the blocking issue was alleviated by using tags that are uniquely defined by the processor performing the calculation (e.g. tag = my\_rank). This resulted in a robust code that did not hang-up during dozens of tests.

## Janus

Janus, also known as the Teraflop, is a MIMD, massively parallel system that consists of 4663 nodes. Each node consists of two Pentium Pro processors, for a total of 9326. The nodes are used for specific purposes, such as computation, service, I/O, communication, hot stand by, and so on.

Because Janus is a distributed memory system, every node has its own memory.

Janus uses a minimalized version of a kernel called Cougar that is run on the 4576 compute nodes of the Teraflop, while the Teraflop Operating System (T O/S) operates the service nodes; this approach was incorporated in order to minimize the amount of memory required by the operating system. For that reason, executables can only run on the compute nodes, while the service nodes are technically used to compile the code. The key idea is that the compute nodes focus on number-crunching, while the rest of the nodes perform all other tasks.

The following compile and link flags were added to the makefile:

```
CC      = /usr/bin/iCC -w
```

**LD** = /usr/bin/iCC

## DEC 8400

The DEC 8400 parallel system consists of 14 computer “clusters,” each with about 12 Alpha processors.

The following compile and link flags were added to the makefile:

**CC** = /bin/cxx -w -lmpi -lrt -pthread

**LD** = /bin/cxx -DUSE\_MPI -lm -lmpi -limc -lrt -threads

To execute the code on a single cluster, type

**dmpirun -np 5 cassandra methodtest.sav**

where dmpirun is the job launcher, np is the flag for number of processors, cassandra is the executable name, and methodtest.sav is the input deck.

After each job completion, the user should type

**mpiclean**

to clear message queues, shared memory, and semaphores. This is a “good citizen” practice.

To run in multi-cluster mode, type

**dmpirun -np 5 -hf myall cassandra methodtest.sav**

where the hf flag tells the system that you want to run on more than one cluster, and the myall file is a dummy name file that contains the names of the clusters that you want to use. A typical file should look like this:

sads141  
sads142  
sads143  
sads144  
sads145  
sads146

---

---

**Table I. Checkout of Parallel Algorithm**

---

<b>Number of Processors</b>	<b>Logic Case</b>	<b>Modulus</b>
-----------------------------	-------------------	----------------

---

1	Abort	N/A
2	3	0
3	3	1
4	3	0
5	3	1
6	3	4
7	3	3
8	3	2
9	3	1
10	2	N/A
11	1	N/A
12	1	N/A
13	1	N/A

## 4 Software Accessibility

The exchange of information between the CRAX GUI, Cassandra, and the physical model can take many forms. Within CRAX is the capability to either recompile the existing software into the Cassandra engine, thereby significantly increasing computational efficiency, or to rely on handshaking between the CRAX GUI, the Cassandra engine, and the existing software. The Tcl/Tk interface was modified to handle either of these situations very easily. In addition, Cassandra is platform-independent and complies with CORBA, permitting easy interface with many of the new engineering design and analysis software packages (Figure 6-3).

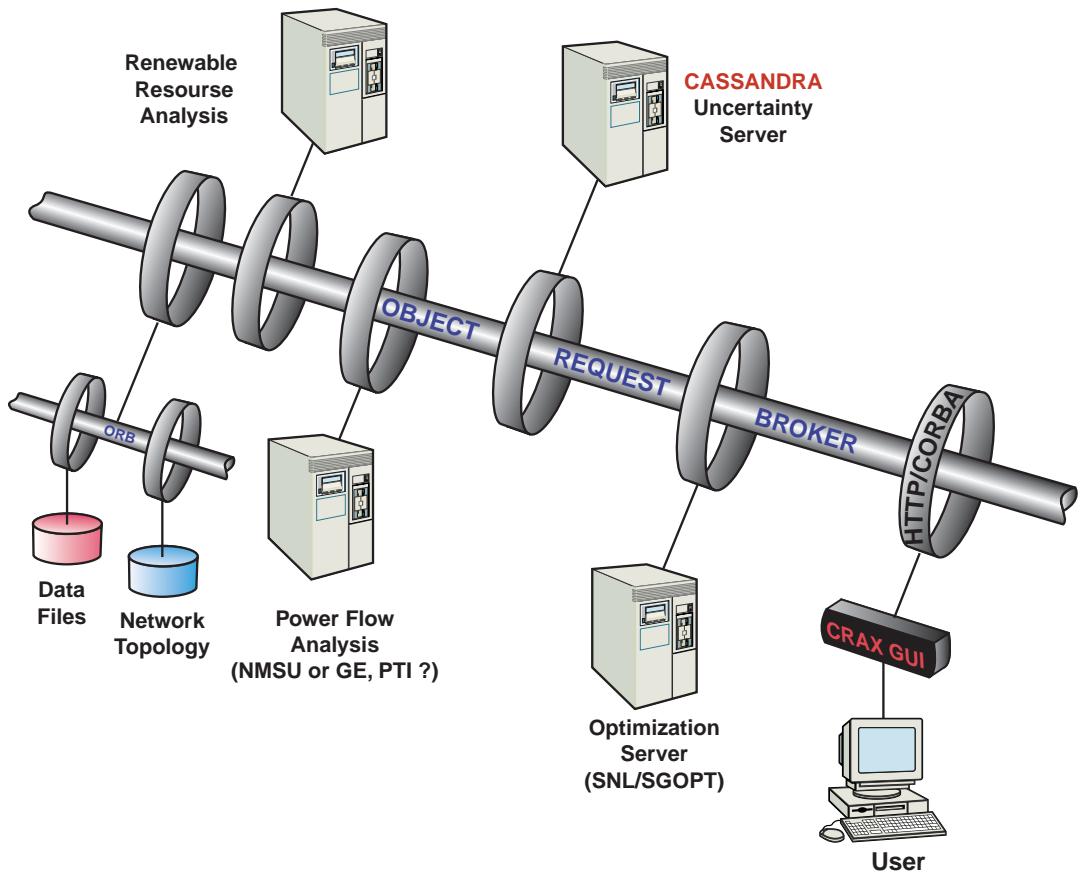


Figure D-1. Network Structure

## References

1. Robinson, David, "CRAX/Cassandra User Manual," Sandia National Laboratories report SAND99-3162, December 1999.
2. Pacheco, Peter S., "Parallel Programming with MPI," University of San Francisco, Morgan Kaufmann Publishers, Inc., 1997.
3. Gropp, William, Lusk, Ewing, and Skjellum, Anthony, "Using MPI Portable Parallel Programming with the Message-Passing Interface," Massachusetts Institute of Technology Press, 1997.
4. Hwang, Kai and Xu, Zhiwei, "Scalable Parallel Computing," McGraw-Hill, 1998.

**DISTRIBUTION:**

MS 0188 D. L. Chavez, 1030  
MS 0188 C. E. Meyers, 1030  
MS 0451 S. G. Varnado, 6500  
MS 0512 J. K. Rice, 2500  
MS 0521 J. T. Cutchen, 2501  
MS 0557 T. L. Paez, 9133  
MS 0557 A. Urbina, 9133  
MS 0613 G. P. Corey, 6251  
MS 0613 J. T. Crow, 2522  
MS 0613 D. H. Doughty, 2521  
MS 0613 R. G. Jungst, 2521  
MS 0613 B. Y. Liaw, 2521  
MS 0614 S. Atcitty, 2522  
MS 0614 R. W. Bickes, 2523  
MS 0614 N. H. Clark, 2522  
MS 0661 D. J. Trujillo, 9512  
MS 0662 P. C. Butler, 2522  
MS 0710 A. A. Akhil, 6251  
MS 0710 J. D. Boyes, 6251  
MS 0736 T. E. Blejwas, 6400  
MS 0739 S. B. Rodriguez, 6415  
MS 0739 G. E. Rochau, 6415  
MS 0741 M. L. Tatro, 6200  
MS 0747 A. L. Camp, 6410  
5 MS 0748 D. M. Kunsman, 6413  
5 MS 0748 D. G. Robinson, 6413  
MS 0748 R. D. Waters, 6413  
MS 0753 P. Klimas, 6219  
MS 0753 J. W. Stevens, 6218  
MS 0828 M. Pilch, 9133  
  
MS 9018 Central Technical Files, 8945-1  
2 MS 0899 Technical Library, 9616  
MS 0612 Review & Approval Desk, 9612

S. J. Ranade  
Klipsch School of Engineering and Computer Engineering  
New Mexico State University  
Las Cruces, New Mexico 88003

This page intentionally left blank